JOURNAL OF PETROLOGY | VOLUME 47 | NUMBER 11 | PAGES 2185–2232 | 2006 | doi:10.1093/petrology/egl041

Contributions of Slab Fluid, Mantle Wedge and Crust to the Origin of Quaternary Lavas in the NE Japan Arc

JUN-ICHI KIMURA[1]* AND TAKEYOSHI YOSHIDA[2]

[1]DEPARTMENT OF GEOSCIENCE, SHIMANE UNIVERSITY, MATSUE 690-8504, JAPAN

[2]INSTITUTE OF MINERALOGY, PETROLOGY AND ECONOMIC GEOLOGY, TOHOKU UNIVERSITY, AOBAKU, SENDAI 980-8578, JAPAN

RECEIVED OCTOBER 10, 2004; ACCEPTED JULY 25, 2006; ADVANCE ACCESS PUBLICATION AUGUST 17, 2006

Quaternary lavas from the NE Japan arc show geochemical evidence of mixing between mantle-derived basalts and crustal melts at the magmatic front, whereas significant crustal signals are not detected in the rear-arc lavas. The along-arc chemical variations in lavas from the magmatic front are attributable almost entirely to geochemical variations in the crustal melts that were mixed with a common mantle-derived basalt. The mantle-derived basalts have slightly enriched Sr–Pb and depleted Nd isotopic compositions relative to the rear-arc lavas, but the variation is less pronounced if crustal contributions are eliminated. Therefore, the source mantle compositions and slab-derived fluxes are relatively uniform, both across and along the arc. Despite this, incompatible element concentrations are significantly higher in the rear-arc basalts. We examine an open-system, fluid-fluxed melting model, assuming that depleted mid-ocean ridge basalt (MORB)-source mantle melted by the addition of fluids derived from subducted oceanic crust (MORB) and sediment (SED) hybrids at mixing proportions of 7% and 3% SED in the frontal- and rear-arc sources, respectively. The results reproduce the chemical variations found across the NE Japan arc with the conditions: 0·2% fluid flux with degree of melting F = 3% at 2 GPa in the garnet peridotite field for the rear arc, and 0·7% fluid flux with F = 20% at 1 GPa in the spinel peridotite field beneath the magmatic front. The chemical process operating in the mantle wedge requires: (1) various SED–MORB hybrid slab fluid sources; (2) variable amounts of fluid; (3) a common depleted mantle source; (4) different melting parameters to explain across-arc chemical variations.

KEY WORDS: *arc magma; crustal melt; depleted mantle; NE Japan; Quaternary; slab fluid*

INTRODUCTION

Island arcs develop because of subduction of oceanic lithosphere. The fluids released from the subducting oceanic plate and their reaction with the overlying mantle wedge provide the prime control on magma genesis (Gill, 1981; Hasegawa *et al.*, 1991; Hawkesworth *et al.*, 1993*a*; Pearce *et al.*, 1995; Tatsumi & Eggins, 1995; Davidson, 1996; Peacock, 1996; Peacock & Wang, 1999; Stern, 2002). Controlling factors for magma genesis along convergent plate boundaries include: (1) adiabatic upwelling of asthenospheric mantle induced by slab penetration (Hasegawa *et al.*, 1991; Peacock, 1996; Peacock & Wang, 1999); (2) partial melting of the mantle wedge as a result of the addition of slab-derived fluids (Arculus & Powell, 1986; Hawkesworth *et al.*, 1993*a*; Pearce & Parkinson, 1993; Poli & Schmidt, 1995; Tatsumi & Eggins, 1995; Davidson, 1996; Iwamori, 1998; Schmidt & Poli, 1998; Hochstaedter *et al.*, 2001); (3) melting of the subducted slab and addition of the resultant melts to the mantle wedge (Defant & Drummond, 1990; Drummond & Defant, 1990; Yogodzinski *et al.*, 1994; Kelemen *et al.*, 1998; Tatsumi & Hanyu, 2003).

Experimental petrology has provided important constraints for understanding melting and dehydration of the subducted slab, including phase relationships and elemental behavior in the slab (Defant & Drummond, 1990; Ayers & Watson, 1993; Poli & Schmidt, 1995; Keppler, 1996; Kogiso *et al.*, 1997; Schmidt & Poli, 1998; Johnson & Plank, 1999). Interactions between mantle peridotite and slab-derived fluid or melt have

*Corresponding author. Telephone: +81 852 32 6462. Fax: +81 852 32 6462. E-mail: jkimura@riko.shimane-u.ac.jp and kmrjunichi2006@yahoo.co.jp

also been studied both experimentally (Wyllie, 1982; Brenan *et al.*, 1995; Ayers *et al.*, 1997; Gaetani *et al.*, 2003; McDade *et al.*, 2003) and theoretically (Kelemen *et al.*, 1998). Geochemical studies of marine sediments, oceanic crust and their metamorphic equivalents have revealed considerable variety in the chemical reservoirs of subduction zones (Staudigel *et al.*, 1996; Plank & Langmuir, 1998; Bebout *et al.*, 1999). Although we now have a much better understanding of the chemical variations of the sources of subduction-related magmas and the nature of subduction zone metamorphism and mantle metasomatic processes, quantitative treatment of the major and trace element geochemistry is still difficult because of the complex phase relationships under hydrous conditions (Poli & Schmidt, 1995; Keppler, 1996; Spandler *et al.*, 2004). Nevertheless, the behavior of trace elements under hydrous conditions has been investigated, and more realistic trace element distribution coefficients have been determined for slab dehydration and hydrous mantle melting processes (Brenan *et al.*, 1995; Ayers *et al.*, 1997; Kogiso *et al.*, 1997; Aizawa *et al.*, 1999; Johnson & Plank, 1999; Green *et al.*, 2000; Gaetani *et al.*, 2003; McDade *et al.*, 2003; Kessel *et al.*, 2005).

Another approach is to investigate the range of chemical variation in the lavas erupted in island arcs. Chemical variations between arcs may originate from the kinematics of plate subduction (e.g. different rates or slab angles) that produce variations in thermal structure beneath arcs (Peacock, 1996; Peacock & Wang, 1999). However, the compositions of arc lavas can also vary across and along individual arcs. This probably results from: (1) differences in subducted slab materials (Plank & Langmuir, 1993); (2) differences in the dehydration or melting conditions of slab materials (Tatsumi, 1986; Defant & Drummond, 1990; Pearce & Parkinson, 1993; Hochstaedter *et al.*, 2001); (3) differences in melting conditions in the mantle wedge (Sakuyama & Nesbitt, 1983; Pearce & Parkinson, 1993); (4) differences in the amounts of slab-derived components added to the overlying mantle wedge (Ishikawa & Nakamura, 1994; Shibata & Nakamura, 1997); (5) pre-existing mantle heterogeneity (Hochstaedter *et al.*, 2001). Identification of the particular causes of chemical diversity in an arc system is difficult because apparently similar effects can have different causes, including modification of the primary magmas during their passage through the arc crust (Davidson, 1996; Davidson *et al.*, 2005).

Northeastern Japan is one of the best-documented volcanic arcs (Kuno, 1966; Sakuyama & Nesbitt, 1983; Tatsumi *et al.*, 1983; Kushiro, 1987; Nakagawa *et al.*, 1988; Nohda *et al.*, 1988; Togashi *et al.*, 1992; Ohki *et al.*, 1994; Kersting *et al.*, 1996; Gust *et al.*, 1997; Yoshida, 2001). The chemical variations within the NE Japan arc lavas have been discussed in terms of their major element, trace element and isotopic compositions, although there are few comprehensive datasets. Proposed geochemical models for the origin of across-arc chemical variations include: (1) different degrees of partial melting (Sakuyama & Nesbitt, 1983; Nakagawa *et al.*, 1988); (2) the presence of two separate dehydration regions (at 100 and 150 km depths) along the slab surface, with hydrated mantle rising through the mantle wedge as diapirs (Tatsumi, 1986; Tatsumi & Eggins, 1995); (3) mixing of slab-derived fluids with the mantle wedge in variable proportions (Shibata & Nakamura, 1997); (4) mantle heterogeneity (Notsu, 1983; Togashi *et al.*, 1992); (5) crustal contamination of mantle-derived magmas (Kersting *et al.*, 1996; Gust *et al.*, 1997; Kobayashi & Nakamura, 2001); (6) remelting of underplated gabbroic rocks at Moho depths in the arc crust to yield andesites (Takahashi, 1986*a*; Kimura *et al.*, 2001*b*). Based on numerical modeling and experimentally determined phase relationships, Iwamori (1998) first simulated fluid transport and partial melting beneath the NE Japan arc. His model assumed that dehydration occurs along the slab surface and that the fluids released are captured by hydration of the overlying mantle peridotite, which is then dragged down to be released at a depth of around 150 km. The fluids released are transported back into the high-temperature mantle wedge via channels and induce melting of the mantle wedge.

Detailed tomographic images have been published for the mantle beneath the NE Japan arc (Hasegawa *et al.*, 1991). These have been revised based on additional seismic data (Zhao *et al.*, 1992; Nakajima & Hasegawa, 2003), and NE Japan is now the best-studied arc in terms of seismology. The tomography results suggest that a region characterized by low P- and S-wave velocities, interpreted to be a zone of relatively high temperatures (and even partial melting), exists in the middle of the mantle wedge. Tamura *et al.* (2002) noted a spatial correlation between volcano distribution and low-velocity regions in the underlying mantle wedge, and proposed that finger-shaped hot regions ('hot fingers') characterize the mantle wedge beneath NE Japan (Tamura *et al.*, 2002). Seismologists argue that the anomalous mantle wedge region forms an inclined sheet rather than fingers, but regions of lower seismic velocity do seem to be concentrated beneath the volcanic front as well as beneath rear-arc volcanoes (Nakajima & Hasegawa, 2003). The origin of heterogeneity in the mantle wedge has become a matter of debate that might stimulate further discussion regarding the origin of the arc magmas.

Because of the large geological, geochemical, and geophysical databases available, the NE Japan arc is one of the best places for examining magma genesis beneath island arcs, although a multiplicity of ideas must be recognized and evaluated. In this paper, we focus on

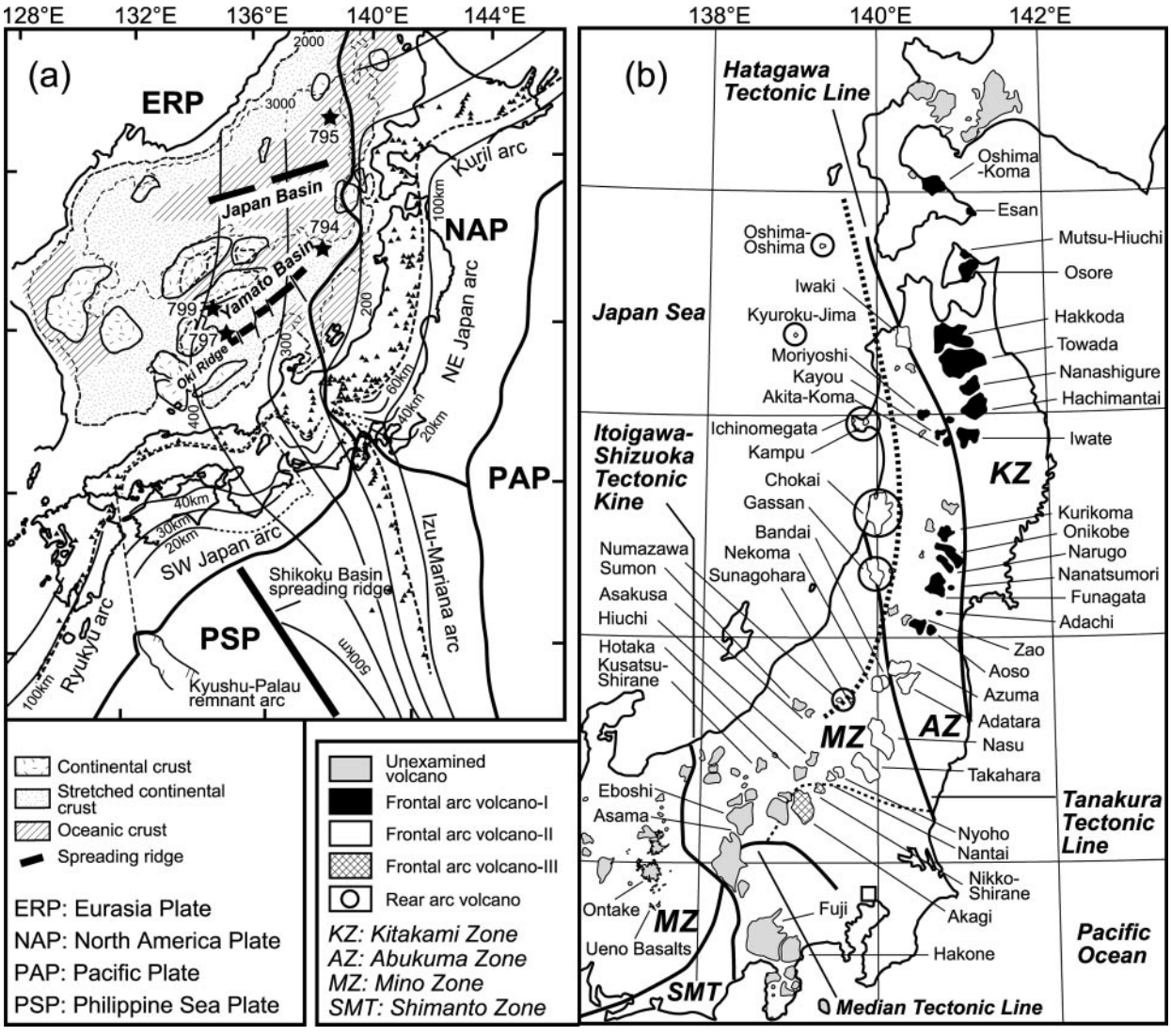

Fig. 1. (a) Tectonic map of the Pacific Plate, Philippine Sea Plate, Japan Sea, and Japan arcs. ERP, Eurasia Plate; NAP, North America Plate; PAP, Pacific Plate; PSP, Philippine Sea Plate. Seafloor tectonic map of the Sea of Japan modified from Tamaki *et al.* (1992). Stars mark ODP sites. (b) Distribution of the Quaternary volcanoes of the NE Japan arc and basement terrane boundaries.

the geochemical variations of the Quaternary lavas along and across the NE Japan arc. We selected 61 lava samples along the volcanic front and rear arc. Of these, 57 were analyzed for trace elements, 54 were further analyzed for Sr isotopes, 43 samples for Nd isotopes and 29 samples for Pb isotopes. Combined with published geochemical data, more than 1100 major element, 198 trace element, and 168 Sr, 138 Nd, and 86 Pb isotope ratio analyses are available for the arc. Based on these data, we discuss the origin of the geochemical variations in the lavas both along and across the NE Japan arc. An important result is the identification of crustal melt contributions to the lava chemistry, particularly in the frontal-arc lavas. By removing the effects of this crustal filter, we conclude that the composition of the parental magma and its source (mantle wedge plus subducted components) is relatively uniform along and across the arc. Different degrees of melting of the common mantle source induced by a relatively constant flux of slab fluids best explain the chemical variations of the basalts within the arc. We propose here a new mantle wedge mass balance model to explain the origin of the Quaternary magmas of the NE Japan arc.

GEOLOGY OF THE NE JAPAN ARC

The NE Japan volcanic arc is located about 500 km west of the Japan Trench, where the Pacific Plate is being subducted at a rate of about 10 cm per year; the arc is about 100 km wide (Fig. 1a and b). Pre-Tertiary

basement rocks beneath the NE Japan arc consist of Carboniferous to Jurassic metamorphic rocks of the Tamba–Ashio–Mino Terrane (MZ in Fig. 1b), Cretaceous sedimentary rocks and granitoids of the Abukuma Terrane (AZ), and an Ordovician to Cretaceous complex known as the Kitakami Terrane (KZ). The Tamba–Ashio–Mino and Abukuma Terranes are in contact along the Tanakura Tectonic Line, which is the main boundary fault between NE and SW Honshu. The Abukuma and Kitakami Terranes are separated by the Hatagawa Tectonic Line (Ichikawa, 1990). A chain of 55 volcanoes obliquely crosses the terrane boundaries. Volcanoes in this arc define two rows, the frontal row and the rear-arc row (Kawano *et al.*, 1961; Fujinawa, 1988; Tatsumi & Eggins, 1995). These have been called the Nasu (front) and Chokai (rear) Volcanic Zones (Kawano *et al.*, 1961). A few volcanoes are located between the chains, and these second-order alignments of volcanoes are regarded as cross chains (Tamura *et al.*, 2002). Quaternary intra-arc basins are always located between the second-order volcanic alignments. Here we follow the classical definition of the two volcanic rows and refer to them as the frontal arc (Nasu Volcanic Zone) and the rear arc (Chokai Volcanic Zone) (Fig. 1b). The two arcs are also geochemically distinct (Kawano *et al.*, 1961). Frontal-arc volcanoes are located parallel to the 110 km depth contour of the Wadati–Benioff zone, whereas the rear-arc volcanoes are located above the 150–190 km depth contours (Fig. 1a). The modern arcs consist mostly of stratocone volcanoes. Establishment of the present volcanic arc dates back to about 1·7 or 2·5 Ma, and preceding stages include large-scale calderas, rather than stratocones (Yoshida, 2001).

Quaternary volcanoes in the NE Japan arc

Volcanism in the NE Japan arc has been thought to have been established in the Quaternary at 1·7 Ma (Yoshida, 2001) or 1 Ma (Umeda *et al.*, 1999). An age data compilation shows that several volcanoes have ages between 2·5 and 1·5 Ma, but these are relatively rare compared with those younger than 1·5 Ma (Fig. 2, based on Committee for Catalog of Quaternary Volcanoes in Japan, 1999). Because of this age gap, we define the Quaternary volcanic arc stage to be younger than 1·5 Ma. Volcanism between 2·5 and 1·5 Ma could be included in the Quaternary stage. We do not preclude this possibility, but focus on the volcanic arc that is younger than 1·5 Ma in this study, because this volcanic activity is typical of the NE Japan arc from that time to the present.

The geochemical definition of the Quaternary volcanic arc relates to the establishment of a strong across-arc variation in the K content of the lavas, which is lower along the volcanic front and gradually increases rearward (Nakagawa *et al.*, 1988; Yoshida, 2001). Medium-K lavas have been erupted along the volcanic front over the past 1·5 Myr, and have been accompanied by low-K lavas from as early as 1·2 Ma (Kimura *et al.*, 2001*b*). The onset of low-K activity in the frontal arc occurred almost simultaneously over the entire arc, including central Japan. Extremely low-K suites occur in the very frontal arc at Osore, Adachi, and Aoso volcanoes (Nakagawa *et al.*, 1988), and also behind the frontal-arc row at Nekoma (Kimura *et al.*, 2001*b*, 2002). Therefore, we include them in the frontal-arc group in this paper. Both medium- and low-K suites were erupted at discrete eruptive centers, but they sometimes occur together in the same center, such as at Bandai, Adatara, Azuma, Zao, Funagata, and Hakkoda (Fujinawa, 1988; Kimura *et al.*, 2001*b*; Fig. 2). The low-K lavas are almost always tholeiitic and the medium-K lavas calc-alkalic, which is the common type in many frontal-arc lavas (Fujinawa, 1988; Kimura *et al.*, 2001*b*) in terms of iron enrichment (Miyashiro, 1974). The activity of rear-arc volcanoes began later than that along the magmatic front. Kimura (1996) first pointed out this temporal variation in the southern part of the NE Japan arc (Kimura, 1996). This observation holds over the entire NE Japan arc; rear-arc volcanoes are as old as 0·8 Ma (Umeda *et al.*, 1999; see Fig. 2). The rear-arc lavas are almost all high-K. The high-K lavas are calc-alkalic, apart from a few exceptions at Chokai. The onset of low-K activity in the frontal arc and high-K activity in the rear arc occurred almost simultaneously over the NE Japan arc, and does not show any distinctive development of the different 'fingers' proposed by Tamura *et al.* (2002). The geochemical distinction between frontal- and rear-arc lavas is well illustrated by the variation of SiO_2 vs K_2O (Fig. 3) as pointed out in previous studies (Kawano *et al.*, 1961; Nakagawa *et al.*, 1988; Yoshida, 2001). There is some overlap between the two geochemical groups in Fig. 3, as some frontal-arc Moriyoshi lavas and high-silica Akagi lavas plot in the field of rear-arc lavas. Low-K to medium-K lavas also occur in the rear-arc Numazawa and Sunagohara volcanoes (Fig. 3). However, such cases are relatively rare.

The frontal and rear arcs also have different magma production rates. The erupted volumes are greater along the magmatic front (total lava volume of ~4·6 km^3/km arc length at a production rate of ~1·5 km^3/ky) than in the rear-arc chain (~0·6 km^3/km arc length at ~0·2 km^3/ky) (Committee for Catalog of Quaternary Volcanoes in Japan, 1999). Eruptions of frontal-arc volcanoes are frequent, whereas activity has been much less frequent in the rear-arc volcanoes, according to tephrochronological studies (Kimura, 1996).

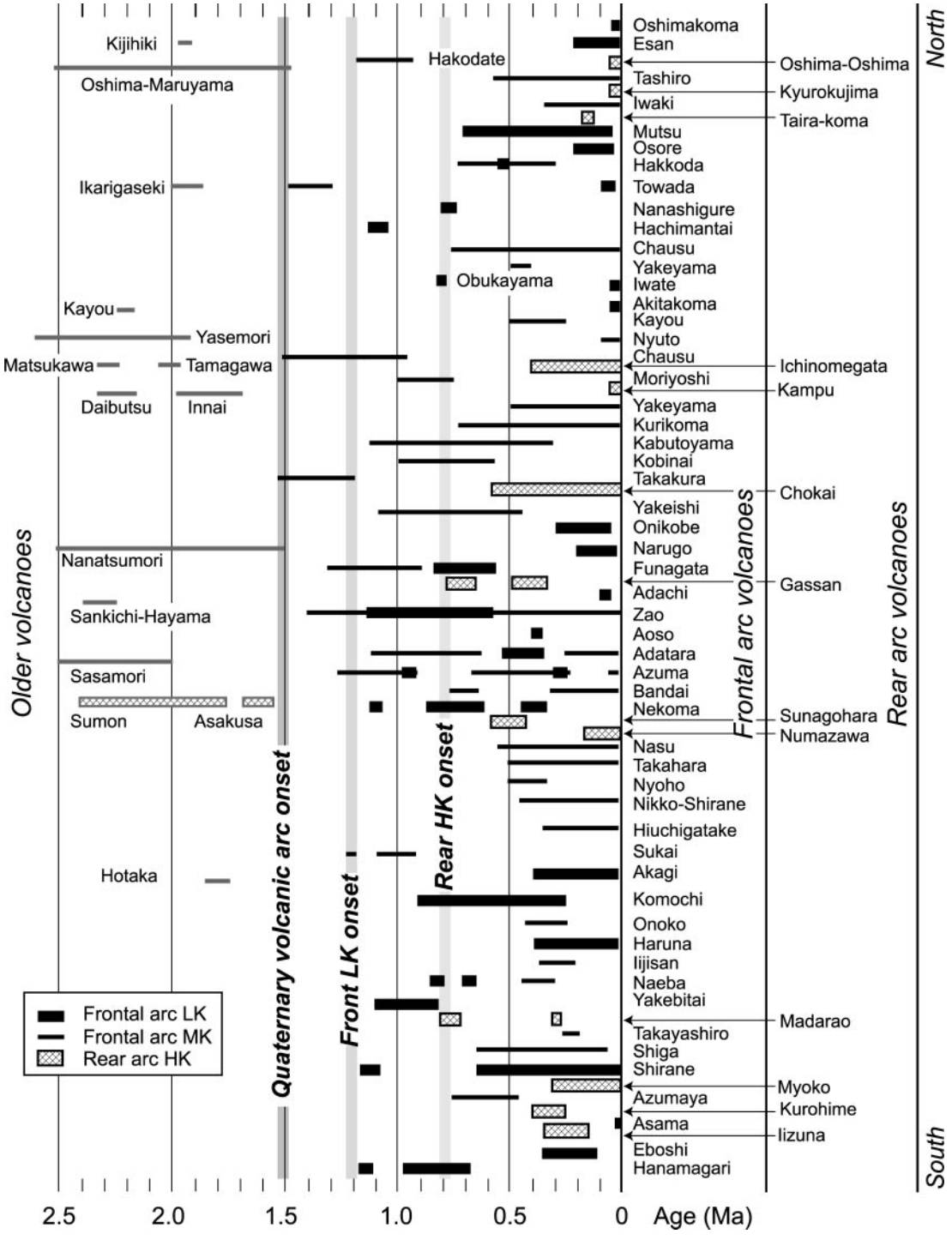

Fig. 2. Temporal variations of volcanic activity and classification of lava suites. Data from Committee for Catalog of Quaternary Volcanoes in Japan (1999) compiled by the authors. LK, low-K; MK, medium-K; HK, high-K.

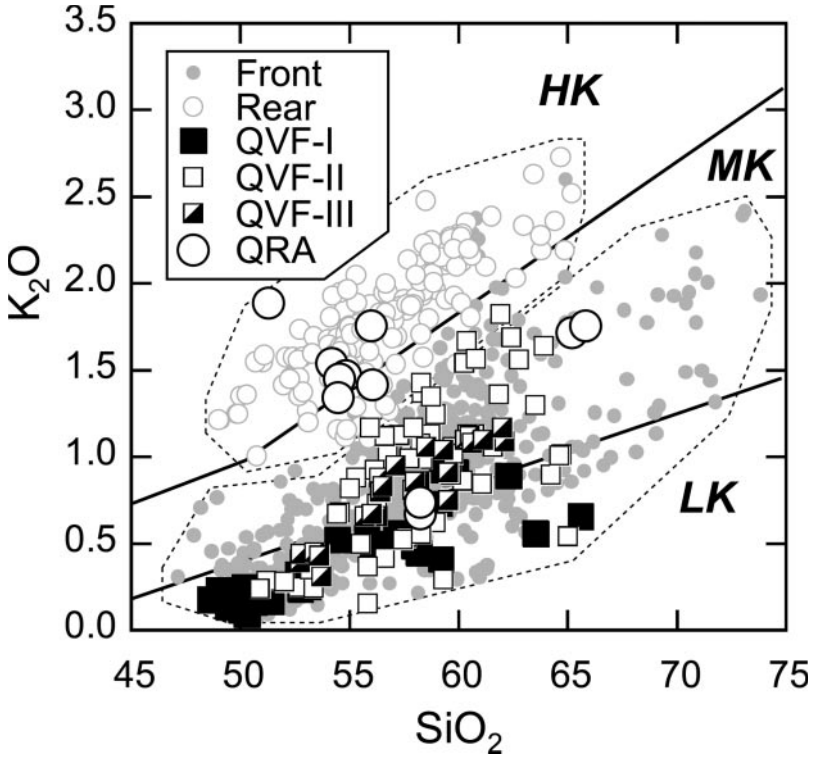

Fig. 3. SiO_2–K_2O variation (wt %) for lavas from the NE Japan arc. Grey shaded data are from the GEOROC database. Bold symbols are lava samples analysed in this study. Boundaries between LK, MK and HK magma series are from Peccerillo & Taylor (1976). Front, frontal-arc lavas; Rear, rear-arc lavas. QVF-I, -II, -III, QRA, classification of lavas based on Nd–Sr isotope systematics (see details in Fig. 5).

SAMPLES AND ANALYTICAL METHODS

Samples

Our samples comprise basalt and intermediate lava pairs from 30 volcanoes. Several researchers have proposed that some intermediate lavas in NE Japan were produced by lower crustal melting (Takahashi, 1986*a*; Fujinawa, 1991; Kobayashi & Nakamura, 2001; Kimura *et al.*, 2002). Therefore, studying intermediate lavas together with the basalts is important for evaluation of the role of crustal filtering. Sample selection was designed to encompass all of the low-K volcanic centers along the volcanic front. Basalt to dacite samples examined range from low-K, through medium-K, to high-K. Two low-K andesite and two medium-K dacite samples are from Numazawa volcano, which has some unusual features for a rear-arc volcano (Fig. 3). Other samples selected from rear-arc high-K volcanoes include those from Kyurokujima, Chokai, Gassan, and Numazawa. We did not analyze frontal-arc medium-K samples because low-K lavas are characteristic of the frontal arc, and the trace element and isotope compositions of medium-K samples covering almost the entire frontal-arc region are available from other studies (Togashi *et al.*, 1992; Kersting *et al.*, 1996; Gust *et al.*, 1997; Shibata & Nakamura, 1997). Analyses made as part of this study include 57 samples for trace elements, 54 for Sr isotopes, 43 for Nd isotopes and 29 for Pb isotopes. Interpretations in this study are based on about 1100 major element analyses from the GEOROC database (http://georoc.mpch-mainz.gwdg.de/georoc/) in addition to our new data. Data coverage for the samples discussed here is shown in Fig. 3.

Analytical methods

Samples were crushed manually in an iron pestle, rinsed with distilled water in an ultrasonic bath, and dried for 2 h at 110°C. Dried chips were then ground in an agate mortar for 30 min. The powder produced was ignited at 1100°C for 3 h. Glass disks with a 2:1 flux:sample ratio were prepared following the method of Kimura & Yamada (1996). The resulting glass disks were analyzed for major and 14 trace elements at Shimane University using a Rigaku RIX 2000 wavelength-dispersive X-ray fluorescence (XRF) spectrometer. Analytical precisions for major and trace elements are better than 1·5% and 8%, respectively.

Additional trace and ultra-trace element analyses were carried out on selected samples using solution inductively coupled plasma mass spectrometry (ICP-MS), following

the methods described by Kimura *et al.* (1995, 2001*a*). Acid reagents used were EL-grade nitric (Kanto Chemicals) and hydrofluoric acid (Tama Chemicals), and analytical grade perchloric acid (Wako Chemicals). Experimental water was distilled and subsequently ion exchanged with a Milli Q filter (Millipore). Procedural blanks were all <1 ppt. The ICP-MS system used was a Thermo ELEMENTAL VG PQ3 at Shimane University, equipped with a normal concentric nebulizer and a water-chilled impact bead-type nebulizer. Instrument settings were fundamentally those of Kimura *et al.* (1995).

The analytical procedure for Sr and Nd isotope analyses follows Iizumi *et al.* (1994, 1995). Acid reagents were Supra grade hydrofluoric and nitric acids (Merck), and precise measurement grade hydrochloric acid (Wako Chemicals). Distilled-ion exchanged water and hydrochloric acid were simmered before use, and procedural blanks were <1 ppt for both Nd and Sr. Samples were analyzed by thermal ionization mass spectrometry (TIMS), using the Ta–Re double filament method, for both Nd and Sr isotopes, using a Finnigan MAT 262 system equipped with five collectors in static mode. The NIST SRM987 Sr standard and La Jolla Nd standard were analyzed before and after each 12 unknowns (Table 1). Standard values during the analyses were $^{87}Sr/^{86}Sr = 0{\cdot}710245 \pm 0{\cdot}000010$ ($n = 3$) and $^{143}Nd/^{144}Nd = 0{\cdot}511847 \pm 0{\cdot}000010$ ($n = 3$) for Nd (errors in 2 SD), respectively. Typical internal 2 SE for sample analyses are ±0·000010 for Sr and ±0·000015 for Nd.

Lead isotopes were analyzed following the conventional TIMS method (Kimura *et al.*, 2003*a*). Lead separation was made using DOWEX 1X8 anion exchange resin and the single column-single bead method (Manton, 1988). Acids used were Tama Chemicals TAMA PURE AA10 grade for HCl, HBr, and HF. Phosphoric acid was TAMA PURE AA100 grade. Procedural blanks for Pb were typically <100 pg. Single Ta filaments were used for analysis. Mass fractionation factors were determined by using NIST SRM981 and normalizing to the $^{207}Pb/^{206}Pb$ ratios reported by Todt *et al.* (1996). Mass fractionation correction factor during the analyses was 0·95 per mil per unit mass. Typical reproducibility of the analyses was within 1 per mil for each isotopic ratio. Analytical results are reported in Table 1.

CHEMICAL VARIATIONS IN THE QUATERNARY LAVAS

Most of the lavas from the frontal arc are olivine basalt through olivine–pyroxene basaltic andesites to pyroxene andesites. Hydrous silicate minerals such as hornblende are occasionally found in dacites. Rear-arc mafic lavas are similar to frontal-arc equivalents. Felsic lavas and ignimbrites commonly contain hornblende and occasionally biotite (Sakuyama, 1983). Plagioclase is ubiquitous in most of the rocks.

Major elements

The most notable chemical feature of the NE Japan arc is the spatial variation of K_2O across strike (see Fig. 3). Based on the total alkalis–silica (TAS) classification (LeMaitre *et al.*, 1989), all samples except for a few alkalic rear-arc lavas fall in the field of basalt–andesite–dacite. Like K_2O, total alkali contents also differ systematically between frontal- and rear-arc lavas (Fig. 4). Iron enrichment features shown by the FeO*/MgO vs silica plot indicate that tholeiitic and calc-alkalic suites exist in both frontal- and rear-arc lavas (Tatsumi & Eggins, 1995); most of the data cluster around the discrimination boundary between high–medium Fe and medium–low Fe (Arculus, 2003). However, low-K lavas are typically tholeiitic, whereas medium-K lavas are calc-alkalic. This feature is common in frontal-arc lavas. Rear-arc high-K lavas are mostly calc-alkalic, as noted above. This across-arc variation is a general characteristic of volcanic rocks in subduction zones (Wilson, 1989). However, coexistence of low-K and medium-K lavas in the frontal arc or even within a single volcano is a notable feature of the NE Japan Quaternary volcanic arc. The occurrence of low- and medium-K lavas in individual volcanoes is not systematic. Low-K lavas tend to occur only in the earliest stages at Azuma and in the Nekoma–Bandai volcano complex, whereas they occur only in the middle stage at Adatara (see Fig. 2). The contents of MgO, TiO_2, Al_2O_3 and P_2O_5 show no systematic differences between frontal- and rear-arc lavas groups at a given SiO_2 content. In contrast, Fe_2O_3 and CaO contents in the rear-arc lavas are systematically lower than those in the frontal-arc lavas (Fig. 4). Such differences in major element compositions have been recognized previously (Sakuyama & Nesbitt, 1983; Nakagawa *et al.*, 1988; Kaneko, 1995; Tatsumi & Eggins, 1995).

Radiogenic isotopes

Trace element and Sr–Nd–Pb isotope data are available from previous studies (Notsu, 1983; Togashi *et al.*, 1992; Kersting *et al.*, 1996; Gust *et al.*, 1997; Shibata & Nakamura, 1997; Kobayashi & Nakamura, 2001; Kimura *et al.*, 2002) and this study. The compositional range of the samples studied for their isotopic composition is from basalt to dacite (SiO_2 48–67 wt %). Only the basaltic lavas are likely to reflect the composition of their mantle source (Shibata & Nakamura, 1997). However, in many cases in the NE Japan arc, the isotopic compositions of lavas of the same K suite from an individual volcano do not differ greatly over

Table 1: Major and trace element and Sr–Nd–Pb isotopic compositions of selected NE Japan lavas

Sample:	Oshimakoma	Esan	Mutsu	Osore	Osore	N-Hakkoda	N-Hakkoda	S-Hakkoda	S-Hakkoda	Towada	Towada	Kyurokujima
Stage:	OKM	ESN	MHU	OSOa	OSOd2	KHD1	KHD2	MHD1	MHD2	TWD1	TWD2	KRJ
Suite:	LK	LK	LK	LK	LK	LK	LK	LK	LK	LK	LK	HK
Type:	QVF-I	QVF-I	QVF-I	QVF-I	QVF-I	QVF-I	QVF-I	QVF-I	QVF-I	QVF-I	QVF-I	QRA
Isotope TIMS												
$^{87}Sr/^{86}Sr$	0·70390	0·70439	0·70373	0·70381	0·70412	0·70394	0·70385	0·70388	0·70398	0·70419	0·70422	
$^{143}Nd/^{144}Nd$	0·51288	0·51286	0·51297	0·51294	0·51288		0·51290	0·51291	0·51294	0·51280	0·51281	
$^{206}Pb/^{204}Pb$	18·469	18·505	18·526	18·491			18·493	18·499		18·515		18·348
$^{207}Pb/^{204}Pb$	15·555	15·583	15·579	15·586			15·577	15·591		15·632		15·617
$^{208}Pb/^{204}Pb$	38·444	38·552	38·540	38·552			38·524	38·567		38·702		38·447
Major XRF (wt %)												
SiO_2	59·65	62·10	—	53·12	65·58	49·51	52·76	49·43	59·19	64·93	68·53	51·29
TiO_2	0·71	0·46	—	0·79	0·58	0·85	0·95	0·95	1·00	—	—	0·90
Al_2O_3	17·51	16·58	—	19·19	16·30	16·81	17·83	17·84	16·20	—	—	17·75
Fe_2O_3*	7·58	7·00	—	9·83	6·37	12·33	10·89	11·63	9·74	—	—	8·60
MnO	0·21	0·16	—	0·18	0·12	0·19	0·18	0·23	0·20	—	—	0·18
MgO	2·87	2·62	—	4·48	1·38	8·38	5·31	4·37	2·59	—	—	4·73
CaO	6·71	6·35	—	9·80	5·06	9·69	9·60	9·88	6·69	—	—	9·35
Na_2O	3·45	3·45	—	2·27	3·13	2·02	2·66	2·18	3·48	—	—	3·18
K_2O	0·93	1·08	—	0·25	0·66	0·16	0·24	0·14	0·41	—	—	1·89
P_2O_5	0·13	0·04	—	0·14	0·12	0·07	0·10	0·06	0·12	—	—	0·25
Total	99·75	99·84	—	100·05	99·30	100·01	100·52	96·71	99·62	—	—	98·12
Trace ICP-MS (ppm)												
Li	8·96	14·5	10·2	5·29	9·57	3·79	5·53	2·64	8·36	8·18	9·85	7·29
Be	0·59	0·43	0·39	0·32	0·59	0·22	0·36	0·34	0·51	0·77	0·89	1·21
Rb	18·5	23·2	11·6	2·94	15·0	2·91	3·08	1·65	6·27	18·3	21·6	55·3
Sr	428	247	233	293	236	324	344	270	303	295	292	
Y	24·9	16·8	20·0	16·1	31·0	13·2	16·4	18·0	29·4	30·5	33·8	25·4
Zr	72·0	60·1	62·4	30·5	86·0	29·2	37·7	38·9	61·7	106	114	122
Nb	1·96	2·25	2·20	0·78	2·81	0·87	1·19	0·88	1·81	4·07	4·36	4·67
Sb	0·21	2·72	0·51	0·28	0·80	0·35	0·25	0·25	0·42	0·52	0·59	
Cs	1·28	4·05	1·28	0·21	0·67	0·34	0·31	1·05	0·30	1·05	0·73	2·79
Ba	245	443	213	101	416	82	105	537	386	318	345	630
La	8·02	6·61	6·17	2·91	8·77	2·45	3·28	2·70	5·36	10·6	11·5	19·2
Ce	20·2	13·8	13·7	7·25	19·3	6·47	8·40	7·67	13·3	25·9	27·2	41·6
Pr	2·78	1·76	1·79	1·10	2·61	1·00	1·34	1·24	2·06	3·42	3·60	5·42
Nd	13·0	7·57	8·04	5·57	12·0	5·19	6·65	6·59	10·5	15·5	16·4	22·4
Sm	3·51	2·02	2·28	1·80	3·38	1·66	2·13	2·28	3·35	4·23	4·52	5·22
Eu	1·21	0·63	0·77	0·72	1·09	0·66	0·82	0·86	1·22	1·25	1·33	1·65
Gd	3·98	2·38	2·78	2·31	4·29	2·09	2·56	2·71	4·13	4·81	5·13	5·16
Tb	0·68	0·42	0·51	0·43	0·77	0·37	0·48	0·52	0·77	0·84	0·91	0·80
Dy	4·50	2·85	3·54	2·91	5·23	2·48	3·11	3·38	5·14	5·48	5·90	4·79
Ho	0·96	0·61	0·74	0·63	1·13	0·52	0·66	0·74	1·11	1·16	1·27	1·01
Er	2·67	1·78	2·13	1·77	3·28	1·45	1·81	1·99	3·12	3·23	3·48	2·86
Tm	0·42	0·30	0·34	0·28	0·53	0·22	0·29	0·31	0·49	0·52	0·55	0·42
Yb	2·87	2·11	2·33	1·90	3·51	1·47	1·88	2·09	3·21	3·46	3·66	2·74
Lu	0·45	0·34	0·38	0·29	0·54	0·22	0·29	0·32	0·50	0·52	0·58	0·43
Hf	2·24	2·05	1·82	0·97	2·73	0·95	1·25	1·14	1·94	3·17	3·31	2·90
Ta	0·14	0·16	0·16	0·05	0·20	0·06	0·08	0·06	0·11	0·29	0·30	0·31
W	0·45	2·05	0·59	0·28	0·45	0·24	0·23	0·26	0·41	0·89	0·97	
Tl	0·12	0·16	0·01	0·01	0·08	0·02	0·03	0·02	0·03	0·14	0·12	
Pb	9·95	16·2	11·0	4·78	9·64	13·6	4·57	4·09	10·4	14·5	13·8	17·9
Th	2·02	1·99	1·34	0·35	2·31	0·33	0·40	0·34	0·77	2·87	2·87	4·07
U	0·67	0·56	0·41	0·11	0·60	0·10	0·12	0·11	0·23	0·70	0·75	1·27

Sample:	Nanashigure	Nanashigure	Hachiman	Hachiman	Iwate	Iwate	Akitakoma	Akitakoma	Ichimonegata	Kampu	Onikobe	Narugo
Stage:	NSG1	NSG2	HCMB	HCMA	IWTB	IWTA	AKMB	AKMA	ICM	KMP	OKB	NRG
Suite:	LK	LK	LK	LK	LK	LK	LK	LK	HK	HK	LK	LK
Type:	QVF-I	QVF-I	QVF-I	QVF-I	QVF-I	QVF-I	QVF-I	QVF-I	QRA	QRA	QVF-I	QVF-I
Isotope TIMS												
$^{87}Sr/^{86}Sr$	0·70492	0·70497	0·70427	0·70422	0·70423	0·70428	0·70409	0·70388			0·70427	0·70410
$^{143}Nd/^{144}Nd$	0·51266	0·51255		0·51284	0·51285	0·51285	0·51287	0·51291			0·51284	0·51287
$^{206}Pb/^{204}Pb$	18·663		18·477		18·539			18·499	18·408		18·502	18·440
$^{207}Pb/^{204}Pb$	15·630		15·584		15·592			15·591	15·560		15·584	15·560
$^{208}Pb/^{204}Pb$	38·790		38·518		38·587			38·567	38·428		38·533	38·400
Major XRF (wt %)												
SiO_2	52·91	58·15	52·85	55·79	50·19	59·11	50·19	54·45	50·72	—	70·75	56·09
TiO_2	0·72	0·65	0·65	0·78	0·80	1·04	0·65	1·11	1·04	—	0·32	0·88
Al_2O_3	20·65	18·81	19·34	15·33	19·33	15·94	17·43	16·36	17·02	—	15·73	17·22
Fe_2O_3*	9·52	8·48	9·85	11·71	10·44	10·15	10·57	11·18	8·65	—	2·60	9·67
MnO	0·19	0·16	0·15	0·14	0·19	0·17	0·10	0·12	0·18	—	0·08	0·19
MgO	3·98	3·15	4·54	3·92	6·17	2·72	6·64	4·44	7·84	—	0·63	4·05
CaO	8·87	7·36	8·74	8·40	10·57	6·69	11·20	9·29	9·56	—	3·62	7·58
Na_2O	0·59	2·20	2·40	2·48	2·14	3·49	1·76	2·32	2·66	—	3·98	3·07
K_2O	0·32	0·45	0·32	0·53	0·19	0·73	0·25	0·52	1·30	—	1·51	0·49
P_2O_5	0·17	0·13	0·10	0·10	0·07	0·12	0·05	0·08	0·19	—	0·04	0·10
Total	97·92	99·54	98·94	99·18	100·09	100·16	98·84	99·87	99·16	—	99·26	99·34
Trace ICP-MS (ppm)												
Li	12·1	9·78	5·72	5·21	3·99	8·91	4·18	5·33	7·77	9·02	15·5	11·4
Be	0·59	0·61	0·44	0·48	0·27	0·63	0·25	0·58	0·74	0·94	0·78	0·50
Rb	6·04	20·3	4·55	8·32	0·73	17·51	3·87	11·2	33·3	36·8	36·3	10·4
Sr	356	325	312	284	319	290	334	294			206	300
Y	12·7	14·1	16·2	22·0	11·6	24·0	11·5	20·4	21·7	18·6	29·7	18·3
Zr	48·2	44·0	43·8	66·84	23·5	83·8	28·9	62·8	72·4	84·8	105	35·5
Nb	2·83	2·89	2·28	2·68	1·13	3·38	1·20	2·91	2·78	2·69	3·99	1·76
Sb	0·31	0·55	0·47	0·24	0·15	0·58	0·32	0·24			0·32	0·11
Cs	0·25	1·69	0·32	0·25	0·04	1·15	0·15	0·31	1·75	2·23	1·42	0·32
Ba	361	224	116	187	59	208	194	164	884		420	377
La	7·73	7·20	4·54	6·43	2·23	6·81	2·95	6·77	18·7	24·7	11·4	4·57
Ce	16·6	15·4	11·4	14·7	5·68	16·8	7·20	15·6	36·8	45·4	26·1	10·8
Pr	1·99	1·97	1·57	2·11	0·87	2·31	1·04	2·11	4·53	5·35	3·32	1·50
Nd	8·32	8·39	7·36	9·68	4·40	11·1	5·00	9·65	18·2	20·0	14·1	7·11
Sm	2·03	2·11	2·14	2·78	1·36	3·16	1·46	2·71	4·12	4·33	3·63	2·11
Eu	0·74	0·72	0·80	0·90	0·63	1·08	0·59	0·85	1·28	1·35	1·05	0·93
Gd	2·20	2·34	2·52	3·28	1·74	3·72	1·85	3·15	4·17	4·32	4·15	2·66
Tb	0·37	0·40	0·46	0·59	0·32	0·68	0·32	0·55	0·63	0·64	0·74	0·49
Dy	2·40	2·55	3·01	3·95	2·17	4·38	2·09	3·69	3·82	3·63	5·00	3·27
Ho	0·49	0·54	0·63	0·83	0·46	0·91	0·44	0·76	0·80	0·80	1·06	0·70
Er	1·38	1·49	1·73	2·28	1·25	2·54	1·20	2·12	2·25	2·26	3·09	2·00
Tm	0·22	0·24	0·28	0·36	0·20	0·41	0·18	0·34	0·34	0·35	0·50	0·32
Yb	1·49	1·58	1·83	2·39	1·34	2·64	1·23	2·24	2·18	2·22	3·55	2·20
Lu	0·24	0·25	0·28	0·37	0·20	0·41	0·19	0·34	0·34	0·34	0·54	0·34
Hf	1·47	1·34	1·33	1·90	0·76	2·46	0·89	1·81	1·94	2·28	3·37	1·39
Ta	0·21	0·22	0·14	0·17	0·06	0·22	0·09	0·18	0·20	0·32	0·30	0·13
W	0·38	0·45	0·62	0·40	0·13	0·48	0·59	0·55			0·60	0·18
Tl	0·04	0·04	0·03	0·03	0·01	0·11	0·03	0·06			0·26	0·04
Pb	15·4	7·70	8·11	10·4	5·62	11·9	9·94	7·74	5·51	6·67	18·2	6·98
Th	2·25	2·05	0·73	1·13	0·12	1·60	0·37	1·28	5·53	6·88	3·42	0·91
U	0·44	0·43	0·18	0·32	0·03	0·44	0·12	0·33	1·48	1·81	0·96	0·18

Table 1: continued

Sample:	Chokai	Funagata	Funagata	Gassan	Nanatsumori	Kurohana	Kurohana	Adachi	Adachi	Zao	Zao	Aoso
Stage:	CHO	FNG1	FNG2	GAS	NTN	KRH1	KRH2	ADCW	ADCG	ZAOB	ZAOA	AOSB
Suite:	HK	LK	LK	HK	LK	LK	LK	LK	LK	LK	LK	LK
Type:	QRA	QVF-I	QVF-I	QVF-I	QVF-I	QVF-I	QVF-I	QVF-I	QVF-I	QVF-I	QVF-I	QVF-I
Isotope TIMS												
$^{87}Sr/^{86}Sr$		0·70413	0·70412	0·70352	0·70464	0·70409	0·70416	0·70442	0·70437	0·70393	0·70381	0·70430
$^{143}Nd/^{144}Nd$		0·51292	0·51278		0·51287	0·51292		0·51283		0·51289	0·51293	0·51282
$^{206}Pb/^{204}Pb$				18·361	18·557			18·475		18·408		18·454
$^{207}Pb/^{204}Pb$				15·543	15·584			15·597		15·563		15·573
$^{208}Pb/^{204}Pb$				38·315	38·572			38·552		38·415		38·480
Major XRF (wt %)												
SiO_2	—	50·62	50·79	54·20	57·15	49·59	50·92	63·51	72·83	48·60	59·22	50·04
TiO_2	—	0·72	0·85	1·09	0·76	0·61	0·68	0·27	0·16	0·95	1·05	1·00
Al_2O_3	—	16·39	17·89	18·49	17·15	16·81	18·69	19·19	13·84	17·81	15·21	20·30
Fe_2O_3*	—	11·46	10·77	9·67	9·14	10·74	9·95	3·11	1·18	11·58	9·50	10·87
MnO	—	0·18	0·17	0·18	0·14	0·18	0·16	0·16	0·10	0·17	0·17	0·17
MgO	—	7·71	6·69	3·98	3·78	8·55	5·18	0·89	0·31	7·36	2·43	4·71
CaO	—	10·14	10·46	6·34	7·71	10·91	11·82	3·72	1·75	11·02	6·21	7·99
Na_2O	—	2·04	2·19	3·11	2·45	1·54	1·97	3·42	4·18	1·91	3·72	2·33
K_2O	—	0·16	0·20	1·54	0·56	0·14	0·20	0·56	1·18	0·18	0·93	0·12
P_2O_5	—	0·08	0·09	0·19	0·09	0·03	0·05	0·10	0·07	0·14	0·30	0·12
Total	—	99·50	100·10	98·79	98·93	99·10	99·62	94·93	95·60	99·72	98·74	97·65
Trace ICP-MS (ppm)												
Li	5·63	3·32	3·79	9·90	9·47	3·17	4·47	21·3	23·9	3·43	5·60	5·18
Be	0·86	0·25	0·31	0·96	0·45	0·18	0·23	0·95	0·93	0·28	0·79	0·49
Rb	16·0	1·56	2·07	35·7	8·41	1·15	1·89	8·80	18·8	1·59	15·9	1·81
Sr		218	297		239	175	204	336	180	305	366	405
Y	30·2	15·0	13·6	23·3	31·6	12·8	15·2	20·4	22·8	13·6	31·8	23·6
Zr	108	29·0	32·9	112	52·3	21·4	29·0	59·0	68·5	33·8	104	44·9
Nb	3·34	1·03	1·37	3·34	2·25	0·55	0·88	3·49	3·80	1·20	3·54	1·83
Sb	0·11	0·16	0·11		0·23	0·10	0·09	0·66	1·29	0·11	0·25	0·36
Cs	0·73	0·06	0·14	0·60	0·26	0·05	0·04	1·73	2·88	0·08	0·59	0·97
Ba	229	71	232	538	274	52	72	533	631	110	338	112
La	14·7	2·68	3·29	16·0	11·9	1·73	2·86	9·14	11·7	3·39	9·23	4·76
Ce	30·4	6·26	7·87	31·6	15·3	4·19	6·57	21·7	27·8	8·10	20·7	9·71
Pr	4·11	0·96	1·19	4·31	2·74	0·70	1·00	3·04	3·63	1·23	3·42	1·74
Nd	18·1	4·84	5·89	17·8	12·3	3·62	4·88	13·4	15·6	5·87	15·6	8·85
Sm	4·54	1·52	1·79	4·34	2·93	1·26	1·53	3·23	3·78	1·79	4·47	2·55
Eu	1·41	0·65	0·72	1·33	1·05	0·51	0·61	0·92	0·73	0·71	1·57	0·90
Gd	4·96	2·04	2·19	4·04	3·96	1·71	2·01	4·00	3·82	2·14	5·09	3·27
Tb	0·81	0·38	0·39	0·72	0·68	0·33	0·39	0·56	0·62	0·39	0·88	0·55
Dy	5·07	2·56	2·55	4·19	4·43	2·26	2·67	3·49	3·88	2·49	5·76	3·52
Ho	1·07	0·56	0·52	0·94	0·98	0·51	0·58	0·72	0·78	0·53	1·20	0·77
Er	3·21	1·55	1·43	2·64	2·77	1·36	1·57	2·02	2·13	1·47	3·27	2·13
Tm	0·46	0·24	0·22	0·41	0·43	0·22	0·25	0·33	0·35	0·23	0·51	0·33
Yb	3·15	1·64	1·45	2·59	2·85	1·43	1·65	2·30	2·47	1·48	3·40	2·19
Lu	0·47	0·25	0·22	0·43	0·45	0·22	0·26	0·38	0·41	0·22	0·52	0·35
Hf	2·77	0·91	1·01	3·07	1·62	0·73	0·96	2·29	2·66	1·08	2·85	1·28
Ta	0·27	0·06	0·07	0·24	0·16	0·03	0·06	0·23	0·29	0·07	0·20	0·10
W	0·02	0·17	0·13		0·45	0·20	2·06	0·56	0·70	0·11	0·32	0·14
Tl		0·02	0·04		0·03	0·01	0·01	0·13		0·01	0·07	0·04
Pb	4·64	3·66	4·31	5·14	6·06	3·37	4·86	18·1	12·39	3·74	7·79	2·99
Th	2·28	0·30	0·34	5·76	1·61	0·23	0·50	1·21	1·44	0·50	1·83	0·31
U	0·75	0·07	0·08	1·59	0·33	0·05	0·09	0·29	0·37	0·11	0·50	0·10

Sample:	Aoso	W-Azuma	W-Azuma	E-Azuma	E-Azuma	Adatara	Adatara	Adatara	Adatara	Adatara	Adatara	Adatara
Stage:	AOSA	NAZ6	NAZ13	HAZ7	HAZ8	ADTA	ADTB	AT8	Hg	AT5	Mt	Se
Suite:	LK	MK	MK	LK	MK	LK	LK	LK	LK	MK	MK	MK
Type:	QVF-I	QVF-II	QVF-II	QVF-II	QVF-II	QVF-II	QVF-II	QVF-II	QVF-II	QVF-II	QVF-II	QVF-II
Isotope TIMS												
$^{87}Sr/^{86}Sr$	0·70438		0·70472	0·70573	0·70546	0·70542	0·70566	0·70564	0·70560	0·70501	0·70485	0·70491
$^{143}Nd/^{144}Nd$			0·51276				0·51265		0·51269	0·51275	0·51277	0·51277
$^{206}Pb/^{204}Pb$							18·487		18·518	18·463		
$^{207}Pb/^{204}Pb$							15·600		15·590	15·570		
$^{208}Pb/^{204}Pb$							38·577		38·587	38·487		
Major XRF (wt %)												
SiO_2	56·45	61·93	58·29	52·60	57·77	56·60	51·99	53·37	51·20	57·27	56·61	56·13
TiO_2	0·81	0·74	0·81	0·66	0·79	0·99	1·02	0·91	0·88	0·82	0·91	0·93
Al_2O_3	18·14	15·51	16·60	18·30	16·32	18·60	20·37	21·34	19·10	16·15	16·83	17·84
Fe_2O_3*	8·82	7·86	9·12	10·26	9·30	9·52	9·60	9·25	11·41	9·35	10·03	9·99
MnO	0·14	0·13	0·14	0·16	0·15	0·15	0·15	0·14	0·19	0·16	0·16	0·16
MgO	3·51	3·19	3·63	6·06	3·99	3·47	3·77	3·02	5·82	3·78	3·80	3·73
CaO	8·04	5·78	7·27	10·59	8·00	7·72	9·79	10·34	9·48	7·54	7·89	7·30
Na_2O	2·88	2·78	2·77	1·70	2·75	2·75	2·39	2·34	2·14	2·54	2·61	2·38
K_2O	0·50	1·83	1·37	0·25	1·05	0·42	0·28	0·24	0·28	1·12	1·12	0·93
P_2O_5	0·12	0·11	0·12	0·07	0·11	0·20	0·21	0·11	0·09	0·12	0·11	0·09
Total	99·41	99·85	100·11	100·69	99·94	100·42	99·57	101·06	100·60	98·85	100·08	99·48
Trace ICP-MS (ppm)												
Li	5·54	25·1	58·0	28·3	24·9	8·15	5·76	31·1	68·0	28·1	36·4	5·20
Be	0·53	0·62	0·60	0·28	0·49	0·63	0·43	0·47	0·41	0·44	0·62	0·53
Rb	5·84	49·4	36·6	3·71	23·9	9·62	4·62	2·66	5·15	29·6	30·4	27·2
Sr	321	270	304	207	170	277	326	371	357	237	253	251
Y	18·9	34·3	24·9	11·6	19·0	24·1	18·8	18·3	16·8	23·6	31·1	21·8
Zr	65·6	154	122	30·7	78·6	65·6	52·8	53·7	54·2	99·8	104	109
Nb	2·48	5·04	1·75	2·00	4·11	4·59	4·07	3·64	3·40	4·23	4·27	4·42
Sb	0·13	0·32	0·30	0·21	0·28	0·25	0·21	0·19	0·18	0·38	0·32	0·30
Cs	0·49	1·54	1·00	0·18	0·48	0·37	0·24	0·29	0·24	0·75	1·60	1·48
Ba	229	486	313	86	172	275	102	115	113	278	272	288
La	10·2	18·4	12·2	3·64	7·97	7·03	4·62	5·00	5·43	8·93	11·6	8·51
Ce	14·7	29·3	27·1	8·07	18·0	16·0	12·1	12·2	12·8	21·8	28·0	20·3
Pr	2·87	5·03	3·54	1·12	2·32	2·35	1·80	1·86	1·73	2·83	3·64	2·56
Nd	12·6	21·0	14·9	4·98	9·98	11·3	8·81	8·64	7·90	12·1	16·2	11·2
Sm	3·06	4·71	3·68	1·40	2·58	3·06	2·46	2·46	2·20	3·05	4·06	2·79
Eu	0·98	1·25	1·06	0·57	0·78	1·06	0·93	0·95	0·81	0·95	1·21	0·94
Gd	3·43	5·40	4·07	1·74	3·05	3·60	2·95	2·87	2·59	3·58	4·92	3·21
Tb	0·57	0·89	0·70	0·32	0·54	0·67	0·53	0·52	0·46	0·66	0·84	0·58
Dy	3·67	5·67	4·48	1·98	3·31	4·33	3·48	3·41	3·04	4·17	5·38	3·77
Ho	0·74	1·21	0·94	0·44	0·72	0·92	0·74	0·75	0·64	0·87	1·15	0·79
Er	2·04	3·22	2·55	1·20	1·97	2·50	1·96	1·95	1·71	2·44	3·13	2·23
Tm	0·33	0·53	0·41	0·19	0·33	0·39	0·31	0·30	0·27	0·39	0·49	0·37
Yb	2·13	3·40	2·68	1·29	2·12	2·54	2·03	1·91	1·77	2·55	3·17	2·46
Lu	0·33	0·54	0·41	0·20	0·31	0·39	0·31	0·30	0·27	0·39	0·48	0·39
Hf	1·93	4·29	3·40	0·94	2·47	1·84	1·45	1·50	1·46	2·84	3·02	2·94
Ta	0·15	0·39	0·38	0·14	0·34	0·24	0·20	0·21	0·17	0·31	0·34	0·33
W	0·30	0·64				0·28	0·29					
Tl	0·04	0·21	0·15	0·01	0·10	0·05	0·02	0·02	0·02	0·12	0·30	0·17
Pb	12·6	7·80	5·72	1·71	5·41	19·8	5·34	2·90	2·42	4·63	5·46	6·39
Th	1·12	5·33	3·83	0·58	2·53	0·83	0·39	0·38	0·61	3·03	3·26	3·57
U	0·26	1·29	0·91	0·12	0·58	0·20	0·09	0·09	0·12	0·78	0·80	0·86

Table 1: continued

Sample:	Nekoma	Nekoma	Nekoma	Bandai	Sunagohara	Numazawa	Numazawa	Numazawa	Numazawa	JB-2	JB-2
Stage:	KU1	SR4	GL4	Bd-16	YD-1	NZS-2	NZS-3	NZP-12	MS-3	Shimane	Reference
Suite:	ELK	LK	MK	MK	MK	LK	LK	MK	MK	Standard	Stamdard
Type:	QVF-II	QVF-II	QVF-II	QVF-II	QVF-II	QVF-II	QRA	QRA	QRA		
Isotope TIMS											
$^{87}Sr/^{86}Sr$	0·70491	0·70506	0·70516	0·70468	0·70429	0·70378	0·70380	0·70389	0·70386	0·70367	0·70375
$^{143}Nd/^{144}Nd$	0·51273	0·51271	0·50261	0·51272	0·51277	0·51293	0·51284			0·51307	0·51313
$^{206}Pb/^{204}Pb$	18·439	18·471	18·444	18·495	18·414	18·407				18·341	*18·343*
$^{207}Pb/^{204}Pb$	15·575	15·602	15·580	15·637	15·573	15·564				15·565	*15·562*
$^{208}Pb/^{204}Pb$	38·494	38·605	38·507	38·715	38·499	38·421				38·268	*38·278*
Major XRF (wt %)											
SiO_2	55·82	57·61	58·35	57·73	77·13	58·18	58·29	65·17	65·73	52·54	52·81
TiO_2	1·05	0·92	0·84	0·81	0·11	0·84	0·83	0·592	0·58	1·18	1·18
Al_2O_3	21·79	17·32	16·22	15·75	13·78	17·90	17·66	15·83	15·76	14·53	14·56
Fe_2O_3*	9·47	9·39	9·31	8·63	0·90	8·05	8·06	5·54	5·44	14·21	14·12
MnO	0·19	0·19	0·16	0·16	0·11	0·23	0·23	0·15	0·15	0·21	0·20
MgO	2·90	2·96	3·77	4·45	0·18	3·08	3·03	2·06	1·91	4·69	4·63
CaO	6·23	7·88	7·06	7·64	0·90	7·15	7·22	4·96	4·87	9·76	9·82
Na_2O	2·63	3·22	2·77	2·96	4·68	3·50	3·53	3·54	3·64	2·07	2·17
K_2O	0·16	0·54	0·99	0·99	2·39	0·69	0·73	1·72	1·75	0·42	0·42
P_2O_5	0·23	0·18	0·12	0·15	0·03	0·31	0·29	0·13	0·06	0·09	0·10
Total	100·47	100·20	99·58	99·26	100·20	99·92	99·85	99·69	99·89	99·69	100·00
Trace ICP-MS (ppm)											
Li	3·16	4·86	7·86		51·6	58·1	25·0	37·8	72·0	7·84	7·78
Be	0·92	0·61	0·70	0·76	1·56	0·8	0·68	0·89	0·89	0·24	0·26
Rb	0·14	9·20	25·0	23·8	59·1	9·96	9·84	36·6	38·4	6·24	*6·62*
Sr	296	341	267	445	89	498	259	364	354	173	170
Y	31·8	25·6	22·4	25·0	42·3	26·8	23·6	20·9	21·1	21·8	24·9
Zr	123	84·1	108	118	51·3	80·5	65·8	74·6	70·9	46·6	*47·9*
Nb	4·93	4·01	4·45	4·58	6·45	2·13	2·03	3·14	3·14	0·486	*0·459*
Sb	0·04	0·06	0·15	0·10	0·12	0·06	0·06	0·12	0·09	0·25	0·25
Cs	0·02	0·24	0·70	0·93	1·83	0·60	0·58	1·63	1·66	0·78	0·85
Ba	137	160	244	386	571	217	161	525	541	223	215
La	9·73	7·84	10·5	11·5	15·4	9·69	8·76	12·3	12·0	2·25	*2·28*
Ce	23·7	18·4	21·3	26·7	37·0	25·0	21·8	27·0	26·1	6·44	*6·48*
Pr	3·17	2·64	2·87	3·27	4·61	3·45	3·17	3·19	3·14	1·12	*1·13*
Nd	14·1	12·1	11·7	14·2	19·4	16·1	14·3	12·9	12·6	6·10	*6·34*
Sm	3·90	3·25	2·84	3·64	5·09	4·20	3·70	2·99	2·98	2·18	*2·20*
Eu	1·34	1·21	0·95	1·14	0·99	1·43	1·28	0·97	0·99	0·818	*0·772*
Gd	4·55	4·03	3·45	3·95	5·95	4·55	4·12	3·30	3·20	2·90	*3·17*
Tb	0·73	0·71	0·60	0·68	1·10	0·78	0·70	0·55	0·55	0·567	*0·552*
Dy	4·82	4·40	3·78	4·31	7·24	4·90	4·33	3·54	3·57	3·90	*4·06*
Ho	1·04	0·97	0·82	0·91	1·54	1·02	0·91	0·76	0·73	0·841	*0·87*
Er	2·83	2·66	2·18	2·51	4·41	2·84	2·45	2·10	2·13	2·36	*2·59*
Tm	0·46	0·43	0·37	0·41	0·73	0·44	0·40	0·35	0·36	0·371	*0·370*
Yb	2·93	2·81	2·45	2·65	4·73	2·97	2·54	2·43	2·49	2·48	*2·67*
Lu	0·46	0·45	0·37	0·41	0·74	0·47	0·41	0·40	0·39	0·380	*0·331*
Hf	2·77	2·38	2·85	3·11	2·36	2·34	2·17	2·37	2·31	1·47	1·49
Ta	0·25	0·21	0·28	0·53	0·63	0·13	0·15	0·33	0·33	0·036	*0·041*
W	0·15	0·19	0·40								
Tl	0·01	0·04	0·12	0·12	0·35	0·14	0·09	0·22	0·24	0·033	0·042
Pb	5·93	5·68	7·30	6·27	12·3	6·67	5·86	10·5	10·2	5·39	*5·27*
Th	1·23	0·99	2·64	3·22	3·24	1·21	1·21	4·58	4·76	0·253	*0·291*
U	0·33	0·26	0·65	0·80	1·77	0·42	0·43	1·40	1·48	0·156	0·168

*Total Fe reported as Fe_2O_3.
JB-2 reference values from Geological Survey of Japan with Hochstaedter *et al*. (2001) trace element values and Pb isotope data from Ishizuka *et al*. (2003) in italics.

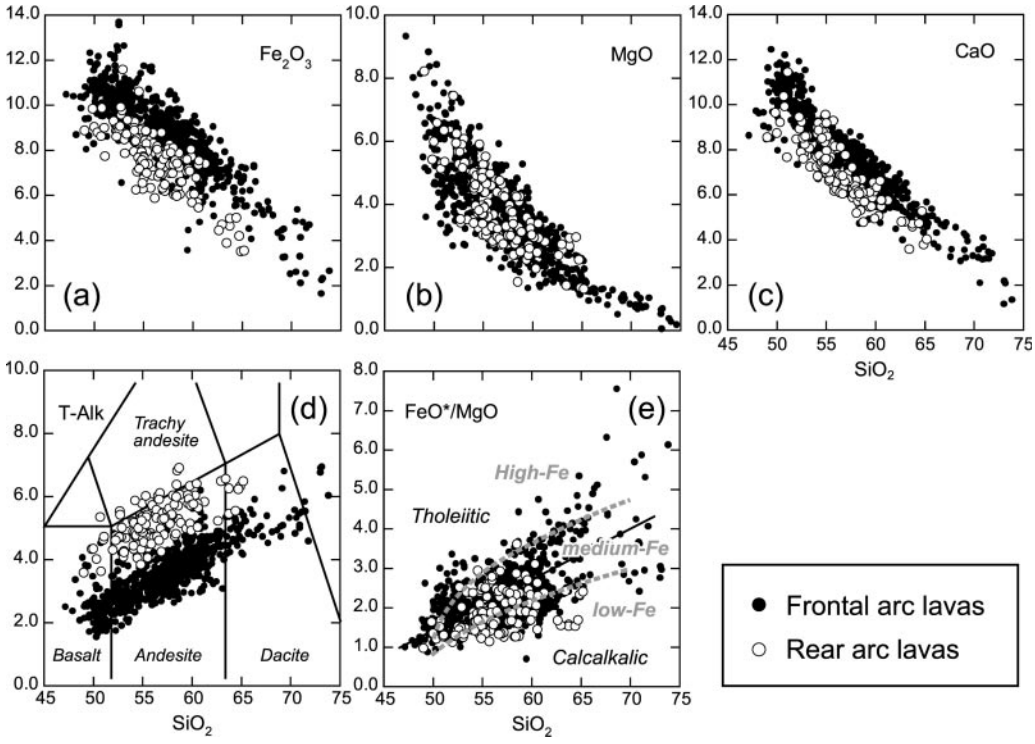

Fig. 4. Major element compositions of lavas from the frontal and rear arcs of the NE Japan arc. Data from GEOROC database. Boundaries in the total alkali–silica diagram are from LeMaitre *et al.* (1989); tholeiite–calc-alkalic boundary in (e) is from Miyashiro (1974), and the high-, medium-, and low-Fe boundaries (grey dashed lines) are from Arculus (2003).

the compositional range (Fujinawa, 1991; Kimura *et al.*, 2001*b*). This is also true for most of the basalt–intermediate lava pairs examined in this study. Nevertheless, there can be complex variations in Nd–Sr–Pb isotope characteristics; for example: (1) Sr isotopic compositions differ between low-K tholeiitic (radiogenic) and medium-K calc-alkalic (less radiogenic) suite lavas at Adatara (Fujinawa, 1991); (2) Sr and Nd isotopic compositions of low-K tholeiitic and medium-K calc-alkalic lavas from the Nekoma–Bandai volcano complex are identical to each other (Kimura *et al.*, 2002); (3), at Akagi volcano, Sr isotope compositions become more radiogenic with increasing silica (Kobayashi & Nakamura, 2001).

Notwithstanding the complexity noted above, in general the NE Japan Quaternary lavas can reasonably be classified into frontal-arc low-K to medium-K and rear-arc high-K groups based on major element compositions, as noted above. Further subdivision is possible based on Sr–Nd isotopic characteristics (Fig. 5). In contrast to the small isotopic variations observed in the rear-arc high-K lavas, which generally appear to have been derived from a more depleted source, the more radiogenic frontal-arc lavas show large variations in Nd–Sr composition that are uncorrelated with K suite affinity. The key feature is that the Nd–Sr isotopic compositions of frontal-arc lavas are similar to those of the neighboring basement granitoids.

Cretaceous to Paleogene granitoids in NE Japan can be divided into three groups based on their Sr–Nd isotope characteristics (Kagami, 2005): the Kitakami (KZ), North (NZ), and South Zones (SZ), in order of increasing Sr isotopic enrichment with Nd isotopic depletion, and from NE to SW (Fig. 5a). The North and South Zones are extensions of the isotopic zones identified in the SW Japan arc (Kagami, 2005). A Transitional Zone (TR) is found between the North and South Zones (Fig. 5a), but is here included in the North Zone for convenience. Such geochemical zoning of the NE Japan basement granitoids was previously recognized for Sr isotopes (Shibata & Ishizaka, 1979), but the proposal by Kagami (2005) extends and reinforces the observation. The zones generally correlate with the basement terranes bordered by major transform faults. However, slight offsets are seen between some of the basement tectonic and isotopic boundaries, particularly between the KZ and NZ (Fig. 5a).

Isotopic variation is rather large in NE Japan lavas of Quaternary age. A southward increase in Sr isotope ratios has been identified along the frontal arc (Notsu, 1983). Kersting *et al.* (1996) first noticed the spatial correlation between Nd–Sr isotopic groups of frontal-arc

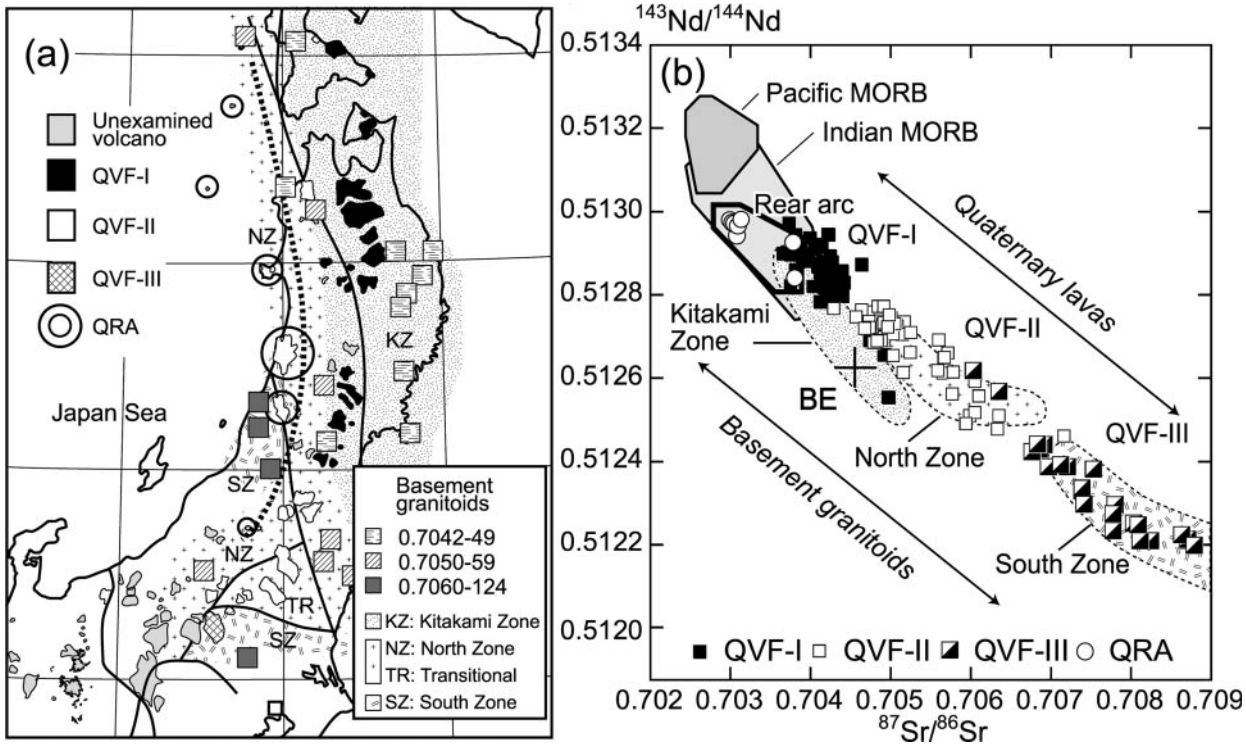

Fig. 5. (a) Distribution of basement granitoids and their isotope zones (Kagami *et al.*, 1992; Kagami, 2005) compared with the Nd–Sr isotopic characteristics of the Quaternary volcanoes; (b) Nd–Sr isotopic compositions of basement granitoids (Kagami *et al.*, 1992, 2005) and Quaternary lavas from the volcanic front and rear arc. Patterned fields show the isotopic compositions of the basement granitoids. Spatial correlations in Nd–Sr isotope composition are evident between the basement granitoids and the lavas for the frontal-arc volcanoes. The Nd and Sr isotopic compositions of the rear-arc lavas do not correlate with their basement. In (a), the bold dotted line is the boundary between the QVF and QRA; continuous lines are major faults between basement terranes. BE, Bulk Earth.

lavas and their underlying basement. The chemical boundaries do not correlate with terrane boundaries as well as they do with the basement granitoid zones (Fig. 5a). Clear spatial–chemical correlations are, however, found between basement granitoids and Quaternary lavas. Frontal-arc Quaternary lavas cluster tightly in three distinct areas in Nd–Sr isotope space; these are classified as QVF-I, -II, and -III (Fig. 5b). These three clusters overlap with those of the basement granitoid zones, namely QVF-I with the Kitakami Zone, QVF-II with the North Zone, and QVF-III with the South Zone (Fig. 5b). The spatial distributions of the three lava groups also correlate well with the basement granitoid zones (Fig. 5a). This striking correlation might reflect strong contributions of the underlying crust and/or mantle to the petrogenesis of the Quaternary lavas, as suggested by previous studies (Kersting *et al.*, 1996; Kobayashi & Nakamura, 2001; Kimura *et al.*, 2002). Hereafter, we use the lava group classification specified above. In contrast, rear-arc Quaternary lavas (QRA), always have a depleted source and plot close to the mid-ocean ridge basalt (MORB) field, notwithstanding the isotopically enriched nature of the granitoid zone (NZ) in which they were erupted. Low- to medium-K lavas from Numazawa and Sunagohara volcanoes are exceptions in the QRA, as they fall in the QVF-I field (the two open circles in Fig. 5b).

Conventional Pb isotope plots indicate that all rear-arc lavas are relatively unradiogenic, and are more similar to Indian MORB than to Pacific MORB (Fig. 6). The isotopic compositions of QRA also overlap those of frontal-arc lavas from the Izu arc (Hochstaedter *et al.*, 2001; Ishizuka *et al.*, 2003), and some Pb isotope compositions are similar to those of Japan Sea floor basalts (Cousens & Allan, 1992; Pouclet *et al.*, 1995). In contrast, lavas from the magmatic front are more radiogenic than the rear-arc lavas. Volcanic front lavas plot between the field for rear-arc lavas and Pacific sediments or between the rear-arc lavas and NE Japan crustal rocks. Among the frontal-arc lavas, the QVF-I group plots closest to the Izu frontal-arc field, although they are more radiogenic. In contrast, QVF-III has the lowest $^{206}Pb/^{204}Pb$ but high $^{207}Pb/^{204}Pb$ and $^{208}Pb/^{204}Pb$ and is close in composition to some Japan Sea oceanic island basalts with EM-I signatures (Tatsumoto & Nakamura, 1991) or global lower crustal compositions (Kobayashi & Nakamura, 2001). QVF-II lavas plot between the other two QVF groups (Fig. 6a and b), as do their Nd–Sr isotopic systematics.

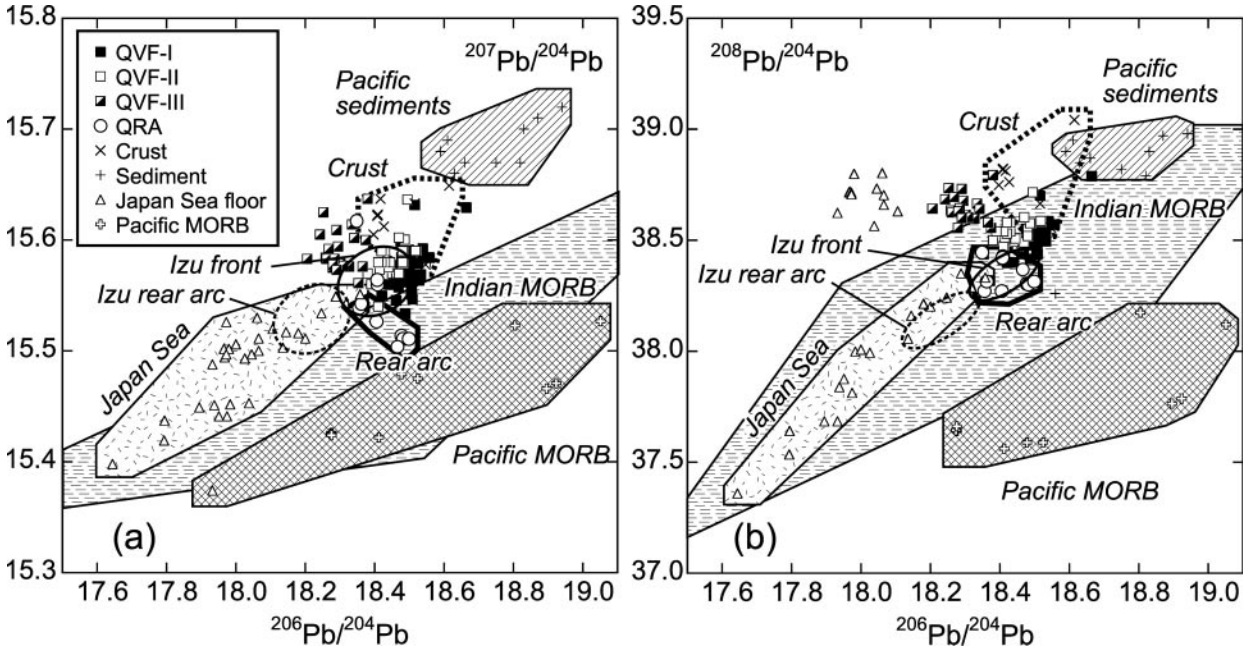

Fig. 6. Variation of $^{207}Pb/^{204}Pb$ (a) and $^{208}Pb/^{204}Pb$ (b) for NE Japan Quaternary lavas. Basement crustal compositions and compositions of Pacific and Indian MORB (GEOROC database), Pacific sediments, Japan Sea MORB (Cousens & Allan, 1992; Pouclet *et al.*, 1995) and Izu front- and rear-arc lavas are also shown.

The QRA and QVF-I groups have somewhat similar and distinctive trends on Sr–Pb and Nd–Pb isotope diagrams (Fig. 7). QRA and QVF-I lavas have flatter trends on both the Sr–Pb and Nd–Pb isotope plots, overlapping the fields of Philippine Sea Plate or Indian MORB. The QRA lavas have relatively high Nd isotope ratios coupled with low Sr isotope ratios (Fig. 7a and b). The QRA lavas almost exactly overlap the Izu rear-arc lava field in both the Sr–Pb and Nd–Pb diagrams, whereas the QVF-I lavas are identical with Izu frontal-arc lavas only for Sr–Pb isotopes. The Izu frontal-arc lavas have higher Nd isotopic ratios than any other lava either from NE Japan or from the Izu rear arc (Fig. 7a and b). In contrast to the rear-arc lavas, QVF-II and -III lavas together define near-vertical linear trends that have end-members lying close to QRA and QVF-I. QVF-III lavas have the highest Sr and lowest Nd isotope ratios, and QVF-II are intermediate between QVF-III and -I. Isotopic data for the NE Japan crust are limited, but those available plot on the vertical QVF-II and -III trends. Isotopic data for QVF-II and QVF-III lavas do not trend towards the isotopic compositions of Pacific seafloor sediments (Fig. 7). QVF-III lavas are from Akagi and Nikko–Shirane volcanoes. It has been argued previously that the intermediate lavas at Akagi are crustal melts (Kobayashi & Nakamura, 2001). QVF-II lavas are from Nekoma volcano. Kimura *et al.* (2002) suggested that the Nekoma lavas represent melts of lower crustal amphibolite. According to these previous studies, the isotopic trends defined by the QVF-II and QVF-III lavas can be explained by mixing of mantle-derived basalt similar to QRA or QVF-I with crustal melts. This is consistent with the isotopic compositions of the crustal rocks.

QVF-I volcanoes are spread over almost three-quarters of the northern frontal arc. QVF-III occurs only at Akagi and Nikko–Shirane (see Fig. 5b). The remaining volcanoes are classified as intermediate QVF-II. Two basaltic andesites from Nikko–Shirane (QVF-III) fall in the field of QVF-II, and a few dacites from Nanashigure (QVF-I) overlap the QVF-II field. A dacite from Nasu (QVF-II) plots in the QVF-III field (Fig. 5b; Table 1). Medium-K basalts in the QVF-I group have been reported from Kayou and Moriyoshi volcanoes (Shibata & Nakamura, 1997). Isotopically, all are classified into the QVF-I group here. However, their Sr–Nd–Pb isotopic compositions fall between those of frontal-arc low-K basalts from Iwate volcano (QVF-I; radiogenic) and rear-arc high-K basalts from Kampu (QRA; less radiogenic) (Shibata & Nakamura, 1997). Low-K to medium-K lavas from Numazawa and Sunagohara (the two most radiogenic QRA lavas in Figs 5 and 6) occur in the rear-arc QRA group. In terms of Nd–Sr–Pb isotope and K suite characteristics, Numazawa–Sunagohara lavas have some affinity with QVF-I (see Fig. 5b and Table 1), which is the reverse case for Kayou and Moriyoshi in the QVF-I group.

Major element classification (e.g. low-K tholeiitic and medium-K calc-alkalic in frontal-arc lavas) seems to correlate with more radiogenic and less radiogenic

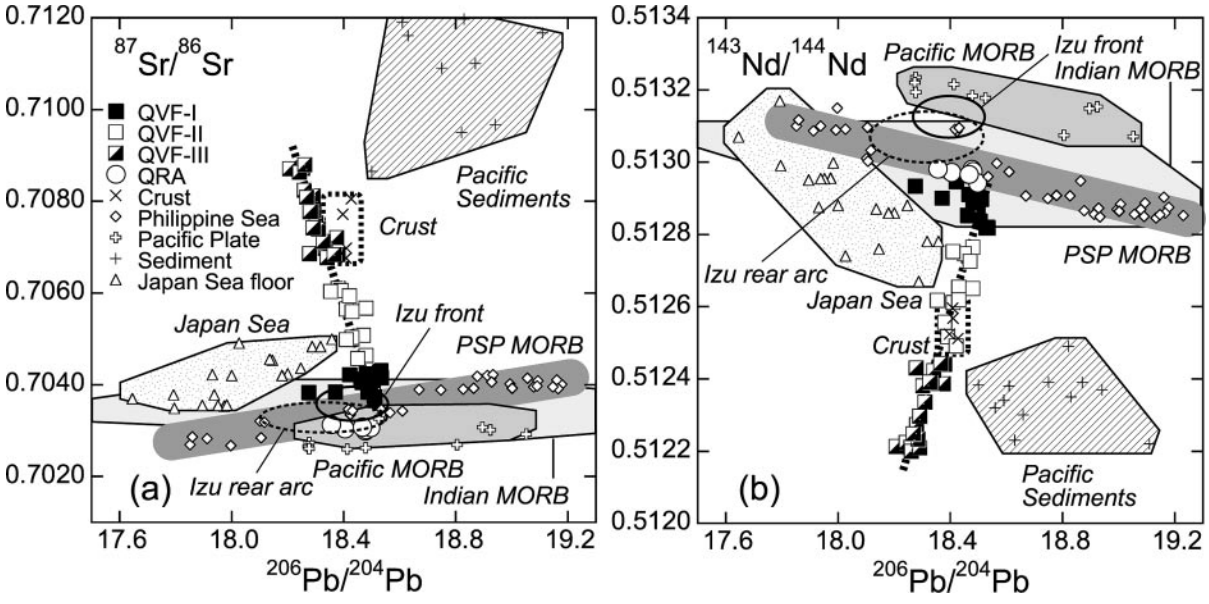

Fig. 7. $^{87}Sr/^{86}Sr$ vs $^{206}Pb/^{204}Pb$ (a) and $^{143}Nd/^{144}Nd$ vs $^{206}Pb/^{204}Pb$ (b) for the NE Japan Quaternary lavas, Pacific and Indian MORB (GEOROC database); Philippine Sea Plate (PSP) MORB (Hickey-Vargas, 1991, 1998; Hickey-Vargas *et al.*, 1995), Japan Sea ocean floor basalts (Cousens & Allan, 1992; Pouclet *et al.*, 1995), Uzu front- and rear-arc lavas and NE Japan crustal rocks (Koide & Nakamura, 1990; Shimoda & Nohda, 1995).

isotopic compositions (respectively) in the cases of Iwate (radiogenic low-K tholeiitic), Kayou and Moriyoshi (less radiogenic medium-K calc-alkalic). The same is true at Adatara volcano for the two K suites, which are radiogenic low-K tholeiitic and less-radiogenic medium-K calc-alkalic (Fujinawa, 1991). Kayou and Moriyoshi medium-K suite lavas have features transitional between low-K Iwate (QVF-I) and high-K Kampu (QRA). However, medium- and low-K Adatara lavas are all in the more radiogenic QVF-II group. Notwithstanding the complexity and systematic variations between major element and isotopic suites, the general isotopic classification of the Quaternary lavas adopted in this study is tenable throughout the NE Japan arc, indicating a genetic link between the crust and the lavas, particularly in the frontal arc.

Trace elements

Primitive mantle normalized multi-element patterns for NE Japan lavas are shown in Fig. 8. The trace element analyses used are from recent publications (Gust *et al.*, 1997; Shibata & Nakamura, 1997; Kobayashi & Nakamura, 2001; Kimura *et al.*, 2002); all data were determined by ICP-MS. Some elemental data that were questionable (e.g. excessive Ta suspected to be caused by contamination) are not plotted.

Rear-arc basalts from six high-K centers have almost identical trace element patterns, replicating the homogeneity shown in their Nd–Sr–Pb isotopic compositions. Low-K basaltic andesite from Numazawa also has a similar trace element pattern, but with lower concentrations of large ion lithophile elements (LILE) (Fig. 8a). The QRA patterns are generally enriched in LILE (Rb, Ba, Th, and U) and light rare earth elements (LREE) and are relatively depleted in high field strength elements (HFSE) (Nb and Ta). Strong enrichments are also seen for K, Pb, and Sr, whereas Zr and Hf are slightly depleted relative to Sm. Similar patterns of relative enrichment and depletion are typical for many island arcs (Pearce & Parkinson, 1993; Davidson, 1996).

QVF-I lavas are subdivided into basalts (SiO_2 <53 wt %: QVF-IB; Fig. 8b) and intermediate lavas (QVF-IA; Fig. 8c). The QVF-I basalts examined here are all low-K and have the most depleted REE abundances. Except for spikes in Ba, Pb, and Sr, QVF-I basalts have flatter normalized patterns than QRA equivalents. Strong depletion in Nb and Ta is also evident, along with minor but clear depletion in Zr–Hf. QVF-I intermediate lavas (QVF-IA) have patterns parallel to QVF-IB, although Sr enrichment diminishes as negative Eu anomalies develop, suggesting control by fractionation of plagioclase. Depletions in Zr–Hf relative to Sm are seen in some samples, but half show no Zr–Hf depletion. Medium-K basalts from Kayou and Moriyoshi of the QVF-I group have incompatible element abundances intermediate between QVF-I low-K and QRA high-K basalts (Shibata & Nakamura, 1997). They retain strong positive LILE anomalies (Ba, Sr, Pb) and negative HFSE anomalies (Nb, Zr, Hf). Positive Ba and Pb spikes are not as prominent compared with the low-K types and slopes in the REE region

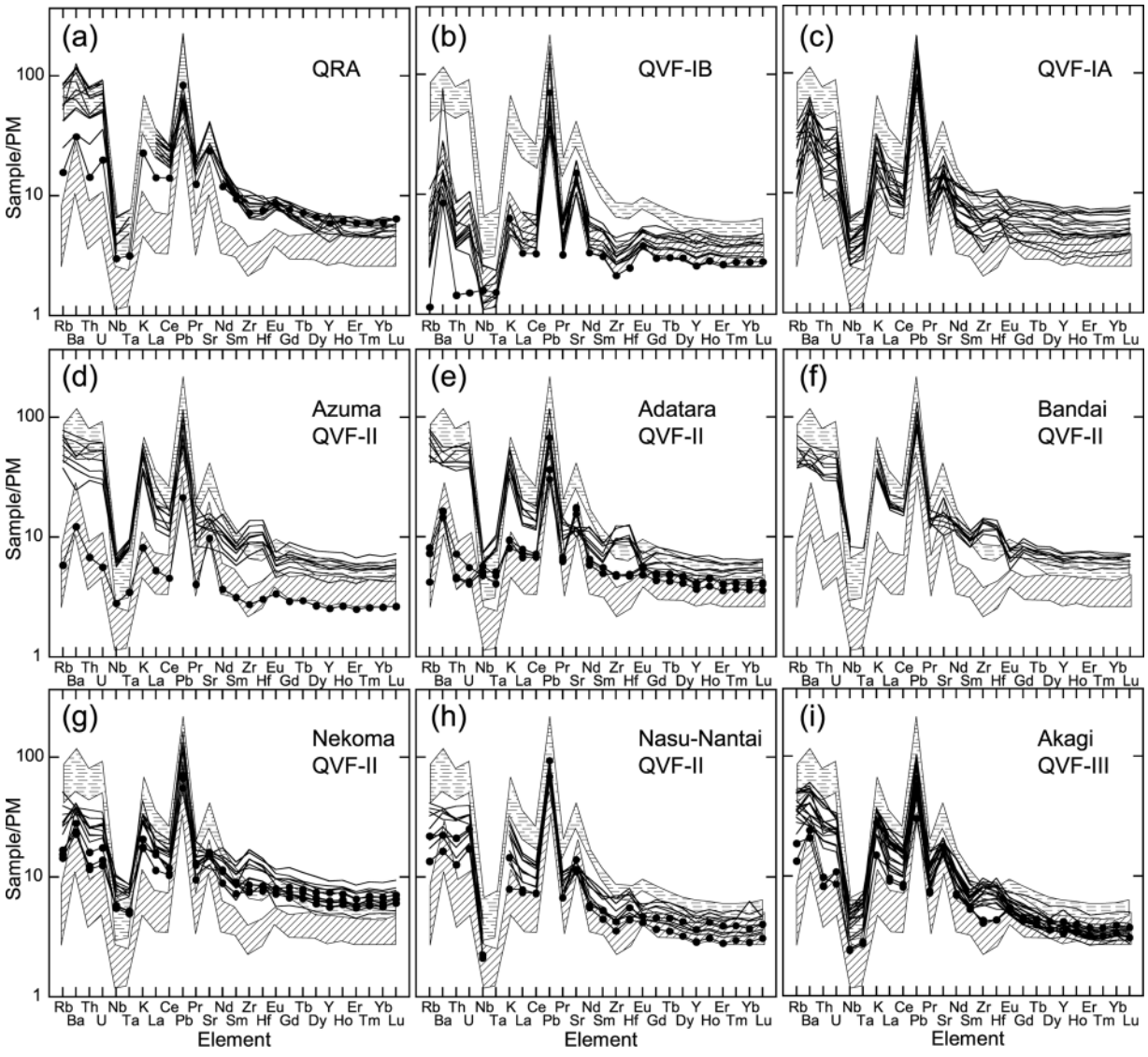

Fig. 8. Primitive mantle (Sun & McDonough, 1989) normalized multi-element patterns of Quaternary lavas from the NE Japan arc. Lava types are as in Fig. 5. (See Fig. 1 for volcano locations.) Shading indicates QRA (diagonal) and QVF-I (dashed horizontal) basalt fields for comparison. QVF-I lavas are separated into basalts (SiO_2 <53 wt %: QVF-IB) and andesite–dacite lavas (QVF-IA; SiO_2 >53 wt %). Lavas from individual volcanic centers are indicated by filled circles: (a) Numazawa low-K basaltic andesite; (b) Iwate basalt; (d) Azuma low-K lavas; (e) Adatara low-K lavas; (g) Nekoma low-K basaltic andesite; (h) Nantai low-K basalts; (I) Akagi low-K basalts.

are intermediate. Medium-K QVF-I basalts have incompatible element abundances and isotopic characteristics intermediate between QVF-I and QRA. This also relates to their geographical distribution across-arc (see Fig. 1).

The QVF-II Azuma and Adatara volcanoes contain both low-K and medium-K lavas. Low-K lavas are identified with filled circle symbols in Fig. 8d and e. The low-K QVF-II lavas are similar to QVF-I basalts in both absolute elemental abundances and patterns. In contrast, medium-K lavas from Azuma and Adatara have chemical abundances similar to QRA basalts. However, substantial differences are also evident, such as the modest Sr and Ba spikes and positive Zr–Hf anomalies shown by Azuma and Adatara medium-K lavas. Similar features are shown by intermediate medium-K QVF-II samples from Bandai (Fig. 8f). Intermediate Nekoma lavas are classified as QVF-II on the basis of isotopic composition. This volcano contains both low-K and medium-K lavas (Kimura *et al.*, 2001*b*, 2002), and the medium-K lavas have similar trace element patterns to other QVF-II lavas (Fig. 8g). Low-K lavas have similar trace element patterns to the medium-K lavas, except for slight positive Ba and Sr

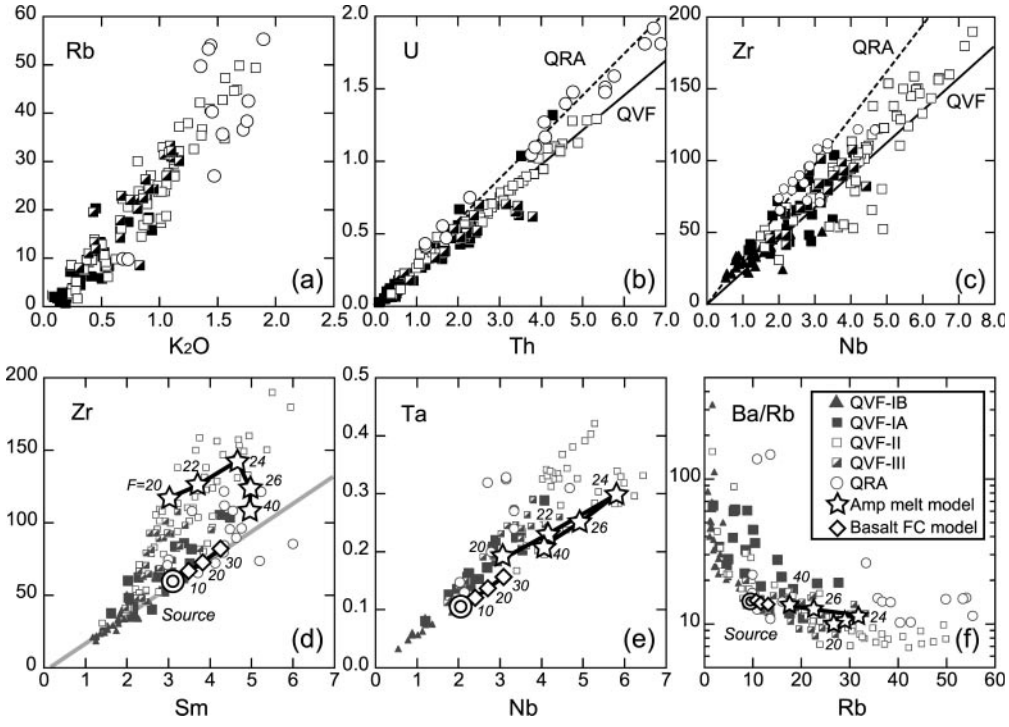

Fig. 9. Binary plots of incompatible element pairs for lavas from the NE Japan arc. Grey symbols in (d)–(f) are lava data; bold symbols are the calculated compositions of the resultant melt from partial melting of underplated mafic magma in the amphibolite facies (double circle) for variable degrees of melting (in per cent; open stars). Fractional crystallization (FC; open diamonds) models from the same mafic magma composition (double circle) are also shown. Numbers adjacent to the stars indicate the percentage melting. (For details of the modeling, see the main text.) Grey line in (d) is a regression line through the QVF-I basalts. This parallels the FC model, suggesting that FC control dominates the trace element ratios in the QVF-I basalts.

spikes with almost no Zr–Hf anomalies. These characteristics are intermediate between those of low-K and medium-K suites (Fig. 8g). Other QVF-II volcanoes (Nasu to Nantai) are all medium-K and show trace element patterns intermediate between those of low-K and medium-K lavas from Adatara (Fig. 8h).

The QVF-III intermediate medium-K calc-alkalic lavas from Akagi have positive Sr spikes (Fig. 8i). Other features such as positive Ba spikes and positive Zr–Hf anomalies are similar to those in the Adatara and Bandai medium-K suite. Akagi low-K tholeiitic basalts, in contrast, are almost identical to low-K lavas from Adatara or to QVF-I basalts (Fig. 8i; patterns with filled circles). The low-K basalts alone plot in the field of QVF-II, and thus are similar to Adatara low-K tholeiitic lavas in terms of trace element and isotope compositions.

Based on incompatible trace element characteristics, the QRA and QVF-I basalts are distinctive in terms of element abundances and slopes of trace element patterns. Frontal-arc low- to medium-K suite intermediate lavas in the QVF-II and -III groups are similar in terms of positive Zr–Hf anomalies and less prominent (or no) Ba and Sr spikes. Akagi lavas differ slightly owing to higher heavy REE (HREE)/LREE. Low-K basaltic lavas from the QVF-II Adatara and Azuma and QVF-III Akagi volcanoes are similar to QVF-I basalts.

Chemical characteristics of QVF-I basalts are commonly found in all basalts of the NE Japan arc, whereas intermediate and evolved lavas from QVF-I volcanoes are distinct from QVF-I or QRA basalts. Combined with the wide isotopic variations observed for frontal-arc intermediate lavas, these geochemical characteristics might reflect significant crustal inputs. The distinctive characteristics of the isotopically depleted QRA and QVF-I basalts, and perhaps some low-K basalts from QVF-II and -III, might thus reflect mantle processes.

Correlations between incompatible element pairs are shown in Fig. 9. Co-variations are seen between K_2O and Rb for all geochemical groups, with decreasing element abundances in the order QRA > QVF-III > QVF-II > QVF-I (Fig. 9a). The same is true for U and Th, with slight relative enrichment of U in QRA, as shown by its differing slope in Fig. 9b. The element pair Zr–Nb also shows strong correlation, but overall enrichments for the groups do not follow the order shown by Rb–K and U–Th. The greatest enrichments in Zr and Nb are seen in QVF-II, whereas QVF-III intermediate lavas and QVF-I basalts are the most

depleted (Fig. 9c). A similar enrichment trend is true for Nb–Ta (Fig. 9e).

Characteristic element fractionation between middle REE (MREE) and HFSE is represented by the Sm–Zr diagram (Fig. 9d). QRA and QVF-I basalts are aligned along a line (Zr/Sm ~20: thick grey line in Fig. 9d). In contrast, intermediate QVF-II and -III lavas depart from this trend.

Elemental fractionation between Ba and Rb (or Ba and Th, not shown) is also apparent in the multi-element plots. The element relationship is shown on a Rb vs Ba/Rb plot (Fig. 9f). Ba/Rb is most elevated in QVF-I basalts, and decreases in response to increasing Rb through QVF-I intermediate lavas, QVF-II and QVF-III. QVF-II and -III intermediate lavas and QVF-I basalts again have contrasting features, but all still lie in a continuum, suggesting that these characteristics result from mixing.

Geochemical summary of NE Japan Quaternary lavas

The characteristics of the NE Japan Quaternary lavas are summarized in Table 2. Significant geochemical variations include: (1) low-, medium- and high-K suites with tholeiitic and calc-alkalic characteristics; (2) variable Sr–Nd–Pb isotopic compositions in frontal-arc lavas; (3) positive and negative Zr–Hf anomalies in primitive mantle normalized multi-element plots; (4) varied Ba/Rb (Ba/Th) ratios, as manifest by the Ba spikes in the multi-element plots.

The QRA lavas commonly have high-K calc-alkalic characteristics, non-radiogenic Sr and Pb and radiogenic Nd isotopic compositions, and negative Zr–Hf and positive Ba anomalies. Tholeiitic lavas occur at Chokai, but these are similar to the calc-alkalic lavas in other respects. Numazawa and Sunagohara lavas have medium- to low-K characteristics with no Zr–Hf and positive Ba anomalies, somewhat similar to those in some frontal-arc low-K tholeiitic lavas.

QVF-I group lavas are commonly low-K tholeiites, are isotopically more radiogenic in Pb and Sr and less radiogenic in Nd than QRA lavas, and have clear negative Zr–Hf and extremely strong positive Ba anomalies. Medium-K calc-alkalic lavas from the Moriyoshi and Kayou centers are intermediate between QVF-I and QRA for all factors.

Most QVF-II lavas are medium-K and calc-alkalic. Isotopic compositions are more radiogenic than in QVF-I, elemental patterns lack Ba anomalies, and Zr–Hf anomalies are zero to positive. Adatara and Azuma low-K tholeiitic basalts are exceptions, and are more radiogenic in Pb and Sr isotope composition than coexisting medium-K basalts. The negative Zr–Hf and strong positive Ba anomalies of these tholeiitic lavas are

Table 2: Geochemical characterization of lavas from NE Japan Quaternary volcanoes

Volcano	Major element	Isotopes	Zr–Hf	Ba spike	Remarks
QRA					
Oshima-Oshima	HKCA	*	–	+	
Kyurokujima	HKCA	*	–	+	
Ichinomegata	HKCA	*	–	+	
Kampu	HKCA	*	–	+	
Chokai	HKCA	*	–	+	
	HKTH	*	–	+	
Gassan	HKCA	*	–	+	
Sunagohara	MKCA	*	0	+	
Numazawa	*LKCA*	**	0	+	*QVF-I like*
QVF-I					
Oshima-koma	LKTH	***	–	+++	
Esan	LKTH	***	–	+++	
Mutsu-Hiuchi	LKTH	***	–	+++	
Osore	LKTH	***	–	+++	
Hakkoda	LKTH	***	–	+++	
Towada	LKTH	***	–	+++	
Nanashigure	LKTH	***	–	+++	
Hachimantai	LKTH	***	–	+++	
Iwate	LKTH	***	–	+++	
Moriyoshi	*MKCA*	**	–	++	*Intermediate*
Kayo	*MKCA*	**	–	++	*between*
Akita-Koma	*MKCA*	**	–	++	*QVF-I and QRA*
Kurikoma	LKTH	***	–	+++	
Onikobe	LKTH	***	–	+++	
Narugo	LKTH	***	–	+++	
Nanatsumori	LKTH	***	–	+++	
Funagata	LKTH	***	–	+++	
Adachi	LKTH	***	–	+++	
Zao	LKTH	***	–	+++	
Aoso	LKTH	***	–	+++	
QVF-II					
Adatara	*LKTH*	*****	–	++	*Akagi like*
	MKCA	****	+	0	
Azuma	*LKTH*	*****	–	+	*Akagi like*
	MKCA	****	+	0	
Nekoma	LKTH	****	0	++	
	MKCA	****	+	0	
Bandai	MKCA	****	0 to +	0	
Nasu	MKCA	****	0 to +	+	
Takahara	MKCA	****	0 to +	0	
Nyoho	MKCA	****	0 to +	0	
Nantai	MKCA	****	0 to +	0	
QVF-III					
Nikko–Shirane	MKCA	******	+	0	
Akagi	*LKTH*	*****	–	++	*Adatara like*
	MKCA	******	+	0~+	

HK, high-K; MK, medium-K; LK, low-K; TH, tholeiitic; CA, calc-alkaline; –, negative anomaly; 0, no anomaly; +, positive anomaly; +++, strong positive anomaly; *, number of asterisks indicates isotopic enrichment (greater number indicates more radiogenic). Italics show exceptions in the group.

similar to those in QVF-I tholeiitic lavas. Nekoma intermediate low-K tholeiitic lavas have slight positive Ba anomalies but lack Zr–Hf anomalies. These features are exceptions for low-K tholeiitic suite lavas.

QVF-III lavas are also characteristically medium-K and calc-alkalic, with trace element characteristics similar to QVF-II medium-K, but have extremely radiogenic isotopic compositions. Akagi low-K tholeiitic basalt is an exception, with characteristics broadly similar to those of Adatara and Azuma low-K tholeiitic lavas.

DISCUSSION

Mantle–crust components for NE Japan lavas

Mantle component in rear-arc lavas

In contrast to the frontal-arc lavas, the rear-arc lavas show no clear characteristics attributable to contamination from basement granitoids, even though they were erupted over the differing NZ and SZ granitoid zones (see Fig. 5). All QRA lavas have the most depleted source compositions and are similar to regional asthenospheric melts such as Japan Sea basalts, Philippine Sea MORB or Indian Ocean MORB (see Figs 5–7). The NE Japan mantle, together with that beneath the Japan Sea, is part of the Indian MORB domain (Hickey-Vargas, 1991, 1998; Tatsumoto & Nakamura, 1991; Jolivet & Tamaki, 1992; Pouclet & Bellon, 1992; Hickey-Vargas *et al.*, 1995; Pouclet *et al.*, 1995; Flower *et al.*, 2001), and QRA lavas indicate derivation from a similar asthenospheric source. In addition, the QRA isotopic compositions are almost identical to those in the Izu arc (Hochstaedter *et al.*, 2001; Ishizuka *et al.*, 2003) suggestive of a common rear-arc asthenosphere beneath the Izu and NE Japan arcs.

Some Japan Sea submarine lavas, however, have a distinctly enriched Nd–Sr isotopic source (see Fig. 7a). This led Cousens & Allan (1992) to infer addition of a subducted Pacific sediment component to the mantle source. However, multiple isotope plots indicate that mixing of NE Japan crust can also generate such enrichments (see Figs 6 and 7) (Tatsumoto & Nakamura, 1991; Pouclet *et al.*, 1995). The Japan Sea was formed by stretching of the Eurasia continental crust, and fragments of the continental crust remain in the basin (see Fig. 1) (Tamaki *et al.*, 1992). Regional upwelling of depleted asthenosphere during opening of the Japan Sea has been proposed by several workers (Nohda *et al.*, 1988; Tatsumi *et al.*, 1989; Cousens & Allan, 1992; Ohki *et al.*, 1994; Pouclet *et al.*, 1995; Okamura *et al.*, 1998, 2005; Kimura *et al.*, 2003*b*, 2005). Consequently, contamination of mafic melts derived from the asthenosphere by remnant crust or lithosphere may cause the isotopic enrichment in the Japan Sea floor basalts. The isotopic trends of the QRA lavas approach those of the most depleted Japan Sea source and are almost identical to Philippine Sea MORB (Fig. 7a and b). The QRA lavas thus appear to represent the isotopic composition of the asthenosphere beneath the rear-arc region, which is comparable with the Sea of Japan back-arc basin mantle asthenosphere (Nohda *et al.*, 1988; Tatsumi *et al.*, 1989; Cousens & Allan, 1992; Ohki *et al.*, 1994; Pouclet *et al.*, 1995; Okamura *et al.*, 1998, 2005; Kimura *et al.*, 2003*b*, 2005).

Mantle component in frontal-arc lavas

Although QVF-I basalts have Sr–Nd isotopic compositions identical to those in the present-day Kitakami Zone granitoids (see Fig. 5), the isotopic characteristics are relatively non-radiogenic Sr and Pb and radiogenic Nd, but not as much as in the QRA basalts (see Fig. 7). Izu frontal-arc basalts have relatively radiogenic Sr and Pb isotope compositions compared with the rear-arc basalts (Hochstaedter *et al.*, 2001; Ishizuka *et al.*, 2003). However, these isotopes in the QVF-I basalts are more radiogenic than those in the Izu arc (see Figs 5–7). Zr–Hf depletions relative to Sm and strong Ba enrichment relative to Th are also similar in QVF-I and QRA basalts, and this differs from other frontal-arc chemical groups (see Fig. 9d). Such trace element characteristics are common in mantle-derived arc basalts (e.g. Arculus, 1981; Tatsumi & Eggins, 1995; Plank & Langmuir, 1998; Hochstaedter *et al.*, 2001; Ishizuka *et al.*, 2003). Therefore, the QVF-I basalts may preserve mantle characteristics, even after modification by crustal processes. Evidence of crustal assimilation would be minimal, because of the less enriched nature of potential crustal assimilants from Kitakami Zone basement (see Fig. 5). Low-K tholeiitic basalt lavas from QVF-II (Adatara and Azuma) and QVF-III (Akagi) also have weaker but similar trace element characteristics to QVF-I, suggesting some preservation of mantle characteristics. The radiogenic Sr and Pb characteristics of these basalts reflect contamination by more radiogenic crustal materials than in QVF-I.

Crustal component in frontal-arc lavas

Quaternary lavas from the volcanic front of the NE Japan arc have isotopic compositions that are almost identical to those of the present-day basement Cretaceous to Paleogene granitoids (see Fig. 5). This suggests four options for QVF magmas: (1) melting of the granitic upper crust; (2) melting of lower crustal rock residues left after yielding the granitoids; (3) melting of mafic cumulates in the lower crust associated with granioids (Kagami *et al.*, 1992; Johannes & Holtz, 1996); or (4) extraction from lithospheric mantle (Tatsumoto &

Nakamura, 1991; Pouclet *et al.*, 1995; Kersting *et al.*, 1996).

Both Kobayashi & Nakamura (2001) and Kimura *et al.* (2002) suggested that intermediate lavas from Nekoma and Akagi were lower crustal melts. A similar proposal has been made for other NE Japan lavas, including production of medium-K andesite by melting of lower crust at Adatara (Fujinawa, 1988, 1991), or melting lower crustal amphibolite to form intermediate calc-alkalic magmas at Ichinomegata (Takahashi, 1986*a*).

Nd–Sr isotope plots strongly support these proposals, at least for the lavas from the frontal arc (see Fig. 5). Conventional Pb isotope plots also show that the frontal-arc lavas have compositions intermediate between the crust and the rear-arc lavas with isotopically depleted source (see Fig. 6). Multiple isotope plots further strengthen the proposal that frontal-arc lavas fall on mixing lines between crustal components and a depleted MORB-type source mantle (see Fig. 7). This crustal contribution is particular to the NE Japan arc, as confirmed by the observation that highly radiogenic Sr and Pb isotopic characteristics are not found in the Izu frontal arc (Hochstaedter *et al.*, 2001; Ishizuka *et al.*, 2003). This feature distinguishes the NE Japan frontal-arc lavas from immature oceanic arcs. Option (4) also has the potential to produce similar isotopic variations between basement granitoids and Quaternary lavas. However, for the reasons given in the next section, we negate this possibility.

Origin of crustal melts

An amphibolite melting model

Intermediate lavas from the frontal arc are either more radiogenic than the associated basalts (e.g. Akagi, Kobayashi & Nakamura, 2001) or isotopically similar (Fujinawa, 1991; Kimura *et al.*, 2001*b*, 2002). These intermediate lavas commonly have distinct geochemical characteristics with positive Zr–Hf anomalies (Fig. 8 and Table 2), a feature that is never shown by the basalts.

Kimura *et al.* (2002) modeled dehydration melting of amphibolite considering the mineralogy and partition coefficients of minerals at different pressures and temperatures. Their model assumed underplating of water-rich basalt magma to form the amphibolite, and that the amphibolite was remelted by heat addition from basalt penetration (Kimura *et al.*, 2002). They used one of the basalt compositions (Aoso basalt) as an analogue of amphibolite, and explained the origin of low-K tholeiitic intermediate lava at Nekoma.

Elemental behavior between Zr–Sm and Ba–Rb was calculated using the same model (amphibolite crust melting model in Fig. 9d–f). The QVF-I basalts, which are possibly of mantle origin, plot on a well-defined linear correlation in the Zr–Sm plot (see Fig. 9d). Consequently, any source compositions lying along the line are appropriate for lower crustal amphibolites derived from under-plated basalts. The solidified basalts may have experienced fractional crystallization or crystal accumulation. The effect of fractional crystallization is estimated by applying the model that Kimura *et al.* (2002) used with a basaltic andesite starting composition (see basalt FC model in Fig. 9d–f). Fractionation and accumulation can alter Zr/Sm, Nb/Ta and Ba/Rb only slightly. The differentiation trend closely follows the straight line defined by the QVF-I basalts. Thus, natural variations of this sort seen in the basalts and intermediate lavas are probably attributable to fractional crystallization. However, the wide compositional variations seen in the intermediate lavas cannot be produced by this mechanism.

The basaltic amphibolite melting calculations indicate elevated Zr relative to Sm for amphibolite melts [$P \sim 0{\cdot}8$ GPa, $T = 1000$–1075°C; calculated model melts have 57–67 wt % SiO_2; see details given by Kimura *et al.* (2002, Table 3)]. Elevated Zr relative to Sm is due to residual amphibole during melting. The amphibolite-melting model reproduces the chemical characteristics of QVF-II and -III intermediate lavas. QVF-I intermediate lavas may also have the same origin, because almost all the andesites plot slightly above the QVF-I basalt regression line (FC model line) on a Zr–Sm plot (Fig. 9d). The large variation in Nb and Ta observed in intermediate lavas is also interpreted as being generated during amphibolite melting rather than by fractional crystallization (Fig. 9e). Although little is known of the behavior of the HFSE, it is clear that fractional crystallization alone cannot account for all the variation observed, but amphibolite melting has the potential to do so.

Kimura *et al.* (2002) also examined the behavior of Sr during amphibolite melting. Sr contents in the resulting melts are buffered by plagioclase formed by incongruent melting of amphibole, and thus relative enrichments in Sr inherited from the parental basalt in the source are almost eliminated from amphibolite melts. This is similar to the chemical character of the intermediate lavas of the QVF-I, -II and -III, as noted above (Fig. 8). Sr fractionation also occurs as a result of fractional crystallization of plagioclase, so the origin of the Sr depletion in the intermediate lavas cannot be distinguished. However, weak or almost no Sr spikes in the lavas can also be explained by partial melting of lower crustal amphibolite.

Ba/Rb (or Ba/Th) ratios also differ between QVF-I basalt and intermediate QVF-II and -III lavas. Ba/Rb ratios reflect the Ba spikes in primitive mantle normalized multi-element diagrams (see Fig. 8). Ba/Rb increases with decreasing Rb (Fig. 9f). Ba/Rb is high in QVF-I basalts and low in QVF-II and -III

intermediate lavas. QVF-I andesites and QRA have intermediate Ba/Rb ratios. Partial melting of lower crustal amphibolite can change Rb but not Ba/Rb (Fig. 9e, amphibolite partial melting model). Rb and Ba partition coefficients for most minerals during fractional crystallization or amphibolite melting are well below unity, although D_{Ba} in plagioclase (0·8–0·2) is greater than D_{Rb} (0·07) (Kimura *et al.*, 2002). Fractional crystallization affects these elements very little (Fig. 9e basalt FC model). Ba/Rb, and thus Ba/Th, in the starting composition cannot be changed much either by fractional crystallization or by amphibolite melting. This suggests that the isotopically less radiogenic QVF-I basalts can be the source for QVF-I andesites with Ba spikes, but cannot be the source for the radiogenic intermediate lavas of other QVF suites because these have no Ba spikes (Fig. 8). QVF-I basalt might largely preserve mantle-derived melt characteristics, and the intermediate lavas could be produced by mixing between a larger amount of melt of pre-existing amphibolitic crust and mantle-derived basalts.

Mixing between mantle-derived basalt and intermediate crustal melts: further decoding of mantle–crust signatures

Low-K tholeiitic basalts occur in the QVF-II and -III suites as noted above, and are regarded as mantle-derived (Fujinawa, 1988, 1991; Kobayashi & Nakamura, 2001). Judging from the Ba and Sr spikes and troughs in the Zr–Hf region in the multi-element plots, these lavas seem to be mantle-derived because of their similarity to the QRA and QVF-I basalts (Fig. 8). The MgO contents of these basalts are, however, <6 wt %, suggesting significant fractional crystallization. All the QVF basalt suites are concentrated in a narrow compositional range on a plot of SiO_2 vs Sr isotopic compositions (Fig. 10a). Sr isotope compositions are more radiogenic in evolved Akagi lavas, whereas the Akagi low-K tholeiitic basalt plots at the non-radiogenic end of the data array. The primary basalt in Akagi could have a less radiogenic Sr isotopic composition than that observed in the basaltic lavas (Kobayashi & Nakamura, 2001). Extrapolation of the Akagi trend intercepts the most primitive QVF-I basalt in this diagram (Fig. 10a). A primitive basalt from Akagi would have had lower SiO_2 (<53 wt %) and higher MgO (>6 wt %) content when the magma last equilibrated with the mantle. Thus the erupted basalt is either fractionated or contaminated by mixing with a crustal melt. As noted by Kobayashi & Nakamura (2001), mixing of radiogenic crustal Sr will strongly affect the isotopic composition of the Akagi low-K tholeiitic basalt. The minimum amount of contamination by crustal melt is estimated to be 20% if the most silica-rich Akagi dacite is taken as representative of the crustal contaminant (see Fig. 10a). We thus conclude that the 'uncontaminated' mantle-derived magma at Akagi is isotopically similar to the QVF-I basalts.

Low-K tholeiitic basalts from Adatara and Azuma also have very similar Nd–Sr isotope and trace element compositions to the Akagi basalts (Figs 8 and 10). This suggests that they had the same origin. Low-K tholeiite basalts at Adatara and Azuma were probably derived by mixing between QVF-I type mantle-derived basalt and a QVF-III type (SZ) crustal melt. Fractional crystallization in a closed magma chamber could maintain the intermediate isotopic composition of the Adatara low-K tholeiitic intermediate lavas (see FC trend in Fig. 10a).

The above process can also explain why medium-K calc-alkalic andesites from Adatara have less radiogenic Sr isotopic characteristics than the low-K tholeiitic Adatara lavas (Fujinawa, 1991). The medium-K calc-alkalic andesites appear to be melts of lower crustal amphibolite that had a less radiogenic Sr isotopic composition, similar to the NZ granitoids (NZ in Fig. 10a). A calculated mixing line between QVF-I basalt and the NZ crustal component almost reproduces the medium-K calc-alkalic trend, which shows slight increase in Sr isotope ratios with increasing SiO_2 (Fig. 10a, low Sr isotope cluster of QVF-II).

The discussion above leads to two important conclusions: (1) QVF-I type parental basalt is widespread beneath the entire magmatic front of the NE Japan arc; (2) QVF-III (SZ) type crust must also exist in areas underlain by QVF-II (NZ) crust.

The apparent Sr isotopic enrichment of the intermediate lavas in the southern segment of the NE Japan arc might be a consequence of crustal contamination. If our model is correct, then it should be able to explain other variations in trace element and isotope pairs. An example involving Nd (MREE) isotope ratios and La/Yb (HREE/LREE) is shown in Fig. 10b. The mixing lines reproduce the chemical variations of the QVF-III and QVF-II lavas. The same model seems applicable for Nb (HFSE) vs La/Yb (REE) shown in Fig. 10c. Relationships between LILE represented by Ba/Rb vs Rb are also in agreement (Fig. 10d). Neither fractional crystallization nor crustal melting significantly changes Ba/Rb as discussed above, but mixing between mantle-derived basalt and various crustal melts can generate large variations in Ba/Rb (see models in Fig. 9f). It should be noted that in each diagram basalts from QVF-II and -III plot closer to the mantle component than the intermediate lavas, which is consistent with the proposed model. Our model suggests that the strongly radiogenic Sr isotope characteristics observed in the frontal arc (Notsu, 1983; Ohki *et al.*, 1994; Kersting *et al.*, 1996; Gust *et al.*, 1997; Shibata & Nakamura, 1997) result from a crustal contribution.

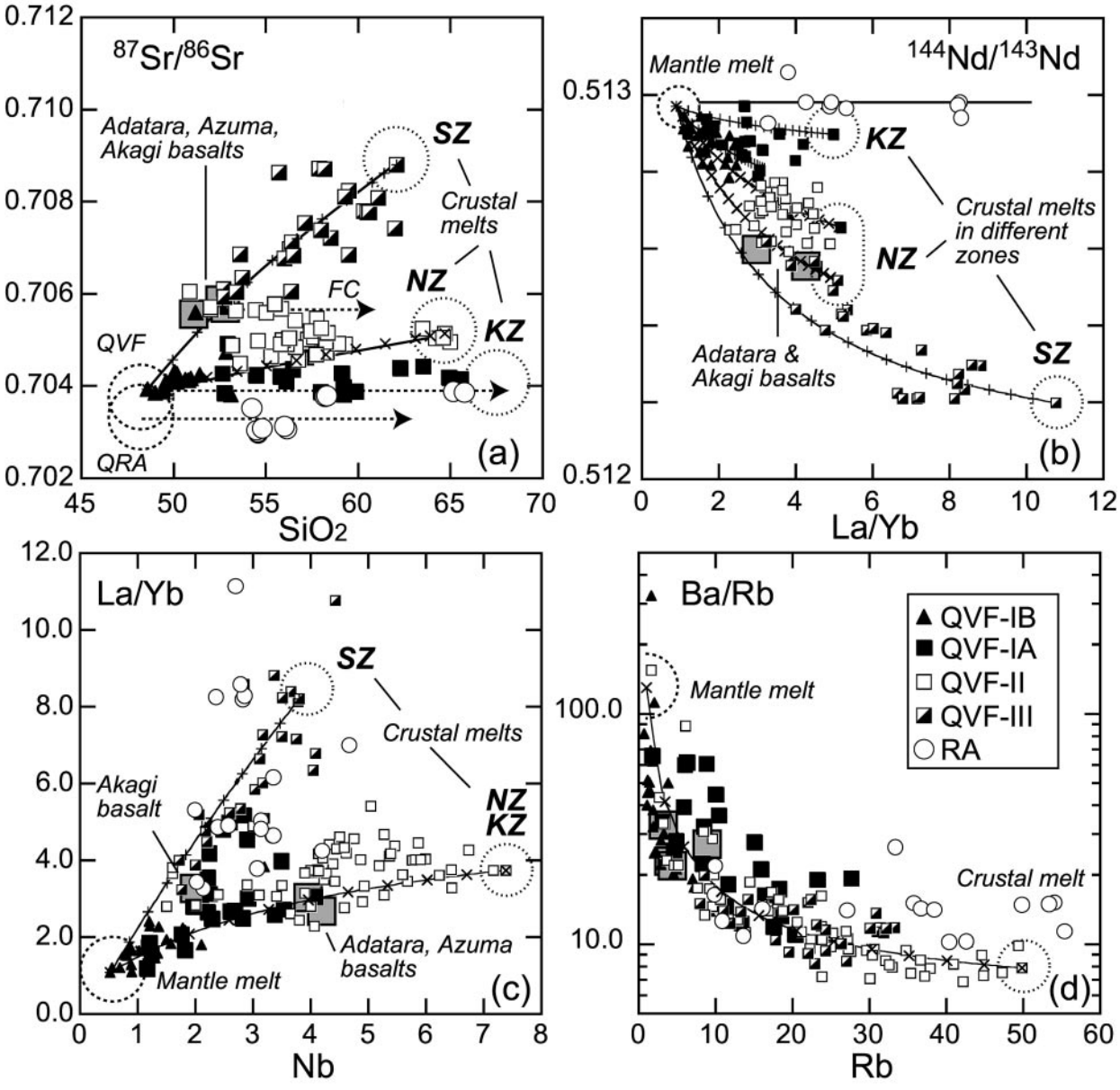

Fig. 10. Mixing calculation models between different crustal sources (KZ, NZ, and SZ) and a common mantle-derived basalt (mantle melt). Basalt compositions from Adatara, Azuma and Akagi are highlighted as shaded squares. Mixing lines are shown as fine lines with tick marks at successive 5% mixing proportions. FC, fractional crystallization trend.

The low-K tholeiitic basalts with QVF-I type characteristics (all QVF-I basalts and Adatara, Azuma, Akagi basalts) strongly reflect the characteristics of the mantle-derived melt. In contrast, medium-K calc-alkalic andesites from the southern frontal arc (QVF-II and -III) could be the products of mixing between primary basalt and low-K tholeiites with a strong crustal signature, or with direct crustal melts. This is supported by weaker mantle signatures in the andesite lavas (Fig. 8). Medium-K calc-alkalic basalts from the QVF-I group (Moriyoshi and Kayou) are exceptions, as they have stronger mantle signatures and less radiogenic Sr and Pb isotopic characteristics intermediate between QVF-I and QRA basalts. These are inferred to be largely mantle-derived, based on their isotopic characteristics. Low-K tholeiitic andesites to dacites from the QVF-I group are all less radiogenic in Sr, similar to the mantle component and KZ granitoids (Fig. 10a). Therefore, distinction of the crustal component by isotopic data alone is difficult. The low-K intermediate

lavas still preserve high Ba/Rb (Fig. 10d), but have no to slightly positive Zr–Hf anomalies (Figs 8c and 9d). The low-K tholeiitic intermediate lavas from Nekoma also have similar trace element characteristics, and appear to be derived from melts of the lower crust (Kimura *et al.*, 2002). We therefore suspect that most of the low-K tholeiitic intermediate lavas are more or less affected by contamination with crustal melts. Basaltic andesite and dacite from Nanashigure have relatively radiogenic Sr and Pb isotopic compositions, which approach the most radiogenic end of the basement KZ granitoids (Fig. 5). The dacite lava has a clear positive Zr–Hf anomaly with a weaker positive Ba spike, and might therefore reflect the characteristics of the crustal melt in the QVF-I suite.

Is the crustal melt of amphibolite origin? Low-K vs medium-K and calc-alkalic vs tholeiite

Contamination by both lower and upper crustal melts has been identified in basalts (lower crustal gneiss) and basaltic andesites (upper crustal granitoids) in the Ueno Basalts, central Japan (Kimura *et al.*, 2001*a*). Involvement of more than one crustal component is similarly suggested here for Adatara and Azuma (SZ and NZ components, see above). Although we have suggested amphibolite melts as the crustal contaminants, the crustal material might actually be highly variable. Consequently, identification of the major crustal component that affects the NE Japan arc lavas remains open.

Compilations of experimental melt compositions of granitoids, sediments, and gneiss (Ariskin *et al.*, 1992) and amphibolite melting experiments (Johannes & Holtz, 1996) are shown in Fig. 11. The K_2O contents of the experimental melts of felsic source rocks are all elevated (>3% K_2O), whereas melts produced by amphibolite melting are relatively K_2O poor (<3% K_2O). Fractional crystallization increases the K_2O content in lavas; however, the general geochemical trends in the frontal-arc lavas still fall between the compositions of mantle-derived basalt and amphibolite melt. The high K_2O contents of the felsic crustal melts are not consistent as mixing end-members for the NE Japan intermediate rocks. High-K intermediate to felsic melts can also be generated from high-K amphibolite (Sisson *et al.*, 2005). This is also confirmed by amphibolite melting model calculations, which showed that a low-K amphibolite source was required for low-K intermediate lavas (Kimura *et al.*, 2002). However, the basement granitoids do not contain any high-K suites (Kagami *et al.*, 1992), and therefore lower crustal igneous amphibolites are likely to be low- to medium-K. This is consistent with the occurrence of low- to medium-K dacites with positive Zr–Hf anomalies. These appear to be derived from lower crustal amphibolite melt (Kimura *et al.*, 2002).

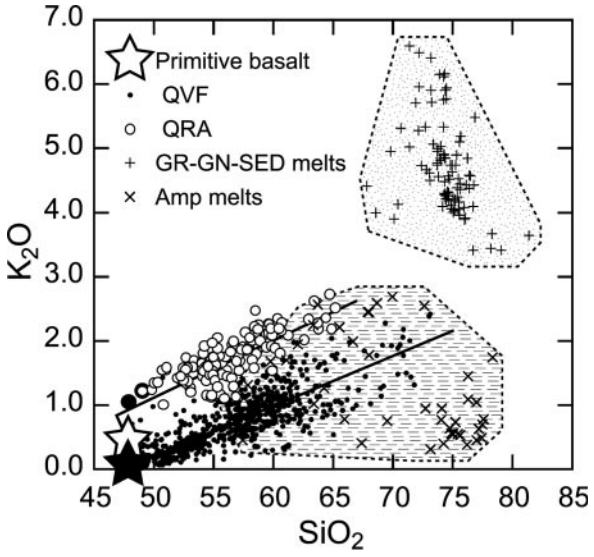

Fig. 11. Comparison of K_2O–SiO_2 contents in experimental silicic crustal (GR–GN–SED) melts, experimental amphibolite (Amp) melts, and intermediate lavas from the NE Japan arc. Experimental compositions for silicic crustal materials are from the INFOREX 4·02 database (Ariskin *et al.*, 1992), including experimental data (Kadik *et al.*, 1971; Clemens *et al.*, 1986; Conrad *et al.*, 1988; Vielzeuf & Holloway, 1988; Johnson & Rutherford, 1989; Beard *et al.*, 1993; Gerke & Kilinc, 1993; Skjerlie *et al.*, 1993; Scaillet *et al.*, 1995; Patiño-Douce, 1996; Gardien *et al.*, 2000). Experimental melt compositions for amphibolite melting are from the compilations of Johannes & Holtz (1996). Open and filled stars are the estimated primitive basalt compositions for the QRA and QVF, respectively. Continuous lines indicate approximate geochemical trends for the QVF and QRA lavas expected as a result of simple fractional crystallization. Dotted field indicates the range of granite–gneiss–sediment partial melt compositions; horizontal dashed field indicates the compositions of partial melts of various amphibolites.

Low-K tholeiitic intermediate lavas are represented by northern QVF-I suite (Nanashigure) and Nekoma lavas. Medium-K calc-alkalic intermediate lavas occur in the southern QVF-II and -III. Derivation of both calc-alkalic and tholeiitic lavas is possible by amphibolite melting, based on reported partial melt compositions from experimental work (Kimura *et al.*, 2002). The critical factor is oxygen fugacity in the melting region, and conditions at $fO_2 <$ NNO (nickel–nickel oxide buffer) can generate tholeiitic intermediate partial melts (Sisson *et al.*, 2005). Therefore, the correlation between K_2O content (source composition) and calc-alkalic or tholeiitic characteristics (fO_2) should logically reflect the oxygen fugacity in the melting region. However, the observed broad correlation between low-K and tholeiitic characteristics and medium-K and calc-alkalic characteristics is prominent in the intermediate lavas in NE Japan. This suggests more reduced conditions for the low-K tholeiitic intermediate lavas. As the low-K suite lavas tend to have stronger mantle signatures (notwithstanding evidence of mixing with crustal melts), reduced conditions could be inherited from the mantle source. As

we have not yet examined the mineralogy of each lava suite, this issue requires further examination.

Mafic gneiss or diorite melts could be an appropriate mixing end-member, but melting of lower crustal amphibolite provides the most plausible crustal component, as discussed in the preceding section. Amphibolite xenoliths have been reported from several Quaternary volcanoes in NE Japan (Aoki, 1987). The wide distribution of amphibolitic lower crust is also suggested by seismic-wave velocity measurements of amphibolite xenoliths at high-pressure and -temperature conditions and comparison of the data with seismic observations (Nishimoto *et al.*, 2005). We suggest that lower crustal amphibolite forms regionally distinct isotopic zones corresponding to the surface granitoids, but is partly heterogeneous, as suggested by the evidence for multiple crustal components (e.g. Adatara and Azuma). For further identification of crustal melt sources and the origin of the lower crust, we must await detailed geochemical and isotopic studies of the basement granitoids. However, our findings provide important constraints on the nature of the lower crust in NE Japan.

We conclude that the large chemical variations found in the lavas of each frontal-arc group fundamentally manifest mixing between various crustal melts and a common mantle-derived basalt. This model applies to the entire magmatic front in NE Japan. The mixing proportion of crustal melt for the Adatara, Azuma, and Akagi basalts is <20% (see Fig. 10). This should be an overestimate of the crustal melt proportion, because we used observed dacite lava compositions to constrain the felsic mixing end-members, and these potentially include a basaltic component to some extent. More critical assessment of the amount of crustal assimilation has been proposed for the Ueno Basalts (<10%, Kimura *et al.*, 2001*a*).

Seismic tomography studies (Hasegawa *et al.*, 1991; Zhao *et al.*, 1992; Nakajima & Hasegawa, 2003; Nakajima *et al.*, 2005) suggest that a low-velocity region exists in the lower crust beneath the volcanic front. Low-frequency earthquakes, which could result from melt movement, are also concentrated around the top of the low-velocity region (Hasegawa *et al.*, 1991; Nakajima & Hasegawa, 2003). Our model for melting of the lower crust beneath the volcanic front is thus further supported by the available seismic data. Such relationships are not observed beneath the rear arc, suggesting little crustal contamination, which is consistent with the petrological observations.

Origin of across-arc chemical variation in basalts

In this section, we further discuss the origin of basalt magmas beneath the NE Japan arc to understand the geochemical variations in the mantle-derived basalts and magma generation processes in the mantle wedge beneath the arc.

Mantle-derived primary basalts in the NE Japan arc

We have discussed the role of a 'crustal filter' in the NE Japan arc, and identified the characteristics of the mantle-derived basalt generated beneath the magmatic front. The chemical composition of this basalt differs significantly from that of the rear-arc basalts (see Fig. 8a and b). As noted above, the frontal- and rear-arc basalts are low–medium K and high-K, respectively (see Fig. 3). Trace element abundances in the rear-arc and frontal-arc basalts are also distinct (see Fig. 8). Strongly fluid-mobile elements, such as Ba and Pb, are enriched in the frontal-arc lavas, whereas HFSE are relatively depleted (see Fig. 8). Rear-arc lavas are unradiogenic in terms of Sr and Pb and radiogenic in Nd isotopic composition. The radiogenic Pb and Sr isotopic compositions of evolved frontal-arc basalts may be due to the assimilation of crustal materials (Kobayashi & Nakamura, 2001). In primitive lavas this radiogenic composition may be imparted by the addition of fluid-mobile LILE (Sr, Pb) via slab-derived fluids (Shibata & Nakamura, 1997), or from enriched lithospheric mantle sources (Kersting *et al.*, 1996). As noted above, the role of crustal assimilation is not negligible. To evaluate mantle melting models, it is essential to estimate the primary basalt composition by removing the effect of the 'crustal filter'. The QVF-I basalts have stronger mantle signatures than the basalts in the other suites. Therefore, we first assess QVF-I before the other basalt suites.

Trace element mixing models suggest that most QVF-I basalts plot on a mixing trend between the most depleted basalt and crustal melts. Mixing may be as much as 20%, as discussed above (see Fig. 10 and relevant discussion). On the other hand, the most magnesian basalt from the frontal arc contains 9 wt % MgO and 95 ppm Ni. These values are below those expected for equilibration of melts with upper mantle peridotite, indicating that even these basalt magmas are somewhat evolved. Taking the Ueno Basalts as an analogue, about 10% crustal melt needs to be added to lower MgO from 11 to 9 wt % (Kimura *et al.*, 2001*a*), and therefore a minimum 10% crustal contamination is likely for QVF-I basalts.

The major element, trace element, and Nd–Sr isotopic compositions of the 'uncontaminated' frontal-arc basalt can be estimated by subtraction of <10% Nanashigure QVF-I dacite from the most magnesian QVF-I basalt. The Nanashigure dacite has a stronger crustal signature in terms of trace elements and Nd–Sr isotopes, and hence most closely represents that of the crustal melt. We used the most magnesian QVF-I basalt (Funagata) for

the starting composition of the 'contaminated basalt'. In the case of Akagi, Adatara, and Azuma, <10% subtraction of Akagi dacite from low-K tholeiitic basalts was made because the crustal melts were assumed to be similar to QVF-III dacite. The QRA basalt composition was also considered in the same manner.

For the frontal-arc basalts, subtraction of >10% crustal melt is unrealistic, as the Rb content in calculated 'uncontaminated basalts' yields negative values. The Rb content in the Iwate basalt (IWTB) is very low, with primitive mantle normalized values as low as Nb and Ta (Table 1 and Fig. 8b). We set the maximum subtraction amount of crustal melt to match the Rb content of an Iwate basalt that shows least contamination. This adjustment allows 3% subtraction for Funagata or Zao, 9% for Azuma and Adatara, and 10% for Akagi, Kayou, Moriyoshi and other QRA lavas. Significant reductions in Rb and Th and U are observed in 'uncontaminated basalt' after deduction of the crustal component, as a result of large contrasts in element abundances between basalts and assumed crustal melts (Fig. 12). In contrast, positive Ba, Pb, and Sr spikes remain or are even enhanced.

The second step is to evaluate whether the major element composition of 'uncontaminated' QRA and QVF-I basalts can result from partial melting of mantle peridotite. Erupted QRA and QVF-I basalts are evolved and are not in equilibrium with upper mantle peridotite, even after subtraction of the crustal contaminant. We calculated an olivine maximum fractionation model (Takahashi, 1986*c*) until the equilibrated olivine reached Fo_{90}. QRA (Chokai) and QVF-I (Funagata) basalts were chosen because of their high MgO contents, and addition of up to 12% olivine for QRA and 21% for QVF was necessary. This results in MgO contents in the primitive basalts as much as 12·4 wt % (QRA) and 14·6 wt % (QVF), respectively (Table 3).

To confirm whether such high-Mg basalt compositions are plausible as primary melts in the NE Japan arc, forward fractional crystallization calculations were made using the Adiabat_1ph MELTS program (Ghiorso & Sack, 1995; Smith & Asimow, 2005*a*, 2005*b*). We assumed fractional crystallization at 1·0 and 0·5 GPa (corresponding to Moho depths and middle crust) and water contents of 2 wt % (Tatsumi *et al.*, 1983). The calculations indicate that 12–20% equilibrium fractional crystallization of olivine alone can occur. Representative primary basalt compositions are shown in Table 3. Important features of the primary magma compositions are the similarities in many elements between QRA and QVF-I, except for lower alkalis and slightly elevated CaO, FeO, and MgO in the QVF-I primary basalt (Table 3).

Finally, incompatible trace element abundances in the primary magmas were calculated from 'uncontaminated basalt' compositions by addition of olivine. Calculations were carried out by simple dilution, because of the incompatibility of most trace elements in olivine. The basic characteristics for the frontal- and rear-arc basalt lavas remain unchanged (Table 3 and Fig. 12). An interesting observation is that the primary Funagata basalt has a similar composition to the Iwate basalt, with strongly depleted primitive mantle normalized Th, as marked as for Nb and Ta (Fig. 12). The same is true for primary low-K tholeiitic basalt compositions from Azuma, Adatara, and Akagi if 10% Akagi dacite is subtracted. U levels in the primary basalts vary from as low as Th (Funagata, Iwate, Azuma and Adatara) to more enriched compositions (Akagi, Zao, Akita-Koma). The U contents appear to correlate with La abundances in the primary basalts, which is consistent with the high mobility of U in fluids (Pearce *et al.*, 1995). In contrast to the frontal-arc basalts, the rear-arc basalts have greater incompatible element abundances than the felsic magmas (Fig. 12). Therefore, crustal contamination cannot greatly alter the primary magma incompatible element contents or isotope compositions. The QRA primary basalt composition has Th and U contents about one to two orders of magnitude greater than frontal-arc primary basalts (Fig. 12a and b).

These features are clearly exhibited in a plot of Th/La vs Sm/La (Plank, 2005; Fig. 12c). Possible crustal contaminants (frontal-arc dacites) have Th/La ratios greater than those of the subducted sediments supplied to the NE Japan arc. Primary basalt compositions therefore have lower Th/La ratios than those of basalts uncorrected for crustal contamination. The corrected Th/La values for frontal-arc basalts approach mantle values or lie close to them, suggesting that slab sediment contribution to the source was small. In contrast, the rear-arc lavas have high Th/La ratios closer to the subducted sediment composition. Although the Th/La–Sm/La systematics indicate greater sediment contribution in the rear arc, the occurrence of basalts with an isotopically depleted source in the rear arc negates a significant sediment contribution. This discrepancy is examined in a subsequent section.

Abundances of Sr, Nd, and Pb in the basalts and crustal melts are almost identical as predicted from the QVF-I basalt and dacite lavas. Therefore, 10% mixing of an isotopically enriched crustal melt can change the isotopic composition of the primitive basalt considerably. Using the Nanashigure dacite end-member and mixing parameter, we can infer the isotopic compositions of the primary QVF-I basalts. These still appear to be slightly enriched relative to the rear-arc basalts (see estimated QVF-I primary basalt isotope compositions in Table 3). The assimilation-corrected QVF-I primary basalt has an isotopic composition very close to that of the Izu frontal-arc basalts [$^{87}Sr/^{86}Sr$ = 0·7035–0·7040 and $^{206}Pb/^{204}Pb$ = 18·50–18·57 in Izu (Hochstaedter

Table 3: Source mantle compositions used in pMELTS calculations

Element:	P1	P2	P3	MP1	MP2	QVF	Primitive basalt				QRA	Primitive basalt			
Remarks:	Fertile	Intermed.	Depleted	Ichinome.	Ichinome.	Original	Funagara	Zao	Azuma	Kayou	Original	Chokai	Kampu	Ichinomegara	Kyurokujima
SiO_2	47·35	45·89	44·43	47·25	—	50·51	48·57				51·15	49·95			
TiO_2	0·24	0·16	0·08	0·10	—	0·73	0·60				1·05	0·93			
Al_2O_3	4·07	2·48	0·88	3·51	—	18·22	14·78				17·16	15·23			
FeO*	8·81	7·98	7·15	7·20	—	10·27	10·74				8·72	9·05			
MnO	0·13	0·12	0·12	0·12	—	0·16	0·16				0·18	0·18			
MgO	34·00	40·00	46·00	37·73	—	7·16	14·62				7·91	12·38			
CaO	3·85	2·23	0·62	3·24	—	11·13	9·03				9·64	8·56			
Na_2O	0·34	0·20	0·07	0·17	—	1·53	1·24				2·68	2·38			
K_2O	0·36	0·23	0·10	0·03	—	0·22	0·18				1·31	1·16			
P_2O_5	0·02	0·02	0·02	0·01	—	0·06	0·05				0·19	0·17			
NiO	0·19	0·25	0·31	0·24	—	—	—				—	—			
Cr_2O_3	0·52	0·42	0·33	0·39	—	—	—				—	—			
H_2O	—	—	—	0·50	—	—	(21% ol added)				—	(12% ol added)			
Total	99·86	99·98	100·10	99·97	—	100·00	99·98				100·00	99·99			
Mg-no.	87·3	89·9	92·0	90·3		60·9	75·2 (Fo_{90})				66·9	75·3 (Fo_{90})			
Trace element (ppm)															
Rb				0·004	0·088		0·294	0·148	0·766	0·582		11·52	39·4	29·1	45·9
Ba				15·2	3·60		50·1	82·6	41·3	85·9		170	592	801	524
Th				0·020	0·013		0·150	0·315	0·204	0·220		1·71	4·40	4·95	3·33
U				0·034	0·008		0·035	0·157	0·043	0·088		0·585	1·21	1·34	1·06
Nb				0·024	0·095		0·737	0·875	1·34	0·865		2·52	1·71	2·32	3·78
Ta				0·001	0·008		0·038	0·051	0·096	—		0·207	—	0·170	0·25
K				257	216		1004	1124	949	1660		9835	9005	9735	13262
La				0·132	0·556		1·95	2·52	1·91	1·71		11·5	16·6	16·8	15·9
Ce				0·189	1·72		4·63	6·13	4·27	4·44		23·8	34·1	32·9	34·5
Pb				0·150	0·159		2·77	2·79	0·898	1·52		3·20	2·87	4·41	14·8
Pr				0·070	0·350		0·731	0·954	0·640	0·760		3·23	4·09	4·03	4·5

Table 3: continued

Element:	P1	P2	P3	MP1	MP2	QVF	Primitive basalt				QRA	Primitive basalt			
Remarks:	Fertile	Intermed.	Depleted	Ichinome.	Ichinome.	Original	Funagara	Zao	Azuma	Kayou	Original	Chokai	Kampu	Ichinomegara	Kyurokujima
Sr				2·30	34·6		172	246	134	280		386	673	435	489
Nd				0·372	1·91		3·76	4·61	2·956	3·89		14·3	17·3	16·2	18·6
Sm				0·184	0·715		1·20	1·43	0·896	1·28		3·58	3·38	3·64	4·32
Zr				4·45	8·78		22·8	26·8	17·1	30·4		85·9	61·9	63·3	101
Hf				0·065	0·262		0·719	0·859	0·545	1·03		2·18	1·68	1·68	2·38
Eu				0·066	0·265		0·524	0·576	0·373	0·700		1·11	1·09	1·12	1·36
Gd				0·307	1·02		1·643	1·72	1·16	1·741		3·90	3·03	3·66	4·25
Tb				0·064	0·181		0·310	0·316	0·218	0·321		0·636	0·469	0·548	0·655
Dy				0·448	1·09		2·08	2·02	1·35	2·23		3·98	2·80	3·32	3·91
Li				1·71	1·26		–	–	–	–		–	–	–	–
Y				2·53	5·87		12·2	11·0	7·89	15·5		23·8	20·8	18·9	20·7
Ho				0·100	0·250		0·461	0·433	0·302	0·522		0·841	0·593	0·694	0·824
Er				0·309	0·685		1·26	1·20	0·826	1·42		2·53	1·66	1·95	2·34
Tm				0·050	0·096		0·195	0·184	0·132	0·215		0·359	0·271	0·294	0·341
Yb				0·331	0·570		1·335	1·19	0·883	1·62		2·47	1·96	1·88	2·23
Lu				0·050	0·086		0·199	0·179	0·135	0·226		0·370	0·288	0·293	0·349
$^{87}Sr/^{86}Sr$							0·70400					0·70295			
$^{143}Nd/^{144}Nd$							0·51300					0·51300			
$^{206}Pb/^{204}Pb$							18·51					18·42			
$^{207}Pb/^{204}Pb$							15·58					15·50			
$^{208}Pb/^{204}Pb$							38·45					38·23			

*Total Fe reported as FeO.
Representative 'uncontaminated' primitive basalt compositions for the NE Japan arc are also shown. P1–P3, mantle peridotite compositions for fertile, intermediate, and depleted sources. Values were calculated from regression equations obtained from the GERM mantle peridotite database. 'Ichinome. MP1' is chemical composition of a depleted Ichinomegata mantle xenolith. 'Original' is the most magnesian basalt used for estimation of primitive basalt; 'Primitive basalt' is estimated primitive basalt compositions for the frontal- and rear-arc lavas of the NE Japan arc (see text for details). Mg-number = Mg/(Mg + Fe) molar proportion.

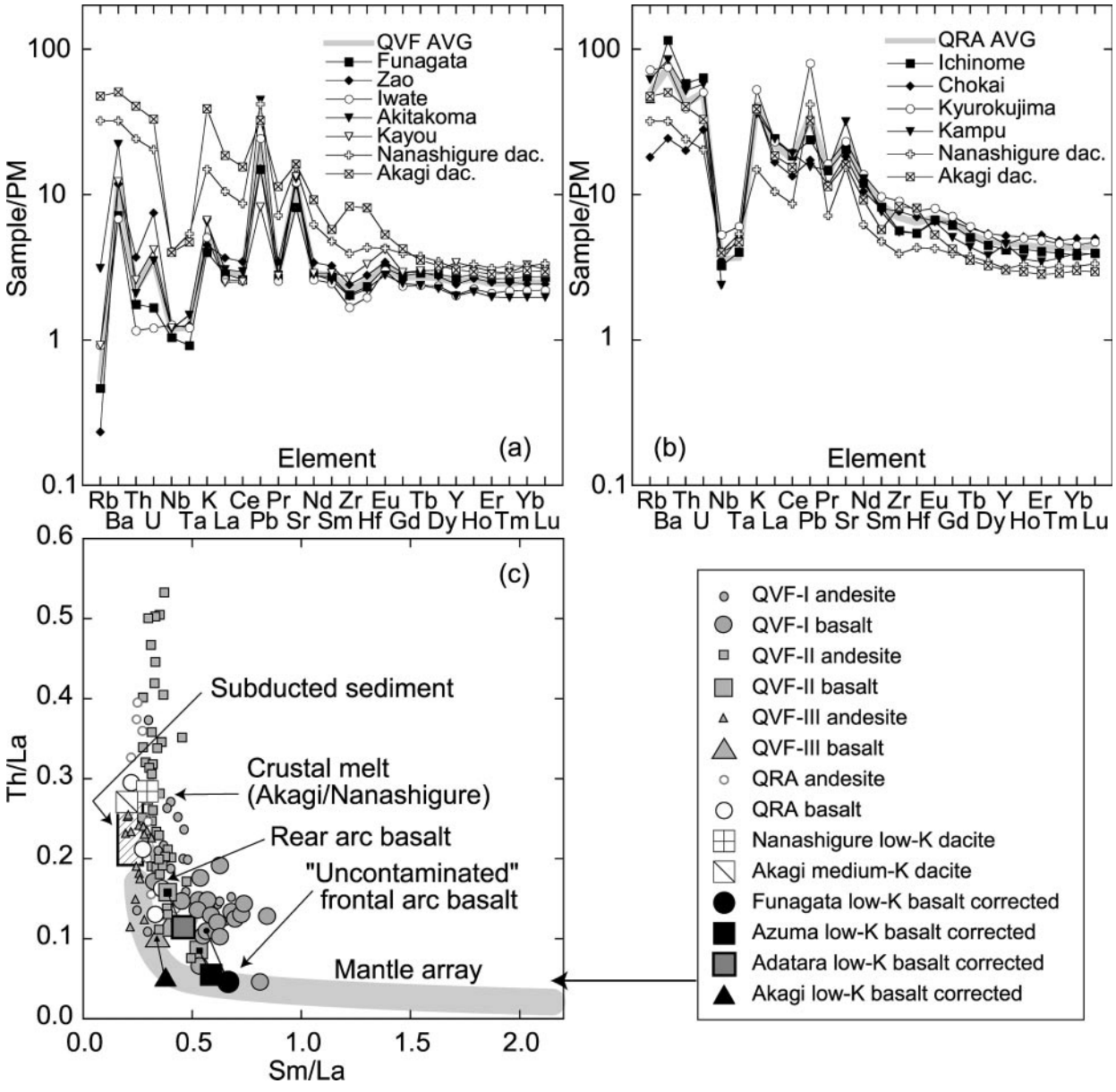

Fig. 12. Uncontaminated primitive basalt compositions for the NE Japan arc. (See Tables 3 and 5 for representative compositions.) (a) Plots of calculated primary basalt compositions for QVF-I, -II, and -III volcanoes with crustal melt compositions used for calculation; (b) plots of calculated primary basalt compositions for QRA; (c) Th/La vs Sm/La plots of uncorrected basalt and andesite compositions with corrected primary basalt compositions. AVG, average; dac., dacite. Shaded field for mantle array indicates mantle melt compositions (Plank, 2005) from a variably depleted mantle source. Subducted sediment composition is for the NE Japan arc (Plank & Langmuir, 1998).

et al., 2001) vs $^{87}Sr/^{86}Sr = 0{\cdot}7040$ and $^{206}Pb/^{204}Pb = 18{\cdot}51$ in the QVF]. The QRA primary basalt is as unradiogenic as the most radiogenic Izu rear-arc basalt ($^{87}Sr/^{86}Sr = 0{\cdot}7028$–$0{\cdot}7032$ and $^{206}Pb/^{204}Pb = 18{\cdot}25$–$18{\cdot}48$ in Izu vs $^{87}Sr/^{86}Sr = 0{\cdot}70295$ and $^{206}Pb/^{204}Pb = 18{\cdot}42$ in the QVF).

This result appears to contradict previous models (Shibata & Nakamura, 1997; Moriguti *et al.*, 2004), which suggested addition of more fluid from the subducted Pacific Plate in NE Japan than in Izu to modify the frontal-arc basalt source, but with insignificant fluid addition in the rear arc (Shibata & Nakamura, 1997), or differing source mantle compositions between Izu and NE Japan (Moriguti *et al.*, 2004). Uniform $^{10}Be/^{9}Be$ (Shimaoka & Kaneoka, 2000) and $\delta^{7}Li$ (Moriguti *et al.*, 2004) in the basalts across the NE Japan arc suggest little variation in the fluid flux at least for Be and Li from the slab to the mantle. This might be consistent with the

observed smaller range of Nd–Sr–Pb isotope variations between the QVF and QRA.

Heterogeneous mantle lithosphere does exist beneath NE Japan, based on the isotopic and chemical heterogeneity of the Ichinomegata mantle xenoliths (Zashu *et al.*, 1980; Aoki, 1987). However, suggested mantle heterogeneity in the basalt source region beneath NE Japan (Ohki *et al.*, 1994; Kersting *et al.*, 1996; Shuto *et al.*, 2006) appears to be minor, at least for the Quaternary lavas. This is strongly supported by the similarities in 'uncontaminated' primary basalt chemistry between the NE Japan and the Izu arcs, which are underlain by thicker continental lithosphere and relatively juvenile lithosphere, respectively. This result is significant for discussion of the origin of across-arc chemical variations.

Source mantle processes: an approach

The factors that control basalt chemistry in arcs are the composition of the mantle source (*Cs*) and slab flux (*Cf*), mineral abundances during melting (*Xa*, melting mineralogy; *Pa*, consumed mineralogy), and element partition coefficients between minerals and melts (*D*) and mode of melting. Estimating these parameters from natural basalts is not easy, because inversion calculations require a dataset from lavas produced by differing degrees of partial melting of the same source (Feigenson *et al.*, 1983; Sakuyama, 1983; Zou & Zindler, 1996; Caroff *et al.*, 1997). We cannot yet identify a site in NE Japan where this requirement is satisfied.

Our approach in this paper uses a forward model for mantle melting. First we approximate the mantle source composition using mantle xenoliths from the NE Japan arc. Then, primary magma compositions for QRA and QVF-I are evaluated to determine whether the mantle compositions are similar to those expected for these primary basalts. Melting phase relationships for the estimated mantle are calculated next, using the pMELTS program (Ghiorso & Sack, 1995; Hirschmann *et al.*, 1998; Ghiorso *et al.*, 2002) with the Aiabat_1ph program (Smith & Asimow, 2005*a*, 2005*b*) and compared with experimental results. Then the fluid composition is estimated, based on slab dehydration experimental results. Finally, the melting parameters *Cs*, *Cf*, *Xa* and *Pa*, and *F* (degree of partial melting) at appropriate *P–T* are applied to simulate the trace element, water, and isotope behaviors for fluid-fluxed melting (Zou, 1998).

Source mantle composition: Ichinomegata mantle peridotite

Direct information on the nature of the mantle peridotite magma source beneath NE Japan can be obtained from mantle xenoliths found at Ichinomegata, a rear-arc volcano located on the Oga Peninsula in NE Japan (Fig. 1; Aoki, 1971, 1987; Arai & Saeki, 1980). These xenoliths are spinel lherzolites or harzburgites that contain amphibole ± minor phlogopite. We analyzed five representative peridotite xenoliths from this site. The most depleted and enriched compositions are given in Table 3 (MP1 and MP2). A global mantle xenolith database has recently become available on the GERM web site (http://earthref.org/GERM/index.html?main.htm). Systematic major element chemical variations in mantle peridotites have been reported (Frey *et al.*, 1985; Herzberg *et al.*, 1988; Wasylenki *et al.*, 1996; Asimow *et al.*, 2001), particularly correlations between MgO, Al_2O_3, FeO, CaO and TiO_2. The range of variation is subdivided into P1 (fertile), P2 (intermediate), and P3 (depleted) compositions (Table 2). The Ichinomegata mantle xenoliths plot on the global trend, and contain ~37 wt % MgO, 3·51 wt % Al_2O_3, and 3·24 wt % CaO. They are classified into the intermediate to depleted peridotite groups in terms of their major element composition.

The Sr isotopic compositions of the xenoliths range between 0·7026 and 0·7035 (Zashu *et al.*, 1980), similar to that of the primary basalt compositions in the NE Japan arc. Incompatible trace element contents of the Ichinomegata xenoliths vary, but are generally depleted (Table 3). Trace element abundances in the peridotite xenoliths show relative HFSE and LREE depletion, in contrast to the intermediate major element characteristics of some of the xenoliths. However, the global database suggests that no systematic relationship exists between major element 'fertility' and trace element depletion (e.g. Niu, 2004). Consequently, the Ichinomegata xenoliths are considered typical depleted mantle peridotite in terms of their trace element and isotopic composition. Some LILE in the xenoliths are elevated, suggesting weak metasomatism, reflecting the presence of interstitial hydrous silicate minerals. The geochemically depleted characteristics of the Ichinomegata peridotites make them appropriate as the source of the Quaternary lavas of the NE Japan arc. This is a common requisite for island arc mantle sources, provided that the basalts originate from fluid-fluxed melting (Hawkesworth *et al.*, 1993*a*; Pearce & Parkinson, 1993; Davidson, 1996).

Can the Ichinomegata peridotites be the source of the primary magmas?

Given the estimated primary basalt compositions (Table 3), the next question is whether the Ichinomegata mantle peridotites can produce such melts under reasonable melting conditions. Partial melting calculations for peridotite compositions using the pMELTS program have been successful, albeit with some limitations (Hirschmann *et al.*, 1998, 1999*a*, 1999*b*). We applied the pMELTS model with Adiabat_1ph (version 1.6.2) program (Smith & Asimow, 2005*a*, 2005*b*) to the mantle peridotite composition of Ichinomegata under

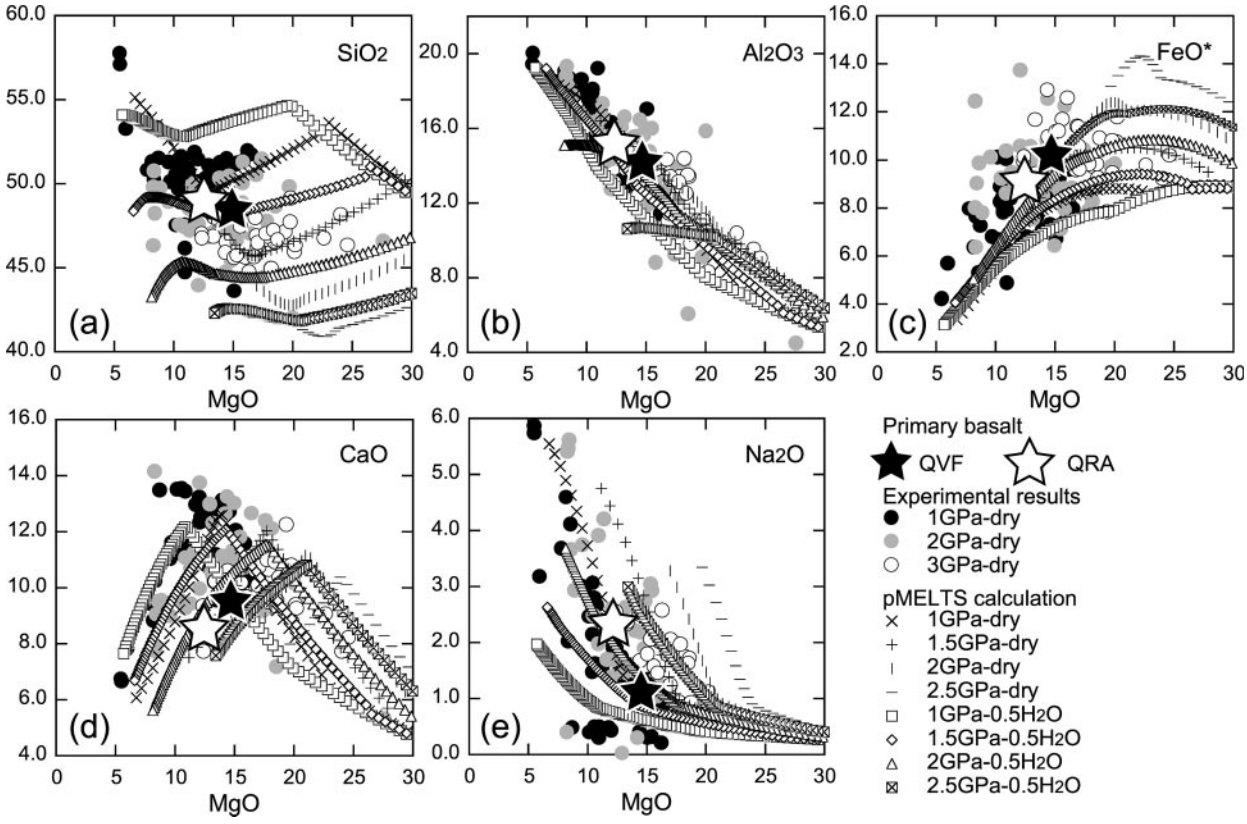

Fig. 13. pMELTS simulation results of partial melting of a depleted mantle peridotite. The starting composition is based on the alkali adjusted depleted mantle composition of the Ichinomegata mantle xenoliths listed in Table 3. Nine simulation experiments were performed for a pressure range of 1–2·5 GPa, degree of melting 2–40%, for dry and 0·5% H_2O conditions using pMELTS. Data points are melt compositions from peridotite melting experiments under dry conditions. Data from INFOREX 4.02 (Ariskin *et al.*, 1992), and experimental data (Ringwood, 1976; Mysen & Kushiro, 1977; Olafsson, 1980; Sen, 1982; Takahashi, 1986*b*; Canil, 1992; Hirose & Kushiro, 1993; Baker & Stolper, 1994; Bertka & Holloway, 1994*a*, 1994*b*; Baker *et al.*, 1995; Hirose & Kawamoto, 1995; Longhi, 1995; Kushiro, 1996; Falloon *et al.*, 1997; Kinzler, 1997; Robinson *et al.*, 1998; Walter, 1998). Calculated primary basalt compositions in Table 3 are shown as stars (filled, QVF; open, QRA).

both dry and water-undersaturated (0·5 wt % H_2O) conditions. An alternative garnet model function (Smith & Asimow, 2005*a*, 2005*b*) was set to accommodate the garnet stability condition problem. Water contents of the mantle beneath the NE Japan arc have been estimated at ~0·5 wt % through examination of the effect of water on basalt crystallization sequences (Sakuyama, 1983). The results of calculations at 1, 2, and 2·5 GPa are given in Fig. 13. Experimental melt compositions under dry and water-undersaturated conditions are also shown in the pressure range 0·7–1·4 GPa (shown as the 1 GPa symbol in Fig. 12), 1·5–2·4 GPa (2 GPa symbol), and 2·5–4 GPa (3 GPa symbol), based on the INFOREX database (Ariskin *et al.*, 1992). The pMELTS results are very similar to experimental results for elements such as Al_2O_3, FeO, CaO, and the alkalis (Fig. 13).

The compositions of peridotites used in melting experiments vary, but generally correspond to those expected for mantle peridotites such as KLB-1 (Takahashi, 1986*b*) or MM3 (Baker & Stolper, 1994). The Ichinomegata peridotite composition is similar to MM3, giving a good fit between modeled and experimental results. The calculation results require an intermediate mantle composition for the source of the NE Japan basalts (shown as open and filled stars in Fig. 12). The Ichinomegata mantle peridotite composition thus appears to be a good natural analogue for the mantle source of the NE Japan basalts.

Melting parameters in the mantle source

If major element compositions are plotted against degree of partial melting (*F*%; Fig. 14), there is no pressure dependence in K_2O contents, because the behavior of K is unrelated to major mantle minerals during melting. 'Biotite' is stabilized in water-bearing pMELTS calculations at lower degrees of melting, and K_2O decreases at lower *F* (Fig. 14a). The degree of partial melting can be estimated from the *F* %–K_2O diagram by plotting the primary basalt compositions for the QVF and QRA (Table 3), suggesting ~3–7% melting for QRA and

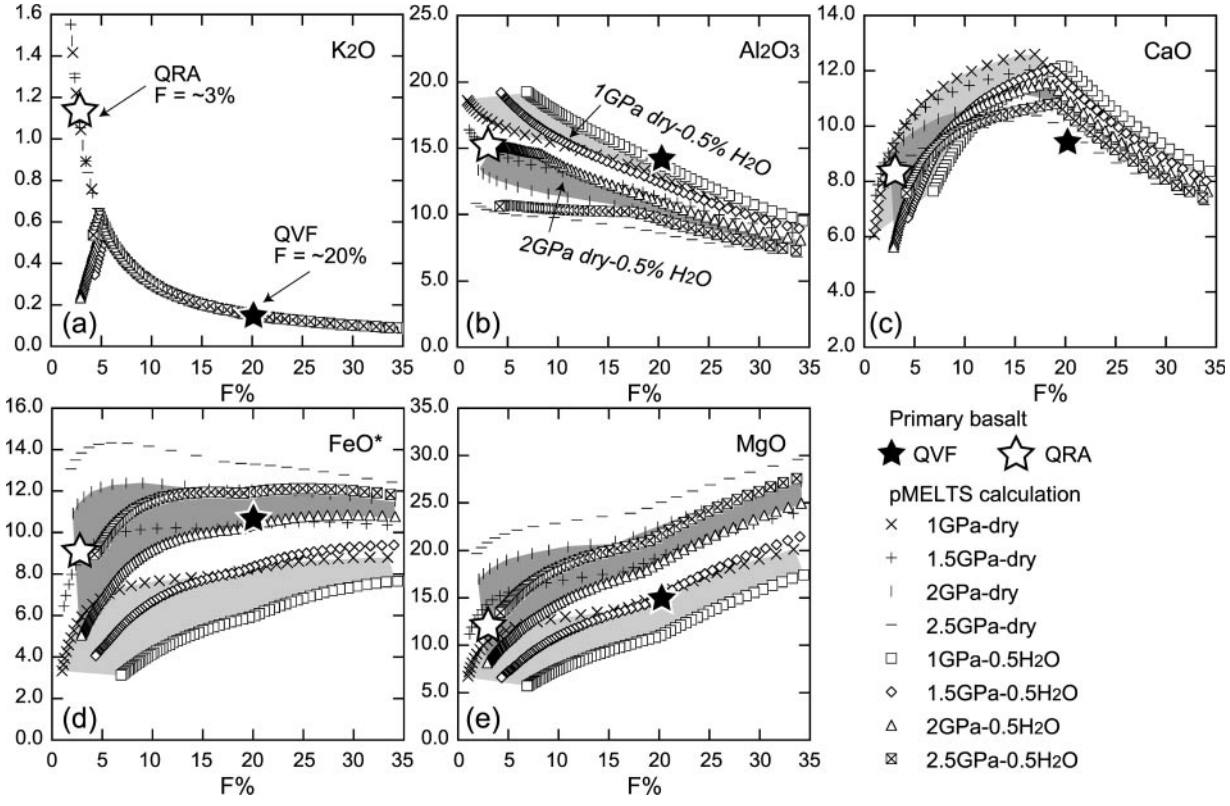

Fig. 14. pMELTS simulation of partial melting of a depleted mantle peridotite, showing wt % oxide vs percent partial melting F(%). Light shaded areas indicate dry to 0·5% H_2O melting regions at 1 GPa. Dark shaded areas indicate dry to 0·5% H_2O melting regions at 2·5 GPa.

~20–25% melting for QVF, provided that the K content of the source mantle is similar. As the isotopic and major element compositions of the source mantle are more or less similar for the QRA and QVF, this assumption appears to be a good first approximation.

The primary QRA and QVF basalt compositions plot in the middle of the 2 GPa experimental melts for SiO_2, Al_2O_3 and FeO (Fig. 13a–c). CaO content is controlled by the stability of clinopyroxene, and CaO increases with increasing MgO until clinopyroxene is consumed. The F at clinopyroxene consumption is about 18%, independent of pressure (Fig. 14c). In contrast, the MgO and FeO (and SiO_2 and Al_2O_3) contents of the melts are pressure-dependent, as a result of changes in the stability field of orthopyroxene. This leads to a systematic shift of the maximum CaO contents in the CaO–MgO diagram (Fig. 13d). The experimental melts also show the same effect when the 1 and 3 GPa results are compared (Fig. 13). The low CaO content in the QRA primitive basalt (Fig. 4 and Table 3) may be due to elevated pressure in the QRA source, resulting in a shift of the melting curve to the right (see 1 GPa and 2 GPa water-bearing melting curves in Fig. 13d). The pressure dependence of the melt composition can be expressed using a MgO–Na_2O diagram (Fig. 13e). The elevated Na_2O content at similar MgO of the QRA basalt compared with QVF suggests a greater pressure of melting of the QRA source; ~1 GPa for the QVF and ~2 GPa for the QRA primary basalts. Decreased SiO_2 contents at greater pressure are suggested by both experimental results and pMELTS calculations (see Fig. 13a). The SiO_2 contents of the estimated primary basalt compositions for the QVF and QRA may be significantly over- or underestimated. Although the SiO_2 contents of the primary basalts are similar in our estimation, the frontal-arc primary basalts may contain several weight per cent more SiO_2 and rear-arc basalt less than our values (see Fig. 13a). However, this discrepancy does not affect the following discussion.

An elevated pressure of melting results in greater FeO and MgO contents (and SiO_2 undersaturation and low Al_2O_3) as shown by element–F diagrams (Fig. 14b–e). The similar FeO and MgO contents in the QRA and QVF-I basalts could be due to the greater degree of partial melting at low pressure required to produce the QVF basalt. This interpretation is consistent with the estimated F values from the F–K_2O diagram. A greater degree of partial melting beneath the frontal arc is also consistent with the depleted incompatible trace element characteristics of the basalts (Fig. 8; Sakuyama, 1983). Based on the 'best fit' on the diagrams in Fig. 14b–e, melting of water-bearing peridotite at a pressure of ~2 GPa and degrees of melting of 3–6% for the QRA and ~1 GPa and 20–25% for the QVF basically explain

the chemical differences between the frontal- and rear-arc primitive basalts.

As shown by available seismic tomography, depths to the top of the low-velocity region in the mantle wedge range from 30 to 60 km, decreasing gradually from beneath the rear arc to beneath the frontal arc (Hasegawa *et al.*, 1991; Zhao *et al.*, 1992; Nakajima & Hasegawa, 2003; Nakajima *et al.*, 2005). Estimated melting pressures are thus consistent with the geophysical observations, suggesting that further mantle melting occurs close the base of the arc crust at a depth of ~30 km (Zhao *et al.*, 1992).

Fluid-fluxed melting beneath the NE Japan arc

In the final modeling step, we calculate the consistency of our model with the trace element and isotopic compositions of the lavas. Both the rear-arc and frontal-arc basalts have trace element characteristics indicative of slab-fluid addition, such as high Ba/Th or elevated LILE and LREE relative to Nb–Ta or Zr–Hf. The isotopic compositions of the primary frontal-arc basalts have slightly radiogenic Pb and Sr, even after removal of the effect of the 'crustal filter'. Such mantle characteristics have been discussed for both the Izu (Hochstaedter *et al.*, 2001; Ishizuka *et al.*, 2003) and NE Japan arcs, and have been explained in terms of the varied flux of slab-derived fluid or melt. In contrast, homogeneous ^{10}Be and δ^7Li (Shimaoka & Kaneoka, 2000; Moriguti *et al.*, 2004) and subtle variations in Nd–Sr–Pb isotope compositions (this study) suggest smaller variations in the amount of slab components than previously thought. Bearing this in mind, we examine the origin of the across-arc chemical variations in the NE Japan arc with a quantitative mantle-melting model.

The potential slab components are: (1) fluid derived from altered oceanic crust (AOC; Staudigel *et al.*, 1996; Kogiso *et al.*, 1997; Bebout *et al.*, 1999; Churikova *et al.*, 2001; Hochstaedter *et al.*, 2001); (2) fluid derived from subducted sediment (Arculus & Johnson, 1981; Arculus & Powell, 1986; Pearce & Parkinson, 1993; Aizawa *et al.*, 1999; Johnson & Plank, 1999); (3) melt of AOC (Defant & Drummond, 1990); (4) sediment melt (Cousens & Allan, 1992; Yogodzinski *et al.*, 1994; Kelemen *et al.*, 1998; Johnson & Plank, 1999; Shimaoka & Kaneoka, 2000; Tatsumi & Hanyu, 2003). Based on geophysical constraints, slab-derived components beneath the NE Japan arc are expected to be fluids rather than melts (Hasegawa *et al.*, 1991; Peacock, 1996; Peacock & Wang, 1999; Nakajima & Hasegawa, 2003; Nakajima *et al.*, 2005), because the seismic structure does not reveal any low-velocity region at the surface of the Pacific Plate slab. This may negate the possibility of slab melting. Thermal models of the mantle wedge also suggest that no slab melting occurs beneath NE Japan (Peacock, 1996; Peacock & Wang, 1999). There is evidence of recycling of ^{10}Be, but the rate of recycling is too small to be due to sediment melt (Shimaoka & Kaneoka, 2000). Addition of slab melt can also be neglected, because this should produce high-Mg andesite but not basalt (Yogodzinski *et al.*, 1994; Kelemen *et al.*, 1998; Johnson & Plank, 1999; Shimaoka & Kaneoka, 2000; Tatsumi & Hanyu, 2003). In the following section we examine a series of model calculations for slab-fluid-fluxed melting of mantle peridotite.

Open-system partial melting: melting parameters

The numerical model for incompatible elements used here is an open-system melting model (Zou, 1998). In this model, the variables are mantle porosity (ϕ), fluid proportion (β), degree of melting (F), mantle mineralogy (Xa), consumed mineral proportion (Pa), mantle composition (Cs), fluid composition (Cf), and partition coefficients (D). Mass balance calculations were based on a dynamic melting equation at a given porosity (ϕ) and degree of melting (F). Additional mass balance is introduced for the fluid influx parameter (β) and composition (Cf) [for details see Zou (1998)]. We first approximate the fluid proportion $\beta = 0{\cdot}5$ wt % of the mantle mass, based on the estimates of the water content of the mantle source, and D values determined from water-saturated experimental run products (Green *et al.*, 2000). D values during hydrous partial melting differ from those under dry or water-undersaturated conditions (Gaetani *et al.*, 2003; McDade *et al.*, 2003). However, the general properties are still similar, and the use of D values determined in water-bearing systems best represents the melting conditions that we expect. The mantle mineralogy during fluid-fluxed melting is difficult to estimate. We simply apply the calculated Xa and Pa at a given F, at 1 and 2 GPa and 0·5 wt % H_2O using pMELTS (Fig. 15, Table 4). The role of hydrous silicate minerals is discarded for simplicity, and modal proportions of the anhydrous silicate minerals are normalized to 100%. The effects of additional silica and other major elements or volatiles other than H_2O from the fluid are not considered (Manning, 2004).

Open-system partial melting: source compositions

Slab-derived fluid compositions were calculated using experimentally determined partition coefficients (D_{fluid}) derived from the MORB dehydration experiments of Kessel *et al.* (2005). Similar experimental results have been published for MORB (Kogiso *et al.*, 1997) and sediments (Aizawa *et al.*, 1999; Johnson & Plank, 1999). As we assume the sediment component contributes little to the composition of the fluid (see below), the D_{fluid} values for MORB dehydration provide the best estimate. The data of Kogiso *et al.* (1997) cannot be used to

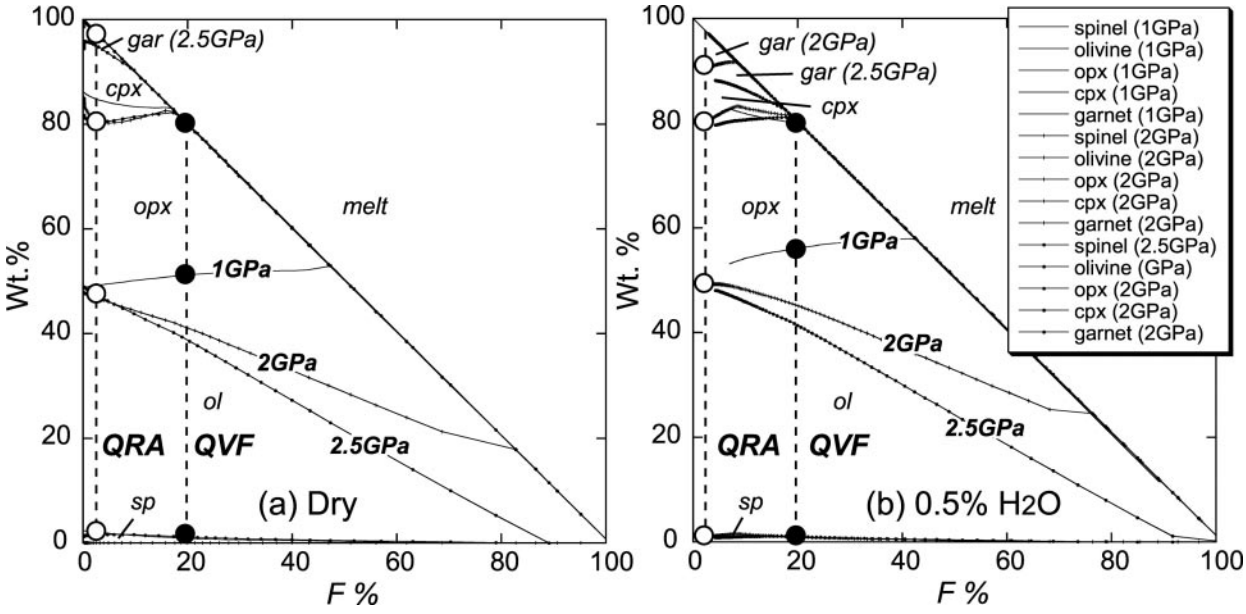

Fig. 15. Mineral modes (wt %) and degrees of partial melting (F%) of Ichinomegata mantle peridotite at 1–2·5 GPa under dry (a) and 0·5 wt % H_2O (b) conditions. Mineral modes and amounts of minerals consumed during melting are given in Table 4. Phase proportion boundaries between olivine and clinopyroxene differ greatly at 1, 2, and 2·5 GPa.

obtain D_{fluid} values directly as they require assumption of the dehydration rate of MORB. Stabilization of phengite may alter D_{fluid} values in the K-bearing eclogite system (Schmidt & Poli, 1998; Kessel *et al.*, 2005), and this effect is discussed in a subsequent section.

The slab sediment and altered oceanic crust (AOC) compositions are from various sources such as terrigeneous sediments (UCC; Taylor & McLennan, 1985), or pelagic sediments (Plank & Langmuir, 1998) and AOC (Staudigel *et al.*, 1996). We found that UCC provides a better fit for our model, particularly in terms of Sr abundance (Fig. 16a). Subducted pelagic sediments (Plank & Langmuir, 1998) have very low Sr contents, and this leads to a deficit in the Sr budget for the source. For this reason, we use the UCC values for our model.

Conventional Pb isotope plots best constrain the contributions of SED and MORB components, because the mixing trends are all linear (Shibata & Nakamura, 1997; Hochstaedter *et al.*, 2001; Hauff *et al.*, 2003; Ishizuka *et al.*, 2003; Moriguti *et al.*, 2004). Estimated mixing amounts range from 3 to 10% SED to MORB. We adopted the results of the Hauff *et al.* (2003) model based on mixing of AOC and SED in the Pacific Plate at Ocean Drilling Program (ODP) Site 1149 and 801, and derived 7% SED for QVF and 3% SED for QRA sources by assuming a depleted mantle wedge (DM) composition at $^{206}Pb/^{204}Pb = 17{\cdot}6$ and $^{208}Pb/^{204}Pb = 37{\cdot}3$.

For the trace element composition of the slab fluid, simple mixing of UCC (Taylor & McLennan, 1985) and N-MORB (Pearce & Parkinson, 1993) was assumed because of the large variability in natural AOC composition (Staudigel *et al.*, 1996). The source region represented by the top of the oceanic slab may be a physical mixture of metamorphosed SED and AOC. Metamorphosed AOC compositions reported in the literature have chemical signatures inherited from adjacent SED components (Kogiso *et al.*, 1997; Spandler *et al.*, 2004). Our simple assumption of a SED–MORB mixed source (hybrid) is acceptable as a first-order approximation. Moreover, we examined various combinations of mixing–melting using SED–fluid, SED–melt, AOC–fluid, and MORB–fluid. However, we found that none of these combinations can satisfy the constraints imposed by trace element and Sr–Nd–Pb isotopes in our fluid-fluxed melting model. We also confirmed that our SED–MORB physical source mixing model does not alter the important constraint from Pb isotopes, and gives the same isotopic mixing proportions as deduced from SED–AOC components (Hauff *et al.*, 2003). The MORB–SED hybrid slab compositions are shown in Table 5 and Fig. 16 as Hybrid_0·07 for QVF and Hybrid_0·03 for QRA.

Experimentally determined D_{fluid} values vary widely, dependent mainly on temperature and fluid states (Kessel *et al.*, 2005). At high pressure (>5 GPa), fluids behave supercritically (above the second critical endpoint; Kessel *et al.*, 2005), increasing the solubility of silicate components. D_{fluid} is also temperature dependent at constant pressure because of the increase in solubility of components with increased temperature (Kessel *et al.*, 2005).

Table 4: Partial melting parameters for trace element model calculations

	F(%)					
	3	5	10	15	20	25
1 GPa, 0·5 wt % H_2O						
Xa(ol)	0·585	0·605	0·655	0·710	0·775	0·828
Xa(opx)	0·307	0·303	0·298	0·281	0·217	0·164
Xa(cpx)	0·092	0·078	0·035	—	—	—
Xa(gar)	—	—	—	—	—	—
Xa(sp)	0·015	0·014	0·011	0·010	0·009	0·008
Pa(ol)	−0·445	−0·403	−0·327	−0·282	−0·248	−0·223
Pa(opx)	0·630	0·581	0·482	0·512	0·681	0·750
Pa(cpx)	0·708	0·726	0·768	0·706	0·515	0·427
Pa(gar)	—	—	—	—	—	—
Pa(sp)	0·106	0·096	0·077	0·063	0·052	0·046
2 GPa, 0·5 wt % H_2O						
Xa(ol)	0·508	0·513	0·530	0·543	0·560	0·570
Xa(opx)	0·354	0·376	0·403	0·437	0·429	0·420
Xa(cpx)	0·098	0·093	0·053	0·004	—	—
Xa(gar)	0·025	0·002	—	—	—	—
Xa(sp)	0·015	0·017	0·014	0·013	0·011	0·010
Pa(ol)	0·129	0·200	0·210	0·228	0·255	0·276
Pa(opx)	−0·793	−0·728	−0·404	−0·327	−0·103	0·018
Pa(cpx)	0·315	0·330	0·552	0·654	0·506	0·418
Pa(gar)	1·498	1·325	0·675	0·452	0·337	0·279
Pa(sp)	−0·149	−0·127	−0·033	−0·007	0·005	0·009

Mantle modal compositions and consumed mineral modes are modeled by the pMELTS program. *F*(%), degree of partial melting; *Xa*(mineral), modal composition of minerals at given *F*; *Pa*(mineral), consumed mineral modes during melting at given *F*. pMELTS (Ghiorso & Sack, 1995; Ghiorso *et al.*, 2002) simulation calculations are performed on DM-Ichinomegata source mantle composition in Table 3 at different pressures. Phase relationships are also shown graphically in Fig. 14, suggesting that addition of trace amounts of water does not significantly affect the phase relationships. *Pa(gar)* at 2 GPa 3% melting condition is intentionally altered by the authors to 0·8, to accommodate the excess HREE problem shown by the trace element model calculations in Fig. 16. Stabilization of trace amount of garnet near the solidus at >2 GPa was also confirmed by Hirschmann *et al.* (1999b).

Our single-stage fluid-fluxed melting model does not assume any chemical reaction of the slab fluids with the mantle peridotite between the site of slab dehydration and the mantle melting regions. This is assumed because of the relatively rapid fluid transport in the mantle wedge deduced from U–Th disequilibria (e.g. Turner *et al.*, 1998), which minimizes trace element fractionation during peridotite–fluid interaction (Hawkesworth *et al.*, 1993*b*). In our model, a fluid with high incompatible element abundances is necessary in the rear arc, because of the limitation imposed on the fluid-flux proportion at low degrees of melting, which affects the water content of the primary basalt. Mainly for this reason, we employ D_{fluid} at 4 GPa, 900°C for QVF and 6 GPa, 1000°C for our QRA models. The resultant hybrid fluid compositions for QVF (4G900FA) and QRA (6G1000RA) are indicated in Table 5 and Fig. 16. The detailed water mass balance model will be considered in a subsequent section.

The trace element composition of the source mantle is also variable and is difficult to assess. We initially assumed that the composition of the entire mantle asthenosphere beneath NE Japan is identical to that of the rear-arc mantle source that produced the MORB of the Japan Sea oceanic crust. The chemical composition of the mantle source was estimated from that of Japan Sea MORB (Cousens & Allan, 1992; Pouclet *et al.*, 1995) by assuming 25% melting at typical MORB-source mantle melting conditions (calculated by pMELTS). This basalt was extracted entirely from the source mantle to calculate the residual mantle composition. The chemical composition calculated by the model compares very well with the most depleted mantle peridotite composition from Ichinomegata except for some LILE added by metasomatism (Fig. 16a and b). We used the composition of this model mantle in subsequent calculations. The source mantle composition (Ichinome DM) used is given in Table 5.

Open-system partial melting: calculation results

Calculations were made using the melting parameters and mantle-fluid compositions discussed above. The results are shown in Figure 16c and d and Table 5. For $F = 20$–25% melting of Ichinome DM peridotite with $\beta = 0{\cdot}7\%$ proportion of 4G900FA fluid with Hybrid_0·03 fluid source reproduces the frontal-arc primary Funagata basalt composition within a range of $\pm \sim 30\%$ in terms of element abundances (Fig. 16c and Table 5). Rb is an exception, because of the very high D_{fluid} values for Rb. In the calculations, the estimated *F* based on the trace element model largely depends on D_{fluid} and β, which consequently alters the fluid element abundances and thus *F*. The fluid proportion β was fixed at $\sim 0{\cdot}5\%$ based on major element modeling. A slight adjustment of β to $0{\cdot}7\%$ does not greatly alter the results. Degrees of melting of 20–25% in the QVF source are consistent with pMELTS calculations for major elements. Therefore, the β and *F* values estimated by the trace element model are generally consistent with the major element modeling.

For the QRA, using 6G1000RA fluid with Hybrid_0·03 fluid source and Ichinome DM, *F* is estimated to be about 3–4% at $\beta = 0{\cdot}2\%$ for Chokai primary basalt (Fig. 16d and Table 5). With the same conditions at an increased flux proportion of $\beta = 0{\cdot}4\%$, the same

Table 5: Chemical compositions used for trace element model calculations and calculated results for QVF and QRA magmas

	Slab source material (ppm)				*D* for dehydration		Hybrid slab fluid (ppm)		Mantle (ppm)
	MORB	UCC	Hybrid_0·07	Hybrid_0·03	4G900	6G1000	4G900FA	6G1000RA	Ichinome. DM
Rb	0·56	112	8·36	3·90	77·296	67·315	646	263	0·004
Ba	6·30	550	44·36	22·61	42·925	179·898	1904	4067	0·075
Th	0·12	10·7	0·86	0·44	6·421	61·649	5·53	26·9	0·0014
U	0·047	2·8	0·24	0·13	5·974	25·010	1·43	3·24	0·0005
Nb	2·33	14·0	3·15	2·68	3·679	6·960	11·58	18·7	0·0241
Ta	0·13	0·96	0·19	0·15	1·772	6·835	0·333	1·06	0·002
K	1079	28225	2979	1894	11·347	74·332	33807	140752	16·0
La	2·50	30·0	4·43	3·33	11·347	74·332	50·2	247	0·060
Ce	7·50	64·0	11·46	9·20	5·192	35·363	59·5	325	0·1892
Pb	0·30	20·0	1·68	0·89	31·405	46·627	52·7	41·5	0·012
Pr	1·32	7·10	1·73	1·49	3·352	27·469	5·78	41·0	0·055
Sr	90·0	350	108	97·8	21·087	82·275	2282	8046	5·30
Nd	7·30	26·0	8·61	7·86	1·513	19·576	13·02	153	0·400
Sm	2·63	4·50	2·76	2·69	0·371	3·753	1·02	10·1	0·150
Zr	74·0	190	82·1	77·5	0·393	3·648	32·3	283	5·00
Hf	2·05	5·8	2·31	2·16	0·519	5·263	1·20	11·4	0·150
Eu	1·02	0·88	1·01	1·02	0·208	2·049	0·210	2·08	0·0900
Gd	3·68	3·80	3·69	3·68	0·094	1·027	0·348	3·78	0·330
Tb	0·67	0·64	0·668	0·669	0·062	0·664	0·041	0·444	0·0642
Dy	4·55	3·50	4·48	4·52	0·030	0·301	0·132	1·36	0·4479
Y	28·0	22·0	27·6	27·8	0·032	0·369	0·882	10·3	2·90
Ho	1·01	0·80	0·995	1·00	0·022	0·221	0·022	0·222	0·100
Er	2·97	2·30	2·92	2·95	0·014	0·140	0·041	0·414	0·309
Tm	0·456	0·33	0·447	0·452	0·013	0·116	0·006	0·053	0·0504
Yb	3·05	2·20	2·99	3·03	0·011	0·092	0·034	0·278	0·3314
Lu	0·455	0·32	0·446	0·451	0·009	0·077	0·004	0·035	0·0501

	Primary basalt composition (ppm)								
	Funagata	QVF *F*20	Diff. (%)	Chokai	QRA *F*3β0·2	Diff. (%)	Kampu	QRA *F*3β0·4	Diff. (%)
Rb	0·294	21·06	7053	11·5	14·3	24·0	39·4	32·0	−18·8
Ba	50·1	62·3	24·6	170	221	30·0	592	495	−16·4
Th	0·15	0·189	26·1	1·71	1·53	−10·6	4·40	3·39	−23·1
U	0·035	0·050	42·0	0·585	0·194	−66·8	1·21	0·416	−65·6
Nb	0·737	0·514	−30·3	2·52	1·65	−34·5	1·71	2·78	63·5
Ta	0·038	0·022	−40·5	0·207	0·111	−46·6	–	0·173	–
K	1003	1217	21·3	9835	8035	−18·3	9005	17416	93·4
La	1·95	2·04	4·4	11·5	14·5	25·7	16·6	30·0	80·5
Ce	4·63	3·14	−32·0	23·8	20·6	−13·3	34·1	39·9	14·3
Pb	2·77	1·89	−31·7	3·20	2·18	−31·8	2·87	4·55	53·9
Pr	0·731	0·528	−27·8	3·23	3·16	−2·2	4·09	5·16	26·0
Sr	172	112	−34·9	386	471	22·0	673	883	31·2
Nd	3·76	2·86	−23·9	14·2	14·9	4·4	17·3	21·2	22·2
Sm	1·20	0·936	−22·2	3·57	3·19	−10·9	3·38	3·33	−1·49
Zr	22·8	30·9	35·5	85·9	82·1	−4·5	61·9	88·2	42·4
Hf	0·719	0·918	27·7	2·18	2·08	−4·3	1·68	2·36	40·2

Table 5: continued

	Primary basalt composition (ppm)								
	Funagata	QVF *f* 20	Diff. (%)	Chokai	QRA *f* 3β0·2	Diff. (%)	Kampu	QRA *f* 3β0·4	Diff. (%)
Eu	0·524	0·547	4·3	1·11	1·45	30·9	1·09	1·39	27·1
Gd	1·64	2·00	21·6	3·90	4·54	16·3	3·03	4·05	33·5
Tb	0·310	0·383	23·7	0·636	0·719	13·1	0·469	0·606	29·1
Dy	2·08	2·64	26·9	3·98	4·01	0·7	2·80	3·23	15·3
Y	12·2	16·5	35·3	23·8	22·4	−6·0	20·8	17·0	−18·4
Ho	0·461	0·569	23·6	0·841	0·766	−9·0	0·593	0·587	−0·91
Er	1·26	1·71	35·6	2·53	2·11	−16·4	1·66	1·601	−3·57
Tm	0·195	0·261	33·7	0·359	0·283	−21·2	0·271	0·216	−20·45
Yb	1·34	1·61	20·2	2·47	1·58	−36·1	1·96	1·21	−38·42
Lu	0·199	0·238	19·2	0·370	0·239	−35·3	0·288	0·181	−37·15

MORB, normal MORB composition of Pearce & Parkinson (1993). UCC, upper crust composition of Taylor & McLennan (1985). Hybrid_0·07, hybrid slab composition calculated by mixing between MORB and UCC in mixing proportions 0·07:0·93. Hybrid_0·03, same as previous composition, but mixing proportions 0·03:0·97. *D*, experimentally determined bulk distribution coefficient between solid and fluid for MORB dehydration by Kessel *et al*. (2005). 4G900FA, fluid composition at 4 GPa, 900°C using Hybrid_0·07 as starting composition. 6G1000RA, fluid composition at 6 GPa, 1000°C using HYBRID_0·03 as starting composition. *D* value for K is assumed to be equal to that for La. Ichinome. DM is depleted mantle composition obtained by subtracting metasomatic composition from a depleted Ichinomegata mantle zenolith. Hybrid slab fluid is slab fluid composition calculated using hybrid slab composition and *D* values. Funagata and Chokai are representatives of QVF and QRA basalt compositions estimated after crustal contamination and fractional crystallization corrections. QVF *F*20 and QRA *F*3 are calculated trace element compositions based on fluid-fluxed melting model of Zou (1993). Melting conditions are given in Table 3 and Fig. 13. Diff. (%) is the per cent difference between primary basalt and calculated primary melt compositions.

calculations almost reproduce the most enriched rear-arc primary basalt from Kampu (Kampu is not shown in Fig. 16d, see Table 5 and Fig. 12 for Kampu primary basalt compositions). The flux proportion and degree of melting are consistent with the pMELTS results of $F = 3$–7% and $\beta = 0{\cdot}5\%$ (Fig. 16). This degree of melting using a mineralogy appropriate for ~2 GPa (Table 4) reproduces the LILE and LREE; however, strongly depleted HREE are not reproduced by the residual mineralogy from the pMELTS calculations. Adjustment of the Pa garnet melting mode from 1·498 to 0·80 reduces the discrepancy between the modeled melts and the QRA primary basalt. The occurrence of garnet is expected at pressures >2 GPa based on garnet stability corrected pMELTS (Smith & Asimow, 2005*a*, 2005*b*). The garnet stability limit in near-solidus experimental studies lies at pressures corresponding to depths of ~70 km (Robinson & Wood, 1998). Involvement of small amounts of garnet is thus expected for the QRA source at lower degrees of partial melting, but the exact amount is not well constrained other than by the trace element modeling. The use of 4G900FA fluid with melting conditions for the rear arc requires a fluid-flux proportion >1%, which is too high for the flux estimated from the major elements. If we accept the melting parameter constraints from pMELTS results and the water content of the primary basalts (see below), slab-derived fluids with very high abundances of incompatible trace elements are required.

Open-system partial melting: H_2O in the primary basalts

The H_2O contents of the calculated primary basalt can be estimated by assuming appropriate mineral–melt partition coefficients for H_2O. The behavior of water is considered to be similar to LREE (e.g. Ce) if the system is not extremely undersaturated in water (Kurosawa, 1993; Stolper & Newman, 1994; Straub & Layne, 2003). By applying the olivine–melt partitioning of H_2O data of Kurosawa (1993) and assumed partition coefficients for the other minerals, open-system melting calculations were performed to determine H_2O contents in the melt (Fig. 17). The H_2O contents in the primary basalts at the given melting conditions are about 1·6–2·8 wt % for the QRA ($\beta = 0{\cdot}2$–$0{\cdot}4\%$, respectively) and 2·5 wt % for the QVF ($\beta = 0{\cdot}7\%$). These estimates are in good agreement with the previous estimates of the amount of mantle-derived water in the NE Japan arc magmas (Sakuyama, 1983; Tatsumi *et al.*, 1983). Equal amounts of water in the primary basalts across-arc of about 2–3 wt % are consistent with melt inclusion studies in other

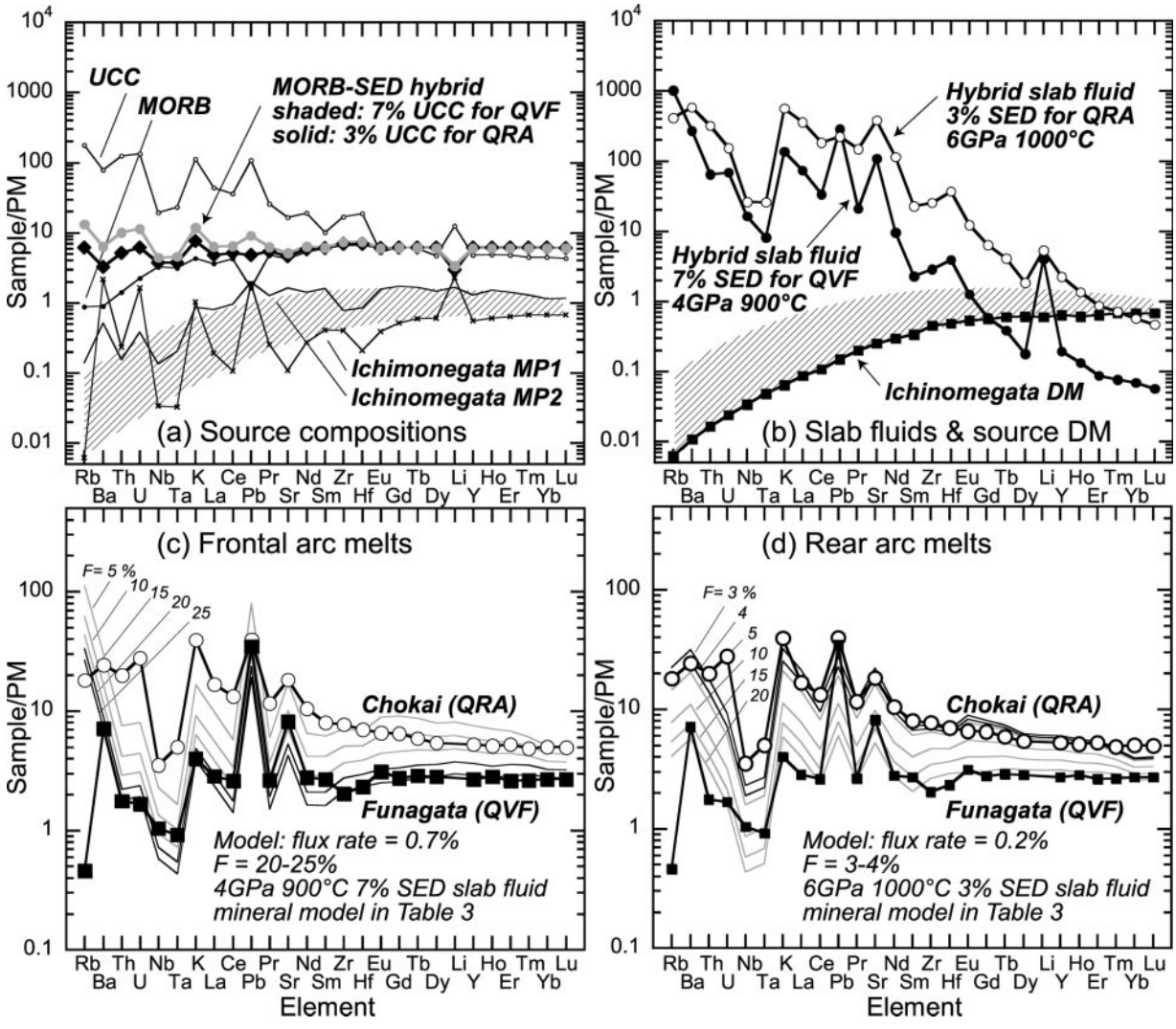

Fig. 16. (a) Primitive mantle normalized trace element patterns of Upper Continental Crust (UCC), terrigeneous sediments (Taylor & McLennan, 1985), MORB (Pearce & Parkinson, 1993), and Ichinomegata mantle peridotites (MP1 and MP2; this study, Table 5). MORB–SED hybrid slab compositions are shown by black diamonds (Hybrid_0.03) and grey filled circles (Hybrid_0.07). (b) Calculated fluid compositions based on (a) and MORB dehydration experiments (Kessel *et al.*, 2005) with 4G900 and 6G1000 distribution coefficients for Hybrid_0·07 and Hybrid_0·04 (Table 5). (c) and (d) show calculated results of open-system melting (Zou, 1998) using the parameters given in Tables 4 and 5 for frontal-arc and rear-arc primary basalts of the NE Japan. *F*, degree of partial melting in per cent. Diagonally shaded areas in (a) and (b) indicate compositional range of possible unmetasomatized Ichinomegata mantle xenoliths compositions.

arcs (Stolper & Newman, 1994). Such water contents obviously require a lower fluid proportion ($\beta = 0{\cdot}2$) in the rear arc, because the degree of partial melting of the rear-arc mantle is smaller.

Open-system partial melting: Sr–Nd–Pb isotope systematics

The same open-system fluxed melting model was used to numerically simulate the behavior of the radiogenic isotopes. To connect the fluid-flux melting model to the AOC, SED, and DM sources, solid–solid slab source mixing calculations between MORB (AOC) and SED were first performed (Fig. 18: source mixing trends). The source mixing calculations were based on the isotopic compositions of AOC and SED (Hauff *et al.*, 2003) and element abundances of UCC and MORB (Table 5). Mixing proportions of 3% and 7% SED were used for the QRA and QVF hybrid slab fluid sources, as noted above. The isotopic compositions at these mixing proportions on the source mixing curves (Fig. 18) correspond to those of Hybrid_0·03 and Hybrid_0·07, and thus 6G1000RA and 4G900FA slab-derived fluid compositions, respectively. It should be noted that the conventional Pb isotope plot of Fig. 18a

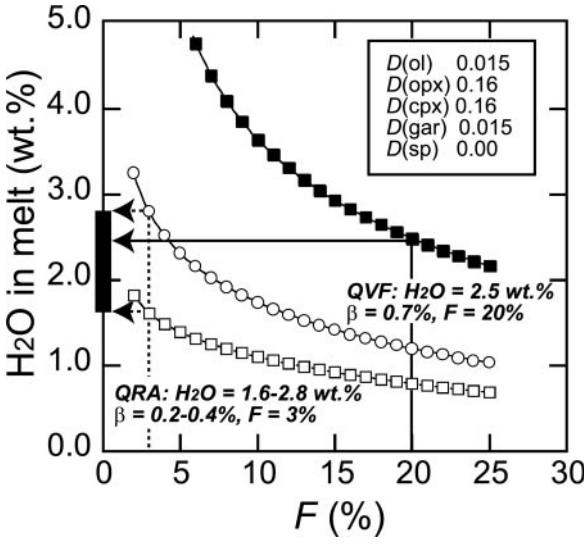

Fig. 17. Calculated water contents in the primary basalts produced by fluid-fluxed open-system mantle melting for QRA and QVF. *D* values used for H_2O partitioning between minerals and melt are given in the figure. ■, Funagata (QVF); □, Chokai (QRA); ○, Kampu QRA. (See text for details of the models.)

was primarily used to satisfy the mass balance between SED, MORB, and DM, as discussed above.

Fluid-fluxed melting calculations were performed for Sr–Nd–Pb isotopes using hybrid slab fluids 6G1000RA and 4G900FA, and Ichinome DM compositions. The isotopic composition of Ichimone DM was assumed from the extremely depleted rear-arc mantle compositions. The necessity for an extremely depleted mantle source is forced by the fluid-fluxed melting model. The melting degree does not significantly affect the isotopic ratios in the primary basalts; rather the amount of fluid flux is the main control (see flux proportion in Fig. 18). With our model, only 0·1% fluid drives the Pb isotopic compositions of the primary basalt very close to the SED–AOC source mixing lines. The trace element compositions of the source fluids largely control the shapes of the melting curves. Calculated results for the QRA and QVF basalts are internally consistent and reproduce the 'uncontaminated' primary basalt compositions (Table 3) at fluid proportions of 0·7% for QVF and of 0·2–0·4% for the QRA basalts (Fig. 18a–d).

The Sr and Pb isotope compositions of the QVF primary basalt are more radiogenic than those of the QRA basalt. This is attributable to a greater SED contribution in the slab fluid source (Fig. 18a). Similarly elevated Nd isotope ratios for the QVF and QRA basalts are a consequence of the low element solubility of Nd in slab fluids during fluid-fluxed melting, leaving a stronger mantle source characteristic in the primary basalts (see flat mixing lines in Sr–Nd and Pb–Nd plots at up to 1% fluid in Fig. 18b and d).

All of the features discussed above are characteristic of our two-stage fluid source mixing–fluid-fluxed mantle melting model. It is possible to alter (1) D_{fluid} during slab dehydration, (2) the proportion of fluid added to the mantle, and (3) the degree of partial melting for the trace element model to obtain similar primary magma compositions in terms of trace element and Sr–Nd–Pb isotopes. However, constraints based on the water content of the primary basalts at a given degree of partial melting and pressures deduced from major elements for the frontal- and rear-arc mantle sources are difficult to reproduce by other models, in particular with greater fluid proportions. The proposed basalt source model maintains the best consistency between multiple petrological and geochemical constraints so far.

Mantle wedge processes and their contributions to the island arc basalts

Our mantle melting model suggests the following: (1) physical slab source mixing occurs between SED and MORB with ~7% SED in the frontal arc and 3% SED in the rear arc; (2) dehydration of slab fluid occurs at pressures of 4 GPa (frontal arc) and 6 GPa (rear arc); (3) slab fluids pass through the mantle wedge without compositional change; (4) fluid-fluxed melting occurs at depths equivalent to pressures of 1 GPa (sp-lherzolite field) in the frontal arc and 2 GPa (garnet lherzolite field) in the rear arc; (5) fluid proportions and degrees of partial melting in the melting region are $\beta = 0{\cdot}7\%$ and $F = 20$–25% for the frontal arc and $\beta = 0{\cdot}2$–$0{\cdot}4\%$ and $F = 3$–4% for the rear arc, to generate the primary basalts in the NE Japan arc (Fig. 19). We further assess the geochemical characteristics of frontal- and rear-arc lavas in relation to our mantle model in the following sections.

Mantle model and major element variations

High FeO and CaO abundances in the frontal-arc basalts (see Fig. 4) are mainly attributable to a greater degree of partial melting in the mantle source. As shown in the pMELTS simulation, CaO in the basalts clearly decreases at lower degrees of partial melting. FeO can also be controlled by pressure, but a lower degree of melting (3–4%) always gives lower FeO than at 20–25% (Fig. 14). The iron-enriched characteristics of the frontal-arc low-K tholeiites might be an inherent feature of the mantle melting conditions. High CaO in the NE Japan frontal-arc basalts suggests that the melting conditions led to total clinopyroxene consumption in the source. High Na_2O and K_2O contents in the rear-arc basalts are also controlled by the degree of partial melting (Figs 13 and 14). Therefore, these major element characteristics found over the entire NE

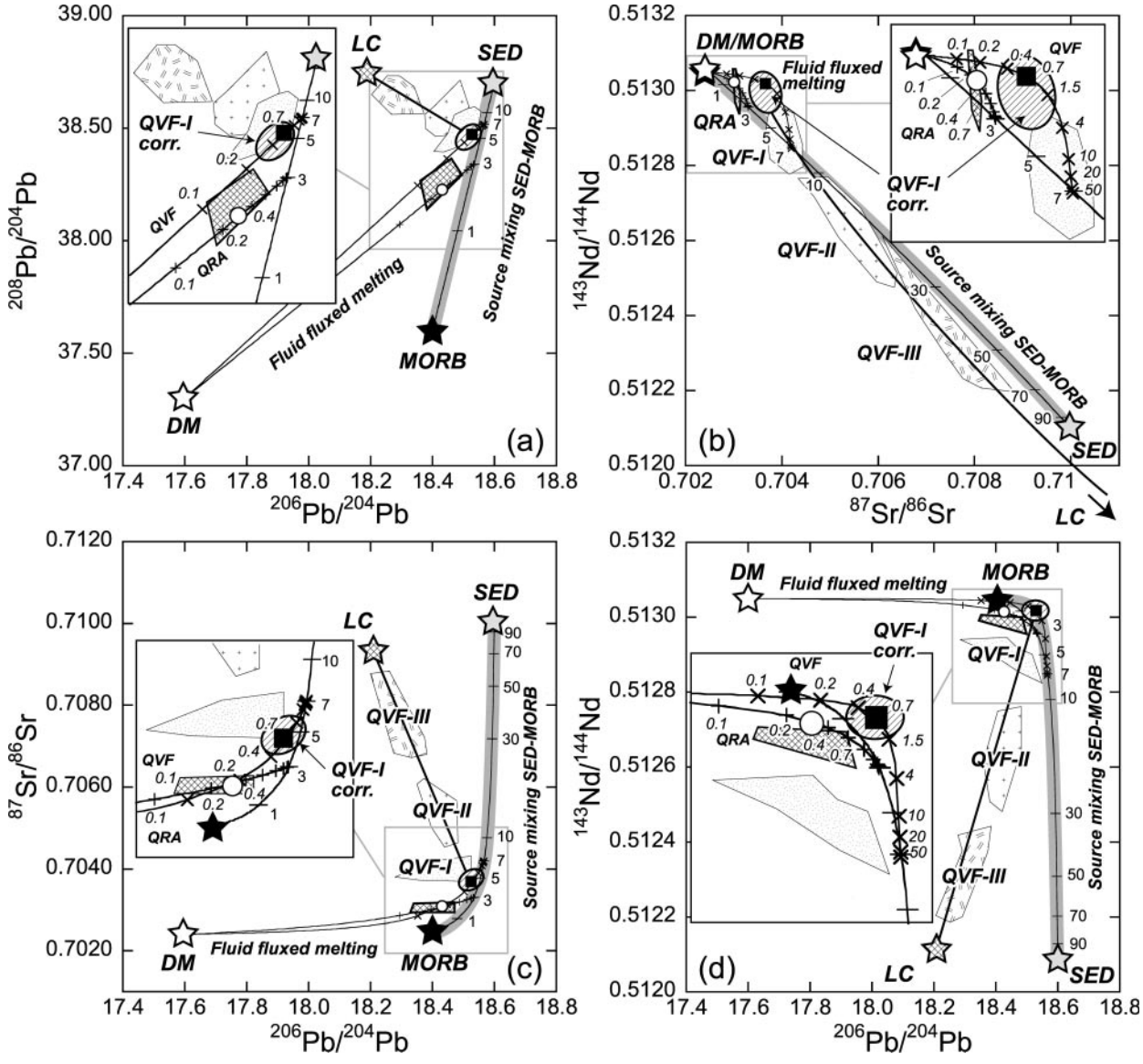

Fig. 18. Results of SED–MORB source mixing and open-system fluid-fluxed melting for Nd–Sr–Pb isotope systematics. SED, sediment component; MORB, oceanic crust component; DM, depleted mantle component; LC, lower crustal amphibolite component. Grey line is source-mixing model for slab fluid flux. The NE Japan basalt compositions are shown by patterned fills (QVF-I to -III, and QRA). Crustal assimilation corrected 'uncontaminated' QVF basalt is shown by the diagonally shaded oval. ■, 'uncontaminated' primary Funagata basalt; ○, 'uncontaminated' primary Chokai basalt.

Japan region and also occurring in arc basalts elsewhere are basically the expression of mantle melting conditions.

Mantle model and trace element variations

Elevated incompatible element abundances in the rear-arc basalts (Fig. 8) fundamentally reflect low degrees of partial melting in the rear-arc mantle. Even if the trace element contents of the slab fluid are low (e.g. 4G900FA used for the frontal-arc model, which results in excess water in the rear-arc basalt), increasing the fluid proportion from 0·4 to 1% can generate high trace element abundances in the rear-arc basalts. This is simply due to the lower degree of partial melting required for the rear-arc source. The presence of garnet in the mantle source is also a requisite for the steeply inclined trace element patterns of the QRA primary basalts in multi-element plots, even if we accept a DM source with very depleted HREE concentrations (Fig. 8). No fluid compositions derived from slab dehydration experiments can achieve such high LILE and LREE

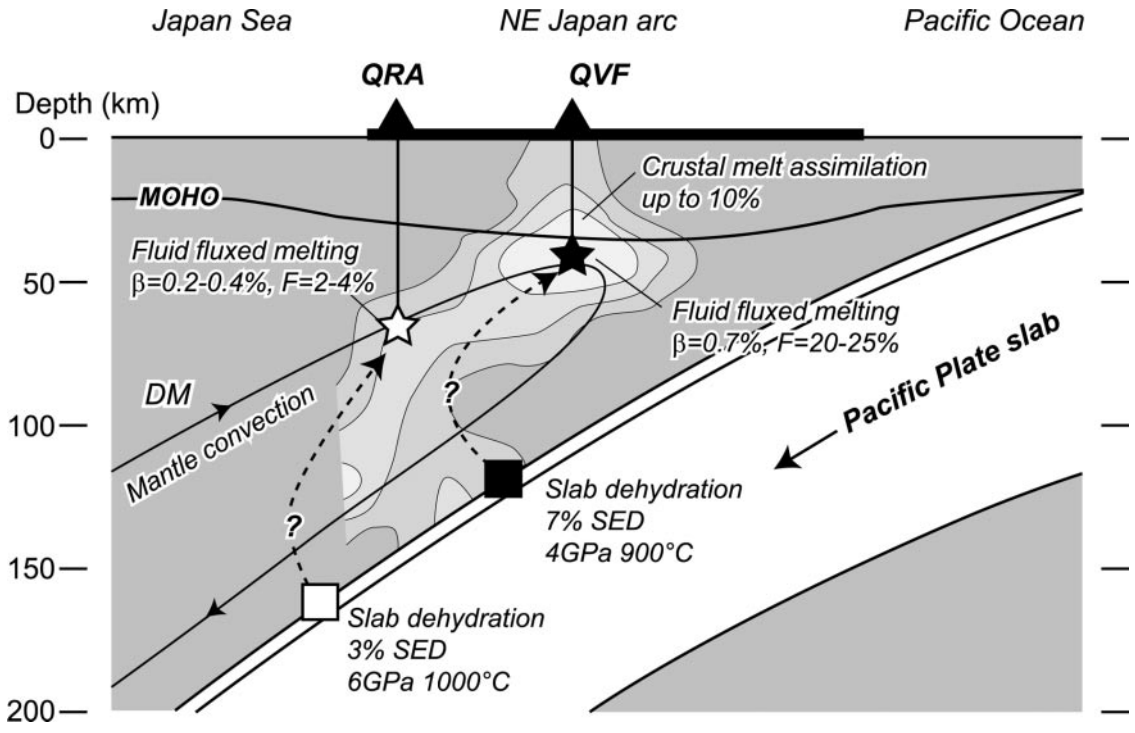

Fig. 19. Schematic diagram showing the locations of slab dehydration, fluid pathways, and partial melting for frontal- and rear-arc basalts in the NE Japan arc. A *P*-wave perturbation seismic tomography image (Nakajima *et al.*, 2005) is superimposed, with lighter colour showing greater perturbation. It should be noted that distinct fluid sources are required for the frontal- and rear-arc basalts, suggesting differing fluid pathways from different slab source regions. Fluid pathways might not be vertical, because of down-drag and upwelling corner flow of the mantle peridotite. The low-velocity region near the slab surface between 100 and 150 km depth could correlate with a region of slab dehydration at 4 GPa.

abundances in the rear-arc basalts without the presence of garnet.

Relatively low Ba/Th (or Ba/Rb and Li/REE) in the rear-arc basalts cannot be attributed to the melting region, but are related to (1) slab dehydration reactions (see different Ba/Th and Li/REE in Fig. 16b) or (2) the role of phlogopite in the mantle melting region. Sheet silicates can retain Ba, Rb, or Li because of their greater partition coefficients (Green *et al.*, 2000). The presence of phengite is confirmed by dehydration experiments on sediments (Johnson & Plank, 1999). The presence of a SED component (particularly K_2O) in the slab fluid source stabilizes K-bearing phase that were intentionally neglected in the MORB dehydration experiments of Kessel *et al.* (2005). Li or Ba can be buffered in the slab fluid source by this mechanism. According to the water-bearing pMELTS calculations, 'biotite' is stabilized at lower degrees of partial melting as a result of water saturation in the system. Although the stability of hydrous silicate minerals is not well constrained by pMELTS, these can provide another possible buffer for Li or Ba in the rear-arc lavas. Stabilization of hydrous mineral phases does not occur at greater degrees of partial melting, because the silicate melts produced can buffer H_2O considerably (Asimow *et al.*, 2004). An alternative solution is the selective depletion of Ba or Li relative to other elements in the slab dehydration region beneath the frontal arc (see Fig. 16b), which may cause depletion of the elements in the slab before it reaches to the rear-arc dehydration region.

Th/La has been used as an indicator of slab sediment melt contribution to the arc basalt source (Plank & Langmuir, 1993; Plank, 2005). The D_{fluid}(Th/La) at 6 GPa is as much as three times higher than at 4 GPa in MORB dehydration experiments, perhaps because of the supercritical behavior of the fluid (Kessel *et al.*, 2005). If our assumption of a pressure of 6 GPa for formation of the rear-arc fluid is correct, then the high Th/La in the rear-arc lavas probably originates from the slab fluid characteristics (Fig. 16b–d). Normalized Th contents as low as those of the HFSE (or LREE) in mantle-normalized trace element diagrams for frontal-arc basalts may suggest a shallow (4 GPa) origin of the slab fluid.

Nb–Ta (as well as Zr–Hf) depletion is also attributable to the stabilization of rutile during slab dehydration reactions (Johnson & Plank, 1999; Kessel *et al.*, 2005). The low HFSE contents of the slab fluids are eventually inherited by the arc basalts. To achieve this, the wedge mantle composition needs to be as depleted as that of Ichinome DM (Fig. 16b) because a low HFSE abundance in the mantle source is a prerequisite for the primary basalts.

Mantle model and isotopic variation

Considering the uniform ^{10}Be characteristics of the NE Japan basalts across and along the arc (Shimaoka & Kaneoka, 2000), the contribution of slab sediments should be uniform over the arc. We use 7% SED and 3% SED component in the slab fluid sources for the frontal and rear arcs, respectively. Enrichment of ^{10}Be should be detected in the frontal-arc lavas, but it is not. The behavior of Be during slab dehydration also differs in supercritical fluids. D_{fluid}(Be) at 6 GPa ranges from 5·6 to 22, several times greater than at 4 GPa (0·9–4·9) (Kessel *et al.*, 2005). Although the ^{10}Be budget in the slab hybrid source is about half that for the rear arc, the ^{10}Be abundance in the rear-arc slab fluids can be similar to that in the frontal arc. The effect of fluid-fluxed melting was not examined because of the poorly constrained partition coefficient data for Be. However, any effect would not be great, because mantle peridotite should have a considerably lower Be content than the slab fluids. Therein greater D_{fluid}(Be) can compensate for the lower fluid proportion in the rear-arc system, resulting in almost equal ^{10}Be in the QVF and QRA primary basalts.

As D_{fluid}(Pb) does not differ between fluid and supercritical fluid (Kessel *et al.*, 2005), except for the 6 GPa, 1200°C data, which include melting, different Pb budgets in the slab hybrid are still preserved even after fluid-fluxed melting (see discrete fluid-fluxed melting lines in Fig. 18a). Therefore, the across-arc variation in Pb isotope could reflect the mixing proportions between SED and MORB. In contrast, the Li isotope compositions of the NE Japan basalts are uniform between QVF-I and QRA basalts (Moriguti *et al.*, 2004). However, D_{fluid}(Li) is similar between fluid and supercritical fluid (Kessel *et al.*, 2005) and therefore gives similar element abundances in both QRA and QVF slab fluids, as for Pb (Fig. 16b). δ^7Li in the Funagata basalt is in the range of 2–4·5, whereas that in the Chokai and Kampu basalts varies in the range of 2–3·4. Although subtle, frontal-arc δ^7Li variations are slightly greater than in the rear arc, perhaps reflecting a greater SED contribution to the slab hybrid. This should be reassessed after correction for crustal contamination, as Li is highly abundant in crustal melts (Table 1).

We have already discussed the internal consistency of the Sr–Nd–Pb isotope compositions with the major and trace element models. All the data are well explained by our model. Although our approach to the removal of the effects of the 'crustal filter' for the QVF basalt could be questioned, our results show that the Nd isotope composition of the QVF primary basalts is identical to that of the QRA basalts (Table 3). The fluid-fluxed melting calculations predict even greater Nd isotope ratios for the QVF basalts at fluid proportions <0·7% (Fig. 18b and d). We have already discussed the isotopic similarity between the primary basalts and the Izu arc basalts. Some Izu frontal-arc basalts have higher Nd isotope ratios than the rear-arc basalts (Hochstaedter *et al.*, 2001; Ishizuka *et al.*, 2003). This observation is consistent with our model.

Hochstaedter *et al.* (2001) and Ishizuka *et al.* (2003) required the involvement of slab sediment melts to explain the near-vertical trends in the Nd–Sr isotope systematics of the arc basalts. They also proposed variable depletion of the mantle wedge to account for differences in Nd isotopic composition. An increase in the slab fluid proportion can yield the vertical trends observed in the Nd–Sr isotope plot (Fig. 18). However, an increase in fluid proportion results in unrealistic amounts of water in the basalt source (Fig. 17). Alternative options are: (1) change in SED–MORB Nd and Sr abundances that alters the Hybrid_0·03 and Hybrid_0·07 isotopic compositions on the mixing hyperbola (Fig. 18b); (2) addition of sediment melt; or (3) introduction of mantle wedge heterogeneity. We prefer models (1) or (3) because there is no particular reason to introduce sediment melt to old and cold subduction zones such as NE Japan and Izu. Indeed, we use a supercritical fluid (6G1000RA) for our QRA basalt model. Introduction of a supercritical fluid would represent the effect of a sediment melt to a certain extent because of its greater element solubility, which approaches that of a melt. The addition of a sediment melt to the mantle wedge cannot account for the vertical trend in our model.

It is difficult to advance discussion of the NE Japan arc mantle melting processes further because of the uncertainty of the contribution of the 'crustal filter' to the petrogenesis of the basalts. We also disregarded slab-fluid reactions with the mantle wedge peridotite, which should occur at the base of the mantle wedge (Hawkesworth *et al.*, 1993*b*; Pearce *et al.*, 1995; Ayers *et al.*, 1997; Manning, 2004). Therefore, the most realistic conclusion of this paper is the necessity for fluids with compositions like 4G900FA or 6G1000RA (Table 5) in the frontal- and rear-arc melting regions, under the melting conditions β, *F*, *Xa* and *Pa* proposed in this study. The role of mantle-fluid reactions should be examined by a combination of (1) development of forward modeling with fluid-peridotite experimental data, and (2) acquisition of comprehensive datasets from juvenile oceanic arc such as the Izu–Mariana, where crustal contamination is minimal.

CONCLUSIONS

We investigated Quaternary basalts and intermediate lavas situated across and along the NE Japan arc. The

major and trace element, and Nd–Sr–Pb isotopic compositions of a new suite of lavas were determined and combined with pre-existing data. Intermediate frontal-arc lavas show the strongest evidence for melting of Cretaceous to Paleogene lower crustal materials (probably amphibolite), as shown by the spatial and geochemical correlations with the underlying crust. Basalt lavas from the frontal arc were produced by mixing of mantle-derived magmas and various intermediate crustal melts. Trace element and Sr–Nd–Pb isotopic compositions suggest that the mantle-derived basalt is uniform along the arc, whereas the intermediate composition melts are variable in composition. Rear-arc basalts are fairly uniform and have the most depleted isotopic compositions. Frontal-arc basalts have similar isotopic compositions to the rear-arc basalts, but are more depleted in incompatible trace elements. Petrogenetic modeling using pMELTS, experimental data, and the geochemical characteristics of Ichinomegata mantle peridotite xenoliths indicates that a similar mantle composition can be the source of the NE Japan basalts before they are modified by interaction with the overlying crust. Numerical modeling using an open-system melting model with (1) various SED–MORB slab hybrid fluid sources (7% SED and 3% SED components for QVF and QRA, respectively), (2) slab dehydration at different depths (4 and 6 GPa for QVF and QRA), (3) fixed depleted mantle component, and (4) variable melting parameters (1 GPa, $F = 20$–25%, $\beta = 0{\cdot}7\%$ for QVF, and 2 GPa, $F = 3$–4%, $\beta = 0{\cdot}2$–$0{\cdot}4\%$ for QRA) reproduce the major and trace element and Sr–Nd–Pb isotopic variations in the basalts across the arc. The relatively simple but semi-quantitative mass balance model proposed here provides important constraints for (1) the volumetric contributions of SED and MORB slab components, (2) the conditions of slab dehydration, and (3) the significance of fluid-induced melting beneath island arcs. Supplementary data that we used in this paper are available for downloading from http://petrology.oxfordjournal.org.

ACKNOWLEDGEMENTS

Our thanks go to Professors R. J. Stern of University of Texas at Dallas and Barry Roser of Shimane University for overall comments on this paper, to Professor A. A. Ariskin and Dr G. Barmina of Vernazky Institute of Russian Academy of Science for comments on the use of thermodynamic modeling and the INFOREX 4.0.2 experimental database, and to Professor A. Hasegawa and Dr J. Nakajima of Tohoku University for geophysical interpretations of seismic tomography. The WINDOWS version MELTS/pMELTS/phMELTS program named Adiabat_1ph (version 1.6.2) was obtained from Dr P. Asimow's California Institute of Technology website (http://www.gps.caltech.edu/~asimow/adiabat/). Discussions with Drs T. Sugawara, Y. Tatsumi, A. Fujinawa, and J. P. Davidson were fruitful for constructing the model. Professors S. Iizumi and Y. Sawada provided free access to the TIMS and XRF facilities at Shimane University. We also thank Professors D. A. Gust, J. B. Gill, R. J. Arculus and M. Wilson for their constructive reviews, which improved this paper significantly. This research was supported by grants-in-aid of the Ministry of Education, Science, and Culture, Japan, 10304038 and 12874058 (Rep. J.-I. Kimura), and 12304031 (Rep. T. Yoshida).

SUPPLEMENTARY DATA

Supplementary data for this paper are available at *Journal of Petrology* online.

REFERENCES

Aizawa, Y., Tatsumi, Y. & Yamada, H. (1999). Element transport by dehydration of subducted sediments: implications for arc and ocean island magmatism. *Island Arc* **8**, 38–46.

Aoki, K. (1971). Petrology of mafic inclusions from Ichinome-gata, Japan. *Contributions to Mineralogy and Petrology* **30**, 314–331.

Aoki, K. (1987). Japanese island arc: xenoliths in alkali basalts, high-alumina basalts, and calc-alkaline andesites and andesites. In: Nixon, P. H. (ed.) *Mantle Xenoliths*. New York: John Wiley, pp. 320–332.

Arai, S. & Saeki, Y. (1980). Ultramafic–mafic inclusions from Sannomegata craters, Oga peninsula, Japan with special reference to the petrological difference from the Ichinomegata inclusions. *Journal of Geological Society of Japan* **86**, 705–708.

Arculus, R. J. (2003). Use and abuse of the terms calcalkaline and calcalkalic. *Journal of Petrology* **44**, 923–935.

Arculus, R. J. & Johnson, R. W. (1981). Island-arc magma sources: a geochemical assessment of the roles of slab-derived components and crustal contamination. *Geochemical Journal* **15**, 109–133.

Arculus, R. J. & Powell, R. (1986). Source component mixing in the regions of arc magma generation. *Journal of Geophysical Research* **91B**, 5913–5926.

Ariskin, A. A., Bouadze, K. V., Meshalkin, S. S. & Tsekhonya, T. I. (1992). INFOREX: a database on experimental studies of phase relations in silicate systems. *American Mineralogist* **77**, 668–669.

Asimow, P. D., Hirschmann, M. M. & Stolper, E. M. (2001). Calculation of peridotite partial melting from thermodynamic models of minerals and melts, IV. Adiabatic decompression and the composition and mean properties of mid-ocean ridge basalts. *Journal of Petrology* **42**, 963–998.

Asimow, P. D., Dixon, J. D. & Langmuir, C. H. (2004). A hydrous melting and fractionation model for mid-ocean ridge basalts: application to the Mid-Atlantic Ridge near Azores. *Geochemistry, Geophysics, Geosystems* **5**, doi:10.1029/2003GC000568.

Ayers, J. C. & Watson, E. B. (1993). Rutile solubility and mobility in supercritical aqueous fluids. *Contributions to Mineralogy and Petrology* **114**, 321–330.

Ayers, J. C., Dittmer, S. K. & Layne, G. D. (1997). Partitioning of elements between peridotite and H_2O at 2·0–3·0 GPa and 900–1100°C, and applications to models of subduction zone processes. *Earth and Planetary Science Letters* **150**, 381–398.

Baker, M. B. & Stolper, E. M. (1994). Determining the composition of high-pressure mantle melts using the diamond aggregates. *Geochimica et Cosmochimica Acta* **58**, 2811–2827.

Baker, M. B., Hirschmann, M. M., Ghiorso, M. S. & Stolper, E. M. (1995). Compositions of near-solidus peridotite melts from experiments and thermodynamic calculations. *Nature* **375**, 308–311.

Beard, J. S., Abitz, R. J. & Lofgren, G. E. (1993). Experimental melting of crustal xenoliths from Kilbourne Hole, New Mexico and implications for the contamination and genesis of magmas. *Contributions to Mineralogy and Petrology* **115**, 88–102.

Bebout, G. E., Ryan, J. G., Leeman, W. P. & Bebout, A. E. (1999). Fractionation of trace elements by subduction-zone metamorphism—effect of convergent-margin thermal evolution. *Earth and Planetary Science Letters* **171**, 63–81.

Bertka, C. M. & Holloway, J. R. (1994a). Anhydrous partial melting of an iron-rich mantle I: subsolidus phase assemblages and partial melting phase relations at 10 to 30 kbar. *Contributions to Mineralogy and Petrology* **115**, 313–322.

Bertka, C. M. & Holloway, J. R. (1994b). Anhydrous partial melting of an iron-rich mantle II: primary melt compositions at 15 kbar. *Contributions to Mineralogy and Petrology* **115**, 323–330.

Brenan, J. M., Shaw, H. F., Ryerson, F. J. & Phinney, D. L. (1995). Mineral–aqueous fluid partitioning of trace elements at 900°C and 2·0 GPa: constraints on the trace element chemistry of mantle and deep crustal fluids. *Geochimica et Cosmochimica Acta* **59**, 3331–3350.

Canil, D. (1992). Orthopyroxene stability along the peridotite solidus and the origin of cratonic lithosphere beneath southern Africa. *Earth and Planetary Science Letters* **111**, 83–95.

Caroff, M., Maury, R. C., Guille, G. & Cotten, J. (1997). Partial melting below Tubuai (Austral Islands, French Polynesia). *Contributions to Mineralogy and Petrology* **127**, 369–382.

Churikova, T., Drendorf, F. & Wörner, G. (2001). Sources and fluids in the mantle wedge below Kamchatka, evidence from across-arc geochemical variation. *Journal of Petrology* **42**, 1567–1593.

Clemens, J. D., Holloway, J. R. & White, A. J. R. (1986). Origin of an A-type granite: experimental constraints. *American Mineralogists* **71**, 317–324.

Committee for Catalog of Quaternary Volcanoes in Japan (1999), *Catalog of Quaternary Volcanoes in Japan*. The Volcanological Society of Japan, Tokyo, Japan.

Conrad, W. K., Nicholls, I. A. & Wall, V. J. (1988). Water-saturated and undersaturated melting of metaluminous and peraluminous crustal compositions at 1 kb: evidence for the origin of silicic magmas in the Taupo volcanic Zone, New Zealand, and other occurrences. *Journal of Petrology* **29**, 765–803.

Cousens, B. L. & Allan, J. F. (1992). A Pb, Sr, and Nd isotopic study of basaltic rocks from the Sea of Japan, LEGS 127/128. In: Tamaki, K., Suyehiro, K., Allan, J. & McWilliams, M. (eds) *Proceedings of the Ocean Drilling Program, Scientific Results*. College Station, TX: Ocean Drilling Program, **127/128**, pp. 805–816.

Davidson, J. P. (1996). Deciphering mantle and crustal signatures in subduction zone magmatism. In: Bebout, G. E., Scholl, D. W., Kibry, S. H., & Platt, J. P. (eds). Subduction: Top to Bottom. American Geophysical Union, **96**, pp. 251–262.

Davidson, J. P., Hora, J. M., Garrison, J. M. & Dungan, M. A. (2005). Crustal forensics in arc magmas. *Journal of Volcanology and Geothermal Research* **140**, 157–170.

Defant, M. J. & Drummond, M. S. (1990). Derivation of some modern arc magmas by melting of young subducted lithosphere. *Nature* **347**, 662–665.

Drummond, M. S. & Defant, M. J. (1990). A model for trondhjemite–tonalite–dacite genesis and crustal growth via slab melting: Archean to modern comparisons. *Journal of Geophysical Research* **95**(B), 503–521.

Falloon, T. J., Green, D. H., O'Neill, H. S. C. & Hibberson, W. O. (1997). Experimental tests of low degree peridotite partial melt compositions: implications for the nature of anhydrous near-solidus peridotite melts at 1 GPa. *Earth and Planetary Science Letters* **152**, 149–162.

Feigenson, M. D., Hofmann, A. W. & Spera, F. J. (1983). Case studies on the origin of basalt. II. The transition from tholeiitic to alkalic volcanism on Kohara volcano, Hawaii. *Contributions to Mineralogy and Petrology* **84**, 390–405.

Flower, M. F. J., Russo, R. M., Tamaki, K. & Hoang, N. (2001). Mantle contamination and the Izu–Bonin–Mariana (IBM) 'high-tide-mark': evidence for mantle extrusion caused by Tethyan closure. *Tectonophysics* **333**, 9–34.

Frey, F. A., Suen, C. J. & Stockman, H. W. (1985). The Ronda high-temperature peridotite: geochemistry and petrogenesis. *Geochimica et Cosmochimica Acta* **49**, 2469–2491.

Fujinawa, A. (1988). Tholeiitic and calc-alkaline magma series at Adatara volcano, Northeast Japan: 1. Geochemical constraints on their origin. *Lithos* **22**, 135–158.

Fujinawa, A. (1991). Tholeiitic and calc-alkaline magma series at Adatara volcano, Northeast Japan: evolution mechanism and genetic relationship. *Bulletin of Volcanological Society of Japan* **36**, 241–254.

Gaetani, G. A., Kent, A. J. R., Grove, T. L., Hutcheon, I. D. & Stolper, E. M. (2003). Mineral/melt partitioning of trace elements during hydrous peridotite partial melting. *Contributions to Mineralogy and Petrology* **145**, 391–405.

Gardien, V., Thompson, A. B. & Ulmer, P. (2000). Melting of biotite + plagioclase + quartz gneisses: the role of H_2O in the stability of amphibole. *Journal of Petrology* **41**, 651–666.

Gerke, T. L. & Kilinc, A. I. (1993). Enrichment of SiO_2 in rhyolites by fractional crystallization: an experimental study of peraluminous granitic rocks from the St. Francois Mountains, Missouri, USA. *Lithos* **29**, 273–283.

Ghiorso, M. S. & Sack, R. O. (1995). Chemical mass transfer in magmatic processes IV. A revised and internally consistent thermodynamic model for the interpolation and extrapolation of liquid–solid equilibria in magmatic systems at elevated temperatures and pressures. *Contributions to Mineralogy and Petrology* **119**, 197–212.

Ghiorso, M. S., Hirschmann, M. M., Reiners, P. W. & Kress, V. C. (2002). The pMELTS: a revision of MELTS for improved calculation of phase relations and major element partitioning related to partial melting of the mantle to 3 GPa. *Geochemistry, Geophysics, Geosystems* **3**, doi: 10.1029/2001GC000217.

Gill, J. B. (1981). *Orogenic Andesites and Plate Tectonics*. Heidelberg: Springer.

Green, T. H., Blundy, J. D., Adam, J. & Yaxley, G. M. (2000). SIMS determination of trace element partition coefficients between garnet, clinopyroxene and hydrous basaltic liquids at 2–7·5 GPa and 1080–1200°C. *Lithos* **25**, 165–187.

Gust, D. A., Arculus, R. J. & Kersting, A. B. (1997). Aspect of magma sources and processes in the Honshu arc. *Canadian Mineralogist* **35**, 347–365.

Hasegawa, A., Zhao, D., Hori, S., Yamamoto, A. & Horiuchi, S. (1991). Deep structure of the northeastern Japan arc and its relationship to seismic and volcanic activity. *Nature* **352**, 683–689.

Hauff, F., Hoernle, K. & Schmidt, A. (2003). Sr–Nd–Pb composition of Mesozoic Pacific oceanic crust (Site 1149 and 801, ODP Leg 185): implications for alteration of ocean crust and the input into the Izu–Bonin–Mariana subduction system. *Geochemistry, Geophysics, Geosystems* **4**, doi:10.1029/2002GC000421.

Hawkesworth, C. J., Gallagher, K., Hergt, J. M. & McDermott, F. (1993a). Mantle and slab contributions in arc magmas. *Annual Review of Earth and Planetary Sciences* **21**, 175–204.

Hawkesworth, C. J., Gallagher, K., Hergt, J. M. & McDermott, F. (1993b). Trace element fractionation processes in the generation of island arc basalts. *Philosophical Transactions of the Royal Society of London, Series A* **342**, 179–191.

Herzberg, C., Feigenson, M., Skuba, C. & Ohtani, E. (1988). Majorite fractionation recorded in the geochemistry of peridotite from South Africa. *Nature* **332**, 823–826.

Hickey-Vargas, R. (1991). Isotope characteristics of submarine lavas from the Philippine Sea: implications for the origin of arc and basin magmas of the Philippine tectonic plate. *Earth and Planetary Science Letters* **107**, 290–304.

Hickey-Vargas, R. (1998). Origin of the Indian Ocean-type isotopic signature in basalts from Philippine Sea plate spreading centers: an assessment of local versus large-scale processes. *Journal of Geophysical Research* **103**, 20963–20979.

Hickey-Vargas, R., Hergt, J. M. & Spadea, P. (1995). The Indian Ocean-type isotopic signature in Western Pacific marginal basins: origin and significance. In: Taylor, B. & Natland, J. (eds) *Active Margins and Marginal Basins of the Western Pacific*. Washington: DC: American Geophysical Union, pp. 175–197.

Hirose, K. & Kawamoto, T. (1995). Hydrous partial melting of lherzolite at 1 GPa: the effect of H_2O on the genesis of basaltic magmas. *Earth and Planetary Science Letters* **133**, 463–473.

Hirose, K. & Kushiro, I. (1993). Partial melting of dry peridotites at high pressures: determination of compositions of melts segregated from peridotite using aggregates of diamond. *Earth and Planetary Science Letters* **114**, 477–489.

Hirschmann, M. M., Ghiorso, M. S., Asimow, P. W., Wasylenki, L. E. & Stolper, E. M. (1998). Calculation of peridotite partial melting from thermodynamic models of minerals and melts. I. Review of methods and comparison with experiments. *Journal of Petrology* **39**, 1091–1115.

Hirschmann, M. M., Asimow, P. D., Ghiorso, M. S. & Stolper, E. M. (1999a). Calculation of peridotite partial melting from thermodynamic models of minerals and melts. III. Controls on isobaric melt production and the effect of water on melt production. *Journal of Petrology* **40**, 831–851.

Hirschmann, M. M., Ghiorso, M. S. & Stolper, E. M. (1999b). Calculation of peridotite partial melting from thermodynamic moels of minerals and melts. II. Isobaric variations in melts near the solidus and owing to variable source composition. *Journal of Petrology* **40**, 297–313.

Hochstaedter, A., Gill, J., Peters, R., Broughton, P., Holden, P. & Taylor, B. (2001). Across-arc geochemical trends in the Izu–Bonin Arc: contributions from the subducting slab. *Geochemistry, Geophysics, Geosystems* **2**, 2000GC000105.

Ichikawa, K. (1990). Pre-Cretaceous Terranes of Japan. In: Ichikawa, K., Mizutani, S., Hara, I., Hada, S. & Yao, A. (eds) *Pre-Cretaceous Terranes of Japan*. Osaka: Nippon Insatsu Shuppan, pp. 1–11.

Iizumi, S., Maehara, K., Morris, P. A. & Sawada, Y. (1994). Sr isotope data of some GSJ rock reference samples. *Memoirs of Faculty of Science, Shimane University* **28**, 83–86.

Iizumi, S., Morris, P. A. & Sawada, Y. (1995). Nd isotope data for GSJ reference samples JB-1a, JB-3 and JG-1a and the La Jolla standard. *Memoirs of Faculty of Science, Shimane University***29**73–76.

Ishikawa, T. & Nakamura, E. (1994). Origin of the slab component in arc lavas from across-arc variation of B and Pb isotopes. *Nature* **370**, 205–208.

Ishizuka, O., Taylor, R. N., Milton, J. A. & Nesbitt, R. W. (2003). Fluid–mantle interaction in an intra-oceanic arc: constraints from high-precision Pb isotopes. *Earth and Planetary Science Letters* **211**, 221–236.

Iwamori, H. (1998). Transport of H_2O in subduction zones. *Earth and Planetary Science Letters* **160**, 65–80.

Johannes, W. & Holtz, F. (1996). *Petrogenesis and Experimental Petrology of Granitic Rocks*. Heidelberg: Springer.

Johnson, M. C. & Plank, T. (1999). Dehydration and melting experiments constrain the fate of subducted sediments. *Geochemistry, Geophysics, Geosystem* **13**, 1999GC000014.

Johnson, M. C. & Rutherford, M. J. (1989). Experimentally determined conditions in the Fish Canyon Tuff, Colorado, magma chamber. *Journal of Petrology* **30**, 711–737.

Jolivet, L. & Tamaki, K. (1992). Neogene kinematics in the Japan Sea region and volcanic activity of the Northeast Japan Arc. In: Tamaki, K., Suyehiro, K., Allan, J. & McWilliams, M. (eds) *Proceedings of the Ocean Drilling Program*. College Station, TX: Ocean Drilling Program, **127/128**, pp. 1311–1327.

Kadik, A. A., Lebedev, E. B. & Khitarov, N. I. (1971). *The Water in Magmatic Melts*. Moscow: Nauka.

Kagami, H. (2005). Formative periods and source materials for Cretaceous–Paleogene granitoids from Honshu arc. *Journal of Geological Society of Japan* **111**, 441–457.

Kagami, H., Iizumi, S., Tainosho, Y. & Owada, M. (1992). Spatial variations of Sr and Nd isotope ratios of Cretaceous–Paleogene granitoid rocks, Southwest Japan. *Contributions to Mineralogy and Petrology* **112**, 165–177.

Kaneko, T. (1995). Geochemistry of Quaternary basaltic lavas in the Norikura area, central Japan: influence of the subcontinental upper mantle on the trace elements and Sr isotope compositions. *Journal of Volcanology and Geothermal Research* **64**, 61–83.

Kawano, Y., Yagi, K. & Aoki, K. (1961). Petrography and petrochemistry of the volcanic rocks of Quaternary volcanoes of northern Japan. *Science Reports of Tohoku University, Series III* **7**, 1–46.

Kelemen, P. B., Hart, S. R. & Bernstein, S. (1998). Silica enrichment in the continental upper mantle via melt/rock reaction. *Earth and Planetary Science Letters* **164**, 387–406.

Keppler, H. (1996). Constraints from partitioning experiments on the composition of subduction-zone fluids. *Nature* **380**, 237–240.

Kersting, A. B., Arculus, R. J. & Gust, D. A. (1996). Lithospheric contributions to arc magmatism: isotope variations along strike in volcanoes of Honshu, Japan. *Science* **272**, 1464–1468.

Kessel, R., Schmidt, M. W., Ulmer, P. & Pettke, T. (2005). Trace element signature of subduction-zone fluids, melts and supercritical liquids at 120–180 km depth. *Nature* **439**, 724–727.

Kimura, J.-I. (1996). Near synchroneity and periodicity of Quaternary explosive volcanism in the southern segment of Tohoku-honshu arc: a study facilitated by tephrochronology. *Quaternary International* **34–36**, 99–105.

Kimura, J.-I. & Yamada, Y. (1996). Evaluation of major and trace element XRF analyses using a flux to sample ratio of two to one glass beads. *Journal of Mineralogy, Petrology and Economic Geology* **91**, 62–72.

Kimura, J.-I., Yoshida, T. & Takaku, Y. (1995). Igneous rock analysis using ICP-MS with internal standardization, isobaric ion overlap correction, and standard addition methods. *Science Reports of Fukushima University* **56**, 1–12.

Kimura, J.-I., Manton, W. I., Sun, C.-H., Iizumi, S., Yoshida, T. & Stern, R. J. (2001a). Chemical diversity of the Ueno Basalts, central Japan: identification of mantle and crustal contributions to arc basalts. *Journal of Petrology* **43**, 1923–1946.

Kimura, J.-I., Tanji, T., Yoshida, T. & Iizumi, S. (2001b). Geology and geochemistry of lavas at Nekoma volcano: implications for origin of Quaternary low-K andesite in the North-eastern Honshu arc, Japan. *Island Arc* **10**, 116–134.

Kimura, J.-I., Yoshida, T. & Iizumi, S. (2002). Origin of Low-K intermediate lavas at Nekoma volcano, NE Honshu arc, Japan: geochemical constraints for lower-crustal melts. *Journal of Petrology* **43**, 631–661.

Kimura, J.-I., Kawahara, M. & Iizumi, S. (2003a). Lead isotope analysis using TIMS following single column–single bead Pb separation. *Geoscience Reports of Shimane University* **22**, 49–53.

Kimura, J.-I., Nagao, T., Yamauchi, S., Kakubuchi, S., Okada, S., Fujibayashi, N., Okada, R., Murakami, H., Kusano, T., Umeda, K., Hayashi, S., Ishimaru, T., Ninomiya, J. & Tanase, A. (2003b). Late Cenozoic volcanic activity in the Chugoku area, Southwest Japan arc during back arc basin opening and re-initiation of subduction. *Island Arc* **12**, 22–45.

Kimura, J.-I., Stern, R. J. & Yoshida, T. (2005). Re-initiation of subduction and magmatic responses in SW Japan during Neogene time. *Geological Society of America Bulletin* **117**, 969–986.

Kinzler, R. J. (1997). Melting of mantle peridotite at pressures approaching the spinel to garnet transition: application to mid-ocean ridge basalt petrogenesis. *Journal of Geophysical Research* **102B**, 853–874.

Kobayashi, K. & Nakamura, E. (2001). Geochemical evolution of Akagi volcano, NE Japan: implications for interaction between island-arc magma and lower crust, and generation of isotopically various magmas. *Journal of Petrology* **42**, 2303–2331.

Kogiso, T., Tatsumi, Y. & Nakano, S. (1997). Trace element transport during dehydration processes in the subducted oceanic crust: 1. Experiments and implications for the origin of oceanic island basalts. *Earth and Planetary Science Letters* **148**, 193–205.

Koide, Y. & Nakamura, E. (1990). Lead isotope analyses of standard rock samples. *Mass Spectroscopy* **38**, 241–252.

Kuno, H. (1966). Lateral variation of basalt magma type across continental margin and island arcs. *Bulletin Volcanologique* **XXIX**, 195–222.

Kurosawa, M. (1993). Water in mantle olivine. *Mineralogical Magazine (Japan)* **22**, 161–166.

Kushiro, I. (1987). A petrological model of the mantle wedge and lower crust in the Japanese island arcs. In: Mysen, B. O. (ed.) *Magmatic Processes: Physicochemical Principles*. Geochemical Society, St. Louis, USA, pp. 165–181.

Kushiro, I. (1996). Partial melting of a fertile mantle peridotite at high pressures: an experimental study using aggregates of diamond. In: Basu, A. & & Hart, S. (eds) *Earth Processes: Reading the Isotopic Code. Geophysical Monograph, Americal Geophysical Union* **95**, 109–122.

LeMaitre, R. W., Bateman, P., Dudek, A., Keller, J., Lameyre-LeBas, M. J., Sabine, P. A., Schmid, R., Sorensen, H., Streckeisen, A., Woolley, A. R. & Zanettin, B. (1989). *A Classification of Igneous Rocks and Glossary of Terms*. Oxford: Blackwell.

Longhi, J. (1995). Liquidus equilibria of some primary lunar and terrestrial melts in the garnet stability field. *Geochimica et Cosmochimica Acta* **59**, 2375–2386.

Manning, C. E. (2004). The chemistry of subduction-zone fluids. *Earth and Planetary Science Letters* **223**, 1–16.

Manton, W. I. (1988). Separation of Pb from young zircons by single-bead ion exchange. *Chemical Geology* **73**, 147–152.

McDade, P., Blundy, J. D. & Wood, B. J. (2003). Trace element partitioning between mantle wedge peridotite and hydrous MgO-rich melt. *American Mineralogist* **88**, 1825–1831.

Miyashiro, A. (1974). Volcanic rock series in island arcs and active continental margins. *American Journal of Science* **274**, 321–355.

Moriguti, T., Shibata, T. & Nakamura, E. (2004). Lithium, boron and lead isotope and trace element systematics of Quaternary basaltic volcanic rocks in northeastern Japan: mineralogical controls on slab-derived fluid composition. *Chemical Geology* **212**, 81–100.

Mysen, B. O. & Kushiro, I. (1977). Compositional variations of coexisting phases with degree of melting of peridotite in the upper mantle. *American Mineralogist* **62**, 843–856.

Nakagawa, M., Shimotori, H. & Yoshida, T. (1988). Across-arc compositional variation of the Quaternary basaltic rocks from the Northeast Japan arc. *Journal of Petrology, Mineralogy and Economic Geology* **83**, 9–25.

Nakajima, J. & Hasegawa, A. (2003). Estimation of thermal structure in the mantle wedge of northeastern Japan from seismic attenuation data. *Geophysical Research Letters* **30**, doi: 10.1029/2003GL017185.

Nakajima, J., Takei, Y. & Hasegawa, A. (2005). Quantitative analysis of the inclined low-velocity zone in the mantle wedge of northern Japan: a systematic change of melt-filled pore shapes with depth and its implications for melt migration. *Earth and Planetary Science Letters* **234**, 59–70.

Nishimoto, S., Ishikawa, M., Arima, M. & Yoshida, T. (2005). Laboratory measurement of P-wave velocity in crustal and upper mantle xenoliths from Ichino-megata, NE Japan: ultrabasic hydrous lower crust beneath the NE Honshu arc. *Tectonophysics* **396**, 245–259.

Niu, Y. (2004). Bulk-rock major and trace element compositions of abyssal peridotites: implications for mantle melting, melt extraction and post-melting processes beneath mid-ocean ridges. *Journal of Petrology* **45**, 2423–2458.

Nohda, S., Tatsumi, Y., Otofuji, Y., Matsuda, T. & Ishikawa, K. (1988). Asthenospheric injection and back-arc opening: isotopic evidence from northeast Japan. *Chemical Geology* **68**, 317–327.

Notsu, K. (1983). Strontium isotope composition in volcanic rocks from the North-east Japan arc. *Journal of Volcanology and Geothermal Research* **18**, 531–548.

Ohki, J., Shuto, K. & Kagami, H. (1994). Middle Miocene bimodal volcanism by asthenospheric upwelling: Se and Nd isotopic evidence from the back-arc region of the Northeast Japan arc. *Geochemical Journal* **38**, 473–483.

Okamura, S., Arculus, R. J., Martynov, Y. A., Kagami, H., Yoshida, T. & Kawano, Y. (1998). Multiple magma sources involved in marginal-sea formation: Pb, Sr, and Nd isotopic evidences from the Japan Sea region. *Geology* **26**, 619–622.

Okamura, S., Arculus, R. J. & Martynov, Y. A. (2005). Cenozoic magmatism of the North-Eastern Eurasian margin: the role of lithosphere versus asthenosphere. *Journal of Petrology* **46**, 221–253.

Olafsson, M. (1980). Partial melting of peridotite in the presence of small amounts of volatiles, with special reference to the low-velocity zone. Masters thesis, Pennsylvania State University, University Park, PA.

Patiño-Douce, A. E. (1996). Effects of pressure and H_2O content on the compositions of primary crustal melts. *Transactions of the Royal Society of Edinburgh: Earth Sciences* **87**, 11–21.

Peacock, S. M. (1996). Thermal and petrologic structure of subduction zones. In: Bebout, G. E., Scholl, D. W., Kirby, S. H. & Platt, J. P. (eds) *Subduction: Top to Bottom. Geophysical Monograph*. American Geophysical Union, **96**, pp. 119–133.

Peacock, S. M. & Wang, K. (1999). Seismic consequence of warm versus cool subduction metamorphism: examples from southwest and northeast Japan. *Science* **286**, 937–939.

Pearce, J. A. & Parkinson, I. J. (1993). Trace element models for mantle melting: application to volcanic arc petrogenesis. In: Prichard, H. M., Alabaster, T., Harris, N. B. W. & Neary, C. R. (eds) *Magmatic Processes and Plate Tectonics. Geological Society, London, Special Publications*, **76**, 373–403.

Pearce, J. A., Baker, P. E., Harvey, P. K. & Luff, I. W. (1995). Geochemical evidence for subduction fluxes, mantle melting and

fractional crystallization beneath the South Sandwich Island arc. *Journal of Petrology* **36**, 1073–1109.

Peccerillo, A. & Taylor, S. R. (1976). Geochemistry of Eocene calc-alkaline volcanic rocks from the Kastamonu area, northern Turkey. *Contributions to Mineralogy and Petrology* **58**, 63–81.

Plank, T. (2005). Constraints from thorium/lanthanum on sediment recycling at subduction zones and the evolution of the continents. *Journal of Petrology* **46**, 921–944.

Plank, T. & Langmuir, C. H. (1993). Tracing trace elements from sediment input to volcanic output at subduction zones. *Nature* **362**, 739–742.

Plank, T. & Langmuir, C. H. (1998). The chemical composition of subducting sediment and its consequence for the crust and mantle. *Chemical Geology* **145**, 325–394.

Poli, S. & Schmidt, M. W. (1995). H_2O transport and release in subduction zones: experimental constraints on basaltic and andesitic systems. *Journal of Geophysical Research* **100B**, 22299–22314.

Pouclet, A. & Bellon, H. (1992). Geochemistry and isotopic composition of volcanic rocks from the Yamato Basin: Hole 794D, Sea of Japan. In: Tamaki, K., Suyehiro, K., Allan, J. & McWilliams, M. (eds) *Proceedings of the Ocean Drilling Program, Scientific Results*. College Station, TX: Ocean Drilling Program, **127/128**, pp. 779–789.

Pouclet, A., Lee, J.-S., Vidal, P., Cousens, B. & Bellon, H. (1995). Cretaceous to Cenozoic volcanism in South Korea and in the Sea of Japan: magmatic constraints on the opening of the back-arc basin. In: Smellie, J. L. (ed.) *Volcanism Associated with Extension at Consuming Plate Margins. Geological Society, London, Special Publications* **81**, 169–191.

Ringwood, A. E. (1976). Limits on the bulk composition of the Moon. *Icarus* **28**, 325–349.

Robinson, J. A. & Wood, B. J. (1998). The depth of the spinel to garnet transition at the peridotite solidus. *Earth and Planetary Science Letters* **164**, 277–284.

Robinson, J. A. C., Wood, B. J. & Blundy, J. D. (1998). The beginning of melting of fertile and depleted peridotite at 1·5 GPa. *Earth and Planetary Science Letters* **155**, 97–111.

Sakuyama, M. (1983). Petrology of arc volcanic rocks and their origin by mantle diapirs. *Journal of Volcanology and Geothermal Research* **18**, 297–320.

Sakuyama, M. & Nesbitt, R. W. (1983). Geochemistry of the Quaternary volcanic rocks of the Northeast Japan arc. *Journal of Volcanology and Geothermal Research* **29**, 413–450.

Scaillet, B., Pichavant, M. & Roux, J. (1995). Experimental crystallization of leucogranite magmas. *Journal of Petrology* **36**, 663–705.

Schmidt, M. W. & Poli, S. (1998). Experimentally based water budget for dehydrating slabs and consequences for arc magma generation. *Earth and Planetary Science Letters* **163**, 361–379.

Sen, G. (1982). Composition of basaltic liquids generated from a partially depleted lherzolite at 9 kbar pressure. *Nature* **299**, 336–338.

Shibata, K. & Ishizaka, S. (1979). $^{87}Sr/^{86}Sr$ ratios of plutonic rocks from Japan. *Contributions to Mineralogy and Petrology* **70**, 381–390.

Shibata, T. & Nakamura, E. (1997). Across-arc variations of isotope and trace element compositions from Quaternary basaltic rocks in northeastern Japan: implications for interaction between subducted oceanic slab and mantle wedge. *Journal of Geophysical Research* **B102**, 8051–8064.

Shimaoka, A. & Kaneoka, I. (2000). Be isotope studies on the contribution of subducted oceanic sediments to arc magma: the Northeast Japan and Hokkaido. *Chigaku-Zassi* **4**, 627–635.

Shimoda, G. & Nohda, S. (1995). Lead isotope analyses: an application to GSJ standard rock samples. *Human and Environmental Studies* **4**, 29–36.

Shuto, K., Ishimoto, H., Hirahara, Y., Sato, M., Matsui, K., Fujibayashi, N., Takazawa, E., Yabuki, K., Sekine, M., Kato, M. & Rezanov, A. I. (2006). Geochemical secular variation of magma source during Early to Middle Miocene time in the Niigata area, NE Japan: asthenospheric mantle upwelling during back-arc basin opening. *Lithos* **86**, 1–33.

Sisson, T. W., Ratajeski, K., Hankins, W. B. & Glazner, A. F. (2005). Voluminous granitic magmas from common basaltic sources. *Contributions to Mineralogy and Petrology* **148**, 635–661.

Skjerlie, K. P., Patiño-Douce, A. E. & Johnston, A. D. (1993). Fluid absent melting of a layered crustal protolith: implications for the generation of anatectic granites. *Contributions to Mineralogy and Petrology* **114**, 365–378.

Smith, P. M. & Asimow, P. D. (2005a). Adiabat_1ph: A new public front-end to the MELTS, pMELTS, and pHMELTS models. *Geochemistry, Geophysics, Geosystems* **6**, doi:10.1029/2004GC000816.

Smith, P. M. & Asimow, P. D. (2005b). Instructions for Adiabat_1ph program and Run_Adiabat.pl script; text driven interfaces for MELTS, pMELTS and pHMELTS. , http://www.gps.caltech.edu/~asimow/adiabat/.

Spandler, C., Hermann, J., Arculus, R. & Mavrogenes, J. (2004). Geochemical heterogeneity and element mobility in deeply subducted oceanic crust; insights from high-pressure mafic rocks from New Caledonia. *Chemical Geology* **206**, 21–42.

Staudigel, H., Plank, T., White, B. & Schmincke, H.-U. (1996) Geochemical fluxes during seafloor alteration of the basaltic upper crust: DSDP Sites 417 and 418. In: Bebout, G. E., Scholl, D. W., Kibry, S. H. & Platt, J. P. (eds) *Subduction: Top to Bottom*. American Geophysical Union, **96**, pp. 19–38.

Stern, R. J. (2002). Subduction zones. *Reviews of Geophysics* **40**, 1012, doi:1029/2001RG000108.

Stolper, E. M. & Newman, S. (1994). The role of water in the petrogenesis of Mariana Trough magmas. *Earth and Planetary Science Letters* **121**, 293–325.

Straub, S. M. & Layne, G. D. (2003). The systematics of chlorine, fluorine, and water in Izu arc front volcanic rocks: implications for volatile recycling in subduction zones. *Geochimica et Cosmochimica Acta* **21**, 4179–4203.

Sun, S.-S & McDonough, W. F. (1989). Chemical and isotopic systematics of oceanic basalts: implications for mantle composition and processes. In: Saunders, A. D. & Norry, M. J. (eds) *Magmatism in the Ocean Basins. Geological Society, London, Special Publications*, **42**, 313–345.

Takahashi, E. (1986a). Genesis of calc-alkali andesite magma in a hydrous mantle–crust boundary: petrology of lherzolite xenoliths from the Ichinomegata crater, Oga Peninsula, northeast Japan, part II. *Journal of Volcanology and Geothermal Research* **29**, 355–395.

Takahashi, E. (1986b). Melting of a dry peridotite KLB-1 up to 14 GPa: implications on the origin of peridotitic upper mantle. *Journal of Geophysical Research* **91B**, 9367–9382.

Takahashi, E. (1986c). Origin of basaltic magmas—implications from peridotite melting experiments and an olivine fractionation model. *Journal of the Volcanological Society of Japan* **20**, S17–S40.

Tamaki, K., Suyehiro, K., Allan, J., Ingle, Jr. J. C. & Pisciotto, K. A. (1992). Tectonic synthesis and implications of Japan sea ODP Drilling. In: Tamaki, K., Suyehiro, K., Allan, J. & McWilliams, M. *et al.* (eds) *Proceedings of the Ocean Drilling Program, Scientific Results*. College Station, TX: Ocean Drilling Program, **127/128**, pp. 1333–1348.

Tamura, Y., Tatsumi, Y., Zhao, D., Kido, Y. & Shukuno, H. (2002). Hot fingers in the mantle wedge: new insights into magma genesis in subduction zones. *Earth and Planetary Science Letters* **197**, 107–118.

Tatsumi, Y. (1986). Formation of volcanic front in subduction zones. *Geophysical Research Letters* **13**, 717–720.

Tatsumi, Y. & Eggins, S. (1995). *Subduction Zone Magmatism*. Oxford: Blackwell Science.

Tatsumi, Y. & Hanyu, T. (2003). Geochemical modeling of dehydration and partial melting of subducting lithosphere: toward a comprehensive understanding of high-Mg andesite formation in the Setouchi volcanic belt, SW Japan. *Geochemistry, Geophysics, Geosystems*, **4**, 10.1029/2003GC000530.

Tatsumi, Y., Sakuyama, M., Fukuyama, H. & Kushiro, I. (1983). Generation of basaltic magmas and thermal structure of the mantle wedge in subduction zone. *Journal of Geophysical Research* **88**, 5815–5825.

Tatsumi, Y., Otofuji, Y., Matsuda, T. & Nohda, S. (1989). Opening of the Japan Sea by asthenospheric injection. *Tectonophysics* **166**, 317–309.

Tatsumoto, M. & Nakamura, Y. (1991). DUPAL anomaly in the Sea of Japan: Pb, Nd, and Sr isotopic variations at the eastern Eurasian continental margin. *Geochimica et Cosmochimica Acta* **55**, 3697–3708.

Taylor, S. R. & McLennan, S. M. (1985). *The Continental Crust: its Composition and Evolution*. Oxford: Blackwell Scientific.

Todt, W., Cliff, R. A., Hanser, A. & Hofmann, A. W. (1996). Evaluation of a ^{202}Pb–^{205}Pb double spike for high-precision lead isotope analysis. In: Basu, A. & Hart S. (eds.) *Earth Processes Reading the Isotopic Code*. American Geophysical Union, **95**, pp. 429–437.

Togashi, S., Tanaka, T., Yoshida, T., Ishikawa, K., Fujinawa, A. & Kurasawa, H. (1992). Trace elements and Nd–Sr isotopes of island arc tholeiites from frontal arc of Northeast Japan. *Geochemical Journal* **26**, 261–277.

Turner, S., McDermott, F., Hawkesworth, C.J. & Kepezhinskas, P. (1998). A U-series study of lavas from Kamchatka and the Aleutians: constraints on source composition and melting processes. *Contributions to Mineralogy and Petrology* **133**, 217–234.

Umeda, K., Hayashi, S., Ban, M., Sasaki, M., Ohba, T. & Akaishi, K. (1999). Sequence of the volcanism and tectonics during the last 2·0 million years along the volcanic front in Tohoku district, NE Japan. *Bulletin of the Volcanological Society of Japan* **44**, 233–249.

Vielzeuf, D. & Holloway, J. R. (1988). Experimental determination of the fluid-absent melting relations in the pelitic system (consequences for crustal differentiation). *Contributions to Mineralogy and Petrology* **98**, 257–276.

Walter, M. J. (1998). Melting of garnet peridotite and the origin of komatiite and depleted lithosphere. *Journal of Petrology* **39**, 29–60.

Wasylenki, L. E., Baker, M. B., Hirschmann, M. M. & Stolper, E. M. (1996). The effect of source depletion on equilibrium mantle melting. *EOS Transactions, American Geophysical Union* **77**, F847.

Wilson, M. (1989). *Igneous Petrogenesis: a Global Tectonic Approach*. London: Unwin Hyman.

Wyllie, P. J. (1982). Subduction products according to experimental prediction. *Geological Society of America Bulletin* **93**, 468–476.

Yogodzinski, G. M., Volynets, O. N., Koloskov, A. V., Seliverstov, N. I. & Matvenkov, V. V. (1994). Magnesian andesites and the subduction component in a strongly calc-alkaline series at the Piip volcano, far Western Aleutian. *Journal of Petrology* **35**, 163–204.

Yoshida, T. (2001). The evolution of arc magmatism in the NE Honshu arc, Japan. *Tohoku Geophysical Journal* **36**, 131–149.

Zashu, S., Kaneoka, I. & Aoki, K. (1980). Sr isotope study of mafic and ultramafic inclusions from Ichinome-gata, Japan. *Geochemical Journal* **14**, 123–128.

Zhao, D., Hasegawa, A. & Horiuchi, S. (1992). Tomographic imaging of P and S wave velocity structure beneath Northeastern Japan. *Journal of Geophysical Research* **97B**, 19909–19928.

Zou, H. (1998). Trace element fractionation during modal and nonmodal dynamic melting and open-system melting: a mathematical treatment. *Geochimica et Cosmochimica Acta* **62**, 1937–1945.

Zou, H. & Zindler, A. (1996). Constraints on the degree of dynamic partial melting and source composition using concentration ratios in magmas. *Geochimica et Cosmochimica Acta* **60**, 711–717.